Wettability and Interfacial Reaction between Liquid Cu-Ti, Al-Ti, Al-Si Alloys and Carbon Materials

Wettability and Interfacial Reaction between Liquid Cu-Ti, Al-Ti, Al-Si Alloys and Carbon Materials

(溶融銅–チタン、アルミニウム–チタン、アルミニウム–シリコン

合金と炭素系材料のぬれおよび界面反応)

By

Weiji Mao

Department of Biological Functions Engineering

Graduate School of Life Science and Systems Engineering

Kyushu Institute of Technology

Table of Contents

Chapter 1 Preface

1.1 Background

1.1.1 Metal matrix composites

There have been many new attempts in materials technology to improve high performance materials. Metal matrix composites (MMCs) are a family of advanced materials which may have many attractive mechanical and physical properties, such as high specific strength and stiffness, high operating temperature, great wear resistance, low coefficient of thermal expansion, decreased life cycle cost, and insensitivity to environment. Metal matrix composites also provide the opportunity to develop new materials with some unique properties that conventional metals or alloys do not possess. However, due to its high cost and limited fabrication experience, the development of metal matrix composites had received only limited attention. In recent decades, higher performance requirements and new applications for the military, automobile and aeronautical manufacturing fields renewed activity [1, 2].

The development of MMCs mainly resulted from the insufficiency of metals and alloys in providing both strength and stiffness to a structure, whereupon the strength and ductility is provided by the metal matrix and the strength and/or stiffness is provided by the reinforcement materials including carbides (e.g., TiC, SiC), nitrides (e.g., Si_3N_4, AlN), oxides (e.g., Al_2O_3, SiO_2), as well as elemental materials (e.g., C, Si) [3]. In general, most of the reinforcement materials are in the form of continuous fibers, chopped fibers, platelets, discontinuous particulates or whiskers. For example, SiC is being used in

aluminium and magnesium MMCs in all of the above mentioned forms and carbon and silicon fibers are being used in aluminium-, magnesium-, and copper-matrix composites [4].

The application of metal matrix composites can be fully exploited once suitable manufacturing techniques are mastered. Fabrication techniques for organic matrix composites have been well developed and applied. However, these fabrication techniques may be not applicable to metal matrix composites, due to high chemical reactivity and poor wettability between solid reinforced phase and liquid metal matrix. Therefore, the process technology of metal matrix composites is still immature and deserves to be studied more deeply.

When liquid metal matrix do not wet the reinforcement phases, an external pressure is necessary to bond them together. Many methods based on this principle have been described: vacuum infiltration, casting, liquid metal pressing and pressure-assisted network infiltration [5]. The fabrication of metal matrix composites by casting is a promising manufacturing method due to the processing conditions have extensive choices and this method is suitable for many materials. Good wetting is a necessary condition for the generation of a satisfactory bond between the reinforcement phase and liquid metal matrix during the manufacture of composites. In spite of the importance of wettability in the process of the fabrication of composites, relatively few researches have been carried out and a lot of essential problems remains unsolved [1].

Generally, the main role of the reinforcements in metal matrix composites is to support most of the applied load, while that of the matrix is to bond the reinforcements together and to transmit and distribute the external loads to the individual reinforcements. Due to transfer of loads depend on a bonding between the metal matrix and the

reinforcement phases, the nature of interface is essential for the property of composites. A sufficiently strong interface is expected to allow transfer and distribution of load from the matrix to the reinforcements without failures [5-10]. With respect to non-wetting systems, application of pressure cannot solve the problem of poor wettability in practical sense due to de-bonding during solidification and void formation in the small channels. Therefore, good wettability is one of the most important aspects during the processing stages of metal matrix composites materials.

On the other hand, the surface tension of liquid metals or alloys, which is both an intrinsic property and a key parameter of technological importance, contributes to deeper understanding the world of wettability. When a substance is liquid, the only forces acting upon it are gravity and the intermolecular attractions that manifest themselves in the phenomenon of surface tension. It follows that the behavior of the liquid materials will be closely related to their surface tensions and that an extension of our knowledge of this property should lead to a greater insight into the peculiarities exhibited by liquid metals. Generally, accurate information on the surface tension of liquid metal or its alloys is beneficial to many materials-related process, such as casting, welding, brazing, and the fabrication of matrix composites [11-13]. Unfortunately, experimental and theoretical investigations of the nature and behavior of surfaces or interfaces between phases are unsatisfactory. This situation results from the difficulty of precise experimental determinations of surface tensions or interfacial tensions. Furthermore, the difference of the measuring method and the experimental condition can also result in inconsistent values of the surface tension [14].

1.1.2 Copper/Aluminium-matrix composites reinforced by carbon materials

In this thesis, we mainly focus on the wetting between metal matrix composites and graphite. Many metals have been considered as a possible matrix: lithium, magnesium, silicon, aluminium, titanium, copper, nickel, zinc, lead, etc. Among these metals, copper and aluminium as two of the most widely used metals in life have attracted particular attention during the last three decades, because their reinforced by graphite have many impressive merits, such as high specific strength and specific stiffness, good thermal and electrical conductivities, superior tribological property without the use of lubricant and low fabrication cost. However, during the processing stages of metal matrix composites, graphite that composes of very thin layers of carbon weakly bond together by Van der Waals forces is very soft and brittle, in addition, it is difficult to uniformly disperse in the metal matrix without dispersants. Therefore, the use of graphite as the reinforcement phase shows a certain limitation. Using carbon fiber instead of the graphite may be an effective way. In fact, carbon fiber can be an equally satisfactory reinforcement material in metal, polymer as well as ceramic matrices because it not only possesses most of the advantages of graphite, but also has some excellent properties that are not available with graphite, such as higher specific strength than graphite, high specific modulus, light weight, good fatigue resistance and low coefficient of thermal expansion (the coefficient of thermal expansion of carbon fiber material in fiber direction is almost zero at room temperature). The composites reinforced by carbon fiber have been more widely used in aerospace, civil engineering, military, and motorsports, along with other competition sports. For this reason, the understanding of the composite of the copper/aluminum alloys

and the carbon fiber appears especially important.

The main purpose of this thesis work is to establish a foundational understanding of wetting behavior and interfacial phenomena between the liquid copper/aluminium or its alloys and carbon materials. In order to demonstrate the concepts developed in this thesis, the nature of the interfacial interactions between Cu-Ti, Al-Ti and Al-Si alloys and graphite/carbon fiber substrates were selected. In addition, the surface tensions of these alloys were measured, which aimed at providing useful and accurate information for any metallurgical and materials-related process.

1.2 Basic Concepts in Wetting

1.2.1 Surface tension

Whenever a liquid droplet is placed down on a horizontal surface of solid substrates, this droplet tends to evolve, till it reaches to an equilibrium state. This may require the drop to either spread across the surface of the solid substrate or remain as a drop or in some cases even try to leave the surface. Such a process depends on properties of the surfaces involved as well as the external conditions, such as temperature and atmosphere. This field is broadly classified as wetting and interfacial phenomena and aims to determine how a liquid behaves on the surface of a substrate [15].

The surface tension, namely the interfacial tension of liquid-vapor, is an intrinsic property of all liquids and is due to an incomplete coordination of the atoms at the liquid-gas interface. In a pure liquid, molecules in the bulk of the liquid are completely surrounded by other molecules, thus they are pulled equally in every direction. However, molecules exposed at the surface do not have surrounding molecules in all directions to provide a balanced net force. Therefore, interatomic attractions cause an uneven pull on the surface molecules, drawing them into the inside of the liquid and resulting in a curvature of the surface as the liquid tries to contracts its surface area to maintain the lowest surface free energy (Figure 1.2.1). Chemical composition and temperature are the two main parameters effecting the surface tension [16-17]. For the liquid phase, the surface tension and surface free energy are a measure of the interatomic forces which reveals how much energy is needed to increase the liquid surface area by one unit, which leads to the thermodynamic definition.

$$\gamma = \left[\frac{\delta G}{\delta A}\right]_{T,V,n} \quad (1.2.1)$$

For the solid phase, surface tension measures the energy required to stretch the surface. The surface tension generally decreases with the increase of the temperature, due to molecules become less tightly bound to the surface with the increase of the kinetic energy.

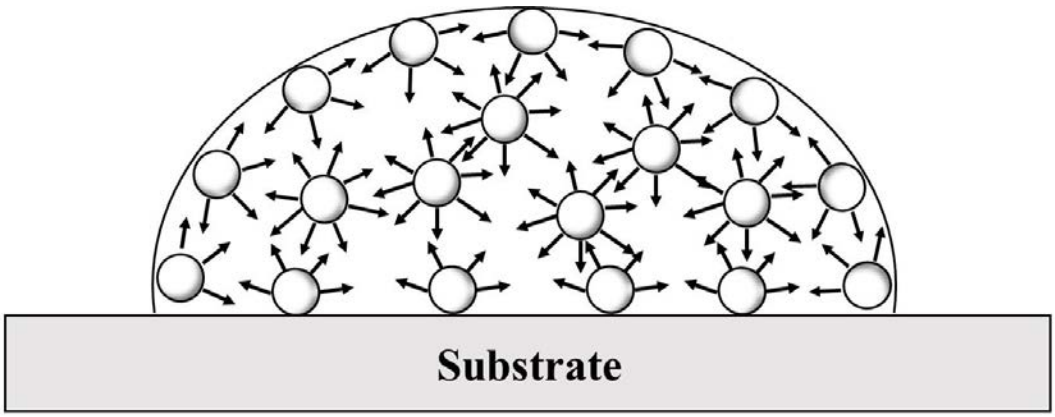

Figure 1.2.1 Surface tension is caused by the unbalanced forces of liquid molecules at the surface

1.2.2 Contact angle

As an important parameter and intuitive judgment, the contact angle formed at the solid-liquid interface is widely used for characterizing the degree of wetting. When a pure liquid is placed on an ideal surface (flat, rigid, perfectly smooth, and chemically homogeneous), three phases exist in the wetting system: the liquid, surface and surrounding atmosphere which is referred to as the vapor. Under equilibrium conditions, the relation between the various interfacial tensions and the contact angle was given by Young's equation [18]:

$$\cos\theta_{eq} = \frac{\gamma_{SV}-\gamma_{SL}}{\gamma_{LV}} \quad (1.2.2)$$

Where γ_{LV} is the interfacial tension of liquid-vapor (the surface tension), γ_{SV} is the interfacial tension of solid-vapor and γ_{SL} is interfacial tension of solid-liquid. θ_{eq} is the equilibrium contact angle as shown in Figure 1.2.2.

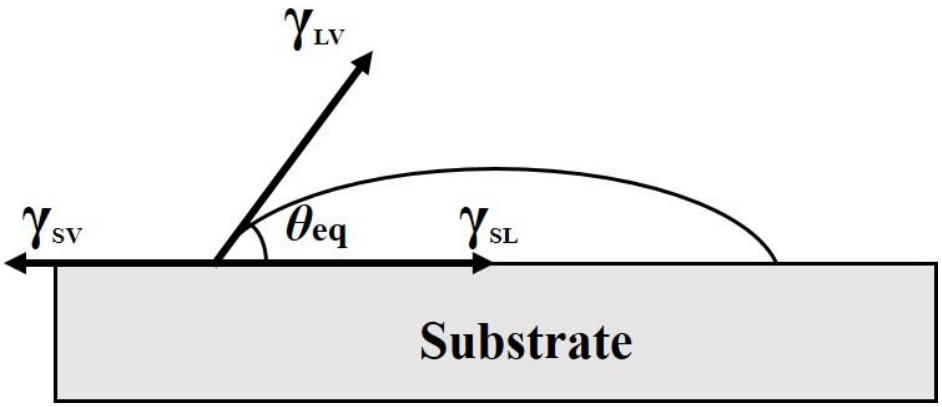

Figure 1.2.2 Young's equation equates the surface tension forces at equilibrium

For a given wetting system, the contact angle θ_{eq} can be obtained from the interfacial tensions involved. Figure 1.2.3 schematically shows these four wetting conditions: highly wetting, partially wetting, partially non-wetting and non-wetting. Small contact angles ($<90°$) correspond to good wetting, while large contact angles ($>90°$) correspond to poor wetting. More specifically, contact angles less than 90° indicate that wetting of the surface is beneficial, and the liquid drop will spread over a large area on the surface, whereas contact angles greater than 90° generally illustrate that wetting of the surface is unbeneficial and the liquid has a tendency to decrease the contact area with the surface,

till it forms a compact liquid drop [19].

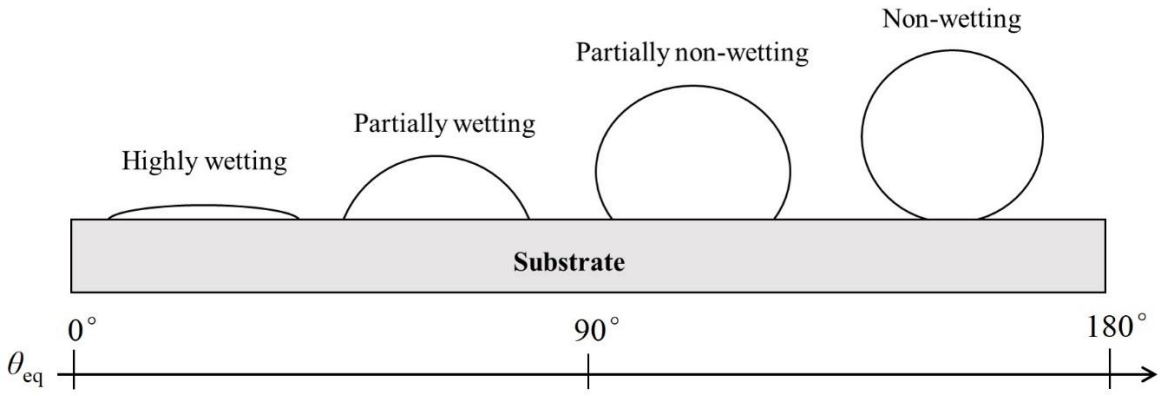

Figure 1.2.3 Liquid drop on a solid substrate under various wetting conditions

As a general rule, the interaction energy between a liquid and a solid substrate is quantified by the work of adhesion W_{ad} related to the characteristic surface energies of the solid (S)–liquid (L)–vapor (V) system by the Dupre equation [20]:

$$W_{ad} = \gamma_{\mathrm{LV}} + \gamma_{\mathrm{SV}} - \gamma_{\mathrm{SL}} \tag{1.2.3}$$

Then combining with the Young's equation (1.2.2), we can finally obtain the Young–Dupre equation, which is more relevant to the contact angle:

$$\cos\theta_{\mathrm{eq}} = \frac{W_{ad}}{\gamma_{\mathrm{LV}}} - 1 \tag{1.2.4}$$

Due to the work of adhesion is regarded as the work per unit area of interface that must be performed to separate reversibly the two phases, thus it is a measure of the strength of the binding between the liquid drop and the solid substrate. Thus, based on the Young–

Dupre equation, the greater the work of adhesion W_{ad}, the smaller the value of contact angle θ. Regarding to complete wetting, the contact angle θ is 0° , which corresponds to $W_{ad}=2\gamma_{LV}$, so it can be viewed as a perfect wetting when $W_{ad}\geqslant 2\gamma_{LV}$ and this means that the adhesion energy between the liquid drop and the solid substrate should be more than twice the surface tension.

The derivation process of Young's and Young–Dupre equations are based on the hypotheses that the liquid spreads on an ideal surface (physically and chemically inert, smooth, homogeneous and rigid) of the solid substrate. In the actual situations, these conditions are very difficult to be met. In any case, Young's and Young–Dupre equations provide a basic starting point for better understanding of the complicated world of wetting [21].

1.2.3 Sessile drop method

Many techniques contribute to measuring the contact angle of the liquid drop on the solid substrate, such as optical reflectometry, contrast interferometry, the capillary rise technique, Wilhelmy plate tensiometry and various goniometric methods [22-25]. Among these, the sessile drop method coupled with digital image analysis is the most commonly used methods to measure the contact angle. In this method, when a liquid drop is formed on the solid substrate, the contour of the drop is captured digitally by a high-resolution digital camera. A number of image analysis algorithms can be subsequently employed to estimate the contact angle from the drop contour such as polynomial fitting, spherical cap approximations [26-28], or direct fitting to numerical solutions of the Young-Laplace equation [29-32]. In addition to the contact angle, the surface tension also can be measured by the sessile drop method, due to its good operability, and the accuracy of the measuring

results at high temperature. The measuring method of the surface tension will be described in detail in the following chapters. However, in sessile-drop techniques, due to some artificial improper operations or optical noise caused by diffraction and scattering [33, 34] which lead to systematic errors in the evaluation of the tangent line, the region near the triple-phase contact line can appear distorted or blurred. Therefore, it should be careful to adjust the camera in order to minimize experimental errors.

1.3 Literature Review

1.3.1 Effect of reactive elements on wetting

The wettability of the copper/carbon and aluminium/carbon systems have been investigated extensively. However, during the fabrication of these two composites, there are some unavoidable issues that need to be improved. For the copper/carbon system, it is well known that the molten copper does not wet the carbon as the contact angle is approximately 140°, besides, neither the mutual solubility nor the formation of carbides would occur at high temperature [35,36]. For the aluminum/carbon system, many researchers have reported that the wettability between carbon and liquid Al is poor at temperature close to the melting point of Al since Al is readily oxidized even if under a high vacuum [37-39]. Although increasing temperature could improve it, Al_4C_3 phase would be formed at the interface in the meanwhile, which is brittle and water soluble, and thus significantly results in the weakening of interfaces and reduces the mechanical properties and corrosion resistance of composites [37, 40]. Therefore, it is necessary to improve the wettability for both the copper/carbon and aluminum/carbon systems and simultaneously avoid the formation of Al_4C_3 at high temperature for aluminum/carbon systems.

In practice, wetting may be improved by adding other reactive elements, such as Ti, Mg, Cr and Si. The beneficial effects of reactive additives on wettability have been addressed as due to two reasons: a reduction of interface energy contributed by the negative free energy of the chemical reaction between the reactive element and the substrate, and by the formation of a reaction product at the liquid-substrate interface [41, 42]. Kritsalis et al. [43] investigated the wetting between NiPd-Ti alloys and alumina substrates. The contact angle decreased with the increase of the Ti content. The interfacial composition analysis revealed that different reaction products have been formed at the interface if the addition amount of Ti changed. Since the free energies of formation of these different reaction products were approximately the same, they concluded that the increase of the contact angle resulted from the formation of different reaction products (titanium oxides) rather than by the negative free energies. A similar result was found by Bougiouri et al. [44], who investigated the wetting of Ni-Si alloys on vitreous carbon (Cv) substrates. They reported that if the addition amount of Si on Ni matrix was less the minimum Si content needed for SiC formation (approximately 35 at. % at 1473 K), no SiC was formed at the interface of the Ni-Si alloys/ Cv systems, and the contact angle of about 123° showed a non-wetting system. On the contrary, when the addition amount of Si was larger than the content of reactivity limit, a thin continuous SiC layer was formed at the interface, resulting in spreading of the liquid alloy. Furthermore, they also compared the immersion energy of the Ni-Si alloys either on reactive substrate of carbon or on non-reactive substrate of SiC at the same Si content, and found that both the values were the same. This result indicated that the change from non-wetting to wetting observed between non-reactive and reactive alloys could be attributed to the replacement of vitreous carbon by wettable SiC at the interface.

However, some investigations indicate that wetting can be improved by the negative free energy of the chemical reaction between the reactive element and the substrate instead of by the formation of reaction products. For instance, in 1993, Fujii et al. [45] investigated the wetting of liquid Al on BN substrates and on AlN substrates. They observed that the reaction product was detected as AlN, and the contact angle of liquid Al on BN at 1173 K decreased to 0°. However, the contact angle of liquid Al on AIN under the same condition was 130°. Clearly, the decrease of contact angle of liquid Al on AlN illustrated that the wetting indeed improved by the chemical reaction itself rather than the formation of AlN at the interface.

A model combining a dynamic process of reaction and equilibrium state of wetting was proposed by Aksay et al. [46]. According to this model, the contact angle would decrease in the initial stage due to the chemical reaction, but then increased by a de-wetting process owing to the formation of a more stable ceramic at the interface. However, such a hypothesis has, to the best of our knowledge, never been verified in experiments [43, 47-49]. In the treatment of reactive wetting, Aksay et al. [46] and Laurent et al. [47] tried to connect the negative free energy and the Young's equation of wetting. However, in principle the use of interface energy is valid only for an equilibrium state of wetting, but not for a dynamic situation like a reactive wetting, where rather the interface tension should be used which of course is not always equal to the interface energy.

After all, the effect of chemical reaction on wetting reported by the previous literatures are still ambiguous and confusing: sometimes, it is effective, but sometimes not. In this thesis, titanium and silicon with high reactivity are selected as carbide-forming element to investigate the wetting behavior of both the copper/carbon and aluminium/carbon systems, and the primary purpose is to probe the essence of the reactive wetting, and to

provide a new insight of the wetting process between the carbon materials and the reactive alloys, which can be applicable to any liquid metal–ceramic reactive system.

1.3.2 Previous studies about wetting between Cu-Ti, Al-Ti, and Al-Si alloys and carbon materials

Numerous studies concerning the wettability of Cu-Ti/carbon, Al-Ti/carbon, and Al-Si/carbon systems have been reported. However, it is a common phenomenon that the reported contact angles are very scattered. This variation can be ascribed to some subtle differences of the samples (different purity of samples, different types, density and surface roughness of carbon substrates, etc.) used in wetting experiments and dissimilar experimental conditions (temperature, atmosphere, holding time and placement state of alloys on carbon substrates, etc.)[43-47].

- **Wetting of Cu-Ti alloys/C systems**

The first study of wetting of Cu-Ti alloys on graphite substrates was carried out by D.A.Mortimer et al. in 1973 [36]. They reported that a change from non-wetting to wetting behavior occurred on the graphite substrate at 1423 K only when the titanium content was over 10 mass %. Meanwhile, a thin TiC layer was observed at the interface and the interfacial morphology of it changed from a continuous layer to a particulate zone with the increasing holding time. Shinozaki et al. [53] reported the contact angle of Cu-Ti alloys/graphite systems decreased with increasing titanium content of alloy and was less than 90° when the alloy containing titanium over 11.6 mass % at 1323 K. Moreover, a reaction layer consisted by numerous TiC granules formed at the interface in the initial stage of alloy melting. LongLong Yang et al. [50] studied the wetting of Cu-Ti/porous

graphite system at 1373 K in argon atmosphere. They demonstrated that an increase in the titanium content from 1 mass % to 5 mass % decreased the stoichiometry of the resultant TiC_X phase and thus improved the wettability, while the final contact angles reached 6° for the Cu-5 mass % Ti alloy. Clearly, in all the examples cited above, it seems that adding titanium into copper can improve the wettability between copper and graphite. However, the reasons for such dependence as well as the large scatter in the reported contact angles have not yet been well understood.

- **Wetting of Al-Ti alloys/C systems**

For the Al/C system, it is expected that the addition of reactive elements (Ti and Si) in Al could not only improve the wettability of the Al/C systems, but also replace the formation of Al_4C_3 by that of other carbide. N. Sobczak et al. [55] reported that adding 6 at. %Ti to Al would get rise to a remarkable change in structure and chemistry of the interfaces between molten Al and vitreous carbon substrate. The formation of undesirable Al_4C_3 was delayed and even prevented because thermodynamically more favorable TiC was formed instead of Al_4C_3. But under certain experimental conditions, they found that TiC existed along with Ti_2AlC and/or Al_4C_3 since the kinetic factors, affecting chemical reactions, dissolution and diffusion processes, are responsible for structural and phase transformations in the system. Despite this, alloying of Al with Ti can improve the wettability of the Al/C systems that has been confirmed by several researchers. K. Landry et al. [56] reported the addition of only 0.1wt. %Ti in Al decreased the contact angle from 77° (for pure Al/C system) to 68° at 1273 K within 30 minutes. N. Eustathopoulos et al. [57] found that addition of Ti in Al up to 0.8 at. % at 1223 K led to the formation of a bilayer of Al_4C_3 and TiC (or may be a Al, Ti ternary carbide) at the interface, and slightly

improved the wetting which the final contact angle decreased from 50° to 46°. In any case, the wettability of the Al-Ti/carbon system deserves to be investigated more deeply due to its complexity and uncertainty at interface.

- **Wetting of Al-Si alloys/C systems**

For the wettability of Al-Si/carbon systems, N. Eustathopoulos et al. [57] measured the contact angle of molten Al-Si alloys on carbon substrates at 1273 K in vacuum by the sessile drop method and reported that with increasing the Si content from zero to 19 mass %, the wettability improved and the equilibrium contact angle decreased from 77° to 58°. They suggested that the Si could lead to rapid dislocation of the oxide film and reacted strongly with the carbon to bring out wetting. K. Landry et al. [56] reported that the contact angle of vitreous carbon substrates by Al alloys containing 0, 13.5 and 20.6 mass% Si were 56°, 45° and 38° respectively at 1190 K, and the addition of Si could not only improve the wettability of Al/carbon systems, but also could replace the formation of Al_4C_3 by that of SiC if the addition amount of Si is high enough. Nevertheless, few researchers have done further discussion about the substantial cause of an improving wettability in Al-Si/carbon systems as increasing the Si content.

References

[1] Oh S Y, Cornie J A, Russell K C. Wetting of ceramic particulates with liquid aluminum alloys: Part I. Experimental techniques[J]. Metallurgical Transactions A, 1989, 20(3): 527-532.

[2] Oh S Y, Cornie J A, Russell K C. Wetting of ceramic particulates with liquid aluminum alloys: Part II. Study of wettability[J]. Metallurgical transactions A, 1989, 20(3): 533-541.

[3] Ibrahim I A, Mohamed F A, Lavernia E J. Particulate reinforced metal matrix composites—a review[J]. Journal of materials science, 1991, 26(5): 1137-1156.

[4] A. L. Geiger and M. Jackson, Adv. Mater. Process 7 (1989) 23.

[5] Delannay F, Froyen L, Deruyttere A. The wetting of solids by molten metals and its relation to the preparation of metal-matrix composites composites[J]. Journal of materials science, 1987, 22(1): 1-16.

[6] Shorowordi K M, Laoui T, Haseeb A, et al. Microstructure and interface characteristics of B 4 C, SiC and Al 2 O 3 reinforced Al matrix composites: a comparative study[J]. Journal of Materials Processing Technology, 2003, 142(3): 738-743.

[7] Surappa M K, Rohatgi P K. Preparation and properties of cast aluminium-ceramic particle composites[J]. Journal of Materials Science, 1981, 16(4): 983-993.

[8] Fundamentals of metal-matrix composites[M]. Elsevier, 2013.

[9] Srivatsan T S, Ibrahim I A, Mohamed F A, et al. Processing techniques for particulate-reinforced metal aluminium matrix composites[J]. Journal of materials science, 1991, 26(22): 5965-5978.

[10] Rajan T P D, Pillai R M, Pai B C. Reinforcement coatings and interfaces in aluminium metal matrix composites[J]. Journal of Materials Science, 1998, 33(14): 3491-3503.

[11] Saravanan R A, Molina J M, Narciso J, et al. Effects of nitrogen on the surface tension of pure aluminium at high temperatures[J]. Scripta materialia, 2001, 44(6): 965-970.

[12] Alchagirov B B, Chochaeva A M, Mozgovoi A G, et al. The surface tension of liquid near-eutectic alloys of lead–bismuth system[J]. High temperature, 2003, 41(6): 755-762.

[13] Park S H, Um Y S, Kum C H, et al. Thermophysical properties of Al and Mg alloys for metal foam fabrication[J]. Colloids and Surfaces A: Physicochemical and Engineering Aspects, 2005, 263(1): 280-283.

[14] Iida T, Guthrie R I L. The physical properties of liquid metals[J]. Clarendon Press, Walton Street, Oxford OX 2 6 DP, UK, 1988., 1988.

[15] Krishnakumar P. Wetting and spreading phenomena[J]. 2010.

[16] Facchini M C, Decesari S, Mircea M, et al. Surface tension of atmospheric wet aerosol and cloud/fog droplets in relation to their organic carbon content and chemical composition[J]. Atmospheric Environment, 2000, 34(28): 4853-4857.

[17] Kingery W D. Surface tension of some liquid oxides and their temperature coefficients[J]. Journal of the American Ceramic Society, 1959, 42(1): 6-10.

[18] Eustathopoulos N. Dynamics of wetting in reactive metal/ceramic systems[J]. Acta Materialia, 1998, 46(7): 2319-2327.

[19] Yuan Y, Lee T R. Contact angle and wetting properties[M]//Surface science techniques. Springer Berlin Heidelberg, 2013: 3-34.

[20] Dezellus O, Eustathopoulos N. Fundamental issues of reactive wetting by liquid

metals[J]. Journal of Materials Science, 2010, 45(16): 4256-4264.

[21] Kumar G, Prabhu K N. Review of non-reactive and reactive wetting of liquids on surfaces[J]. Advances in colloid and interface science, 2007, 133(2): 61-89.

[22] Deák A, Hild E, Kovács A L, et al. Contact angle determination of nanoparticles: film balance and scanning angle reflectometry studies[J]. Physical Chemistry Chemical Physics, 2007, 9(48): 6359-6370.

[23] Srinivasan S, McKinley G H, Cohen R E. Assessing the accuracy of contact angle measurements for sessile drops on liquid-repellent surfaces[J]. Langmuir, 2011, 27(22): 13582-13589.

[24] Wang J Y, Betelu S, Law B M. Line tension approaching a first-order wetting transition: Experimental results from contact angle measurements[J]. Physical Review E, 2001, 63(3): 031601.

[25] Shang J, Flury M, Harsh J B, et al. Comparison of different methods to measure contact angles of soil colloids[J]. Journal of colloid and interface science, 2008, 328(2): 299-307.

[26] Mack G L. The Determination of Contact Angles from Measurements of the Dimensions of Small Bubbles and Drops. I. The Spheroidal Segment Method for Acute Angles[J]. The Journal of Physical Chemistry, 1936, 40(2): 159-167.

[27] Mack G L, Lee D A. The determination of contact angles from measurements of the dimensions of small bubbles and drops. II. the sessile drop method for obtuse angles[J]. The Journal of Physical Chemistry, 1936, 40(2): 169-176.

[28] Yang M W, Lin S Y. A method for correcting the contact angle from the θ/2 method[J]. Colloids and Surfaces A: Physicochemical and Engineering Aspects, 2003, 220(1): 199-210.

[29] Rotenberg Y, Boruvka L, Neumann A W. Determination of surface tension and contact angle from the shapes of axisymmetric fluid interfaces[J]. Journal of colloid and interface science, 1983, 93(1): 169-183.

[30] Skinner F K, Rotenberg Y, Neumann A W. Contact angle measurements from the contact diameter of sessile drops by means of a modified axisymmetric drop shape analysis[J]. Journal of Colloid and Interface Science, 1989, 130(1): 25-34.

[31] Cheng P, Li D, Boruvka L, et al. Automation of axisymmetric drop shape analysis for measurements of interfacial tensions and contact angles[J]. Colloids and Surfaces, 1990, 43(2): 151-167.

[32] Stalder A F, Melchior T, Müller M, et al. Low-bond axisymmetric drop shape analysis for surface tension and contact angle measurements of sessile drops[J]. Colloids and Surfaces A: Physicochemical and Engineering Aspects, 2010, 364(1): 72-81.

[33] Starov V M, Zhdanov S A, Kosvintsev S R, et al. Spreading of liquid drops over porous substrates[J]. Advances in Colloid and Interface Science, 2003, 104(1): 123-158.

[34] Zuo Y Y, Do C, Neumann A W. Automatic measurement of surface tension from noisy images using a component labeling method[J]. Colloids and Surfaces A: Physicochemical and Engineering Aspects, 2007, 299(1): 109-116.

[35] Ishii T, Koishi M, Tsunoda T. Wettability Technology Hand book. 2th ed. Tokyo: Techno-System; 2001.

[36] Mortimer D A, Nicholas M. The wetting of carbon by copper and copper alloys. J. Mater. Sci 1970; 5(2): 149-155.

[37] Cong X S, Shen P, Wang Y, et al. Wetting of polycrystalline SiC by molten Al and Al− Si alloys[J]. Applied Surface Science, 2014, 317: 140-146.

[38] Laurent V, Chatain D, Eustathopoulos N. Wettability of SiC by aluminium and Al-Si alloys[J]. Journal of materials science, 1987, 22(1): 244-250.

[39] Kimura Y, Mishima Y, Umekawa S, et al. Compatibility between carbon fibre and binary aluminium alloys[J]. Journal of materials science, 1984, 19(9): 3107-3114.

[40] Eustathopoulos N, Joud J C, Desre P, et al. The wetting of carbon by aluminium and aluminium alloys[J]. Journal of Materials Science, 1974, 9(8): 1233-1242.

[41] Zhou X B, De Hosson J T M. Reactive wetting of liquid metals on ceramic substrates[J]. Acta Materialia, 1996, 44(2): 421-426.

[42] Intermetallic and ceramic coatings[M]. CRC Press, 1999.

[43] Kritsalis P, Drevet B, Valignat N, et al. Wetting transitions in reactive metal/oxide systems[J]. Scripta metallurgica et materialia, 1994, 30(9): 1127-1132.

[44] Bougiouri V, Voytovych R, Dezellus O, et al. Wetting and reactivity in Ni–Si/C system: experiments versus model predictions[J]. Journal of materials science, 2007, 42(6): 2016-2023.

[45] Fujii H, Nakae H, Okada K. Interfacial reaction wetting in the boron nitride/molten aluminum system[J]. Acta metallurgica et materialia, 1993, 41(10): 2963-2971.

[46] Aksay I A, Hoge C E, Pask J A. Wetting under chemical equilibrium and nonequilibrium conditions[J]. The Journal of Physical Chemistry, 1974, 78(12): 1178-1183.

[47] Laurent V, Chatain D, Eustathopoulos N. Wettability of SiO 2 and oxidized SiC by aluminium[J]. Materials Science and Engineering: A, 1991, 135: 89-94.

[48] Ip S W, Kucharski M, Toguri J M. Wetting behaviour of aluminium and aluminium alloys on Al 2 O 3 and CaO[J]. Journal of materials science letters, 1993, 12(21): 1699-1702.

[49] Laurent V, Chatain D, Eustathopoulos N. Wettability of SiC by aluminium and Al-Si alloys[J]. Journal of materials science, 1987, 22(1): 244-250.

[50] Yang L, Shen P, Lin Q, Qiu F, Jiang Q. Wetting of porous graphite by Cu–Ti alloys at 1373K. Mater. Chem. Phys 2010; 124(1): 499-503.

[51] Landry K, Kalogeropoulou S, Eustathopoulos N. Wettability of carbon by aluminum and aluminum alloys. Mater. Sci. Eng., A 1998; 254(1): 99-111.

[52] Li J G. Kinetics of wetting and spreading of Cu-Ti alloys on alumina and glassy carbon substrates. J. Mater. Sci. Lett 1992; 11(23), 1551-1554.

[53] Shinozaki N, Katayama Y, Umezawa Y, Wasai K. Reaction and wetting between molten Cu-Ti alloy and graphite. J. JRICu 2008; 47: 187-191.

[54] Dahan I, Admon U, Frage N, Sariel J, Dariel M P. Diffusion in Ti/TiC multilayer coatings. Thin solid films 2000; 377: 687-693.

[55] Sobczak N, Sobczak J, Seal S, et al. TEM examination of the effect of titanium on the Al/C interface structure[J]. Materials chemistry and physics, 2003, 81(2): 319-322.

[56] Landry K, Kalogeropoulou S, Eustathopoulos N. Wettability of carbon by aluminum and aluminum alloys[J]. Materials Science and Engineering: A, 1998, 254(1): 99-111.

[57] Eustathopoulos N. Wettability of carbon by aluminum and aluminum alloys[J]. Materials Science & Engineering A, 1998, 1(254): 99-111.

Chapter 2 Wettability and Interfacial Reaction between Cu-Ti Alloys and Graphite

2.1 Introduction

In spite of numerous researches about the wetting of the Cu-Ti alloy/graphite systems that have been performed, few or even no researchers have investigated that whether the wetting behavior would be affected by the placement state of Cu-Ti alloys on graphite substrates. In general, there are two kinds of the placement states that are usually employed in previous studies: (1) Pure Cu is alloyed with pure Ti by arc-melting to fabricate Cu-Ti alloys before wetting experiments and then placed on graphite substrates [1]; (2) Drops of Cu-Ti alloys were prepared in situ by melting pure Ti and Cu, which were directly placed on the graphite substrate in some configuration [2, 3]. Although the wetting results reported previously suggest that adding titanium into copper can improve the wettability between copper and graphite, since the placement states of Cu-Ti sample in each study are not uniform completely, it may have a certain impact on the wetting results.

In this chapter, the wettability and interfacial reaction between graphite substrate and liquid Cu-Ti alloys with titanium content of 4 mass%, 6 mass% and 10 mass% by changing the placement state of copper and titanium was studied at 1373 K using the sessile drop method. This investigation was devoted to obtaining a new insight of the wetting process between the graphite and the Cu-Ti alloys, which is applicable to any liquid metal–ceramic reactive system.

2.2 Experimental

2.2.1 Materials

High purity copper (99.99 wt. %) and titanium (99.99 wt. %) plates were employed in this study and there were placed on the graphite substrates in three states which were separately defined as the placement state A (Figure 2.2.1(a)), B (Figure 2.2.1(b)) and C (Figure 2.2.1(c)). As shown in Figure 2.2.1(a), the placement of state A, from top to bottom, was settled as pre-alloyed Cu-Ti/C. The pre-alloyed Cu-Ti alloys with titanium content of 4 mass%, 6 mass% and 10 mass% were prepared from pure copper and titanium by arc-melting in a Ti (99.8 wt. %)-gettered argon (99.999% purity) atmosphere, and were machined into a small cylinder with 5mm ± 0.5mm in height and 4mm ± 0.5mm in diameter and weighting approximately 0.4 g for the experiment. The placement of state B and C, from top to bottom, was settled as Ti/Cu/C and Cu/Ti/C, respectively, shown as Figure 2.2.1(b) and 2.2.1(c). The drops of Cu-Ti alloys were prepared in situ by melting the pure Ti and Cu plates, which were directly piled on the graphite substrate. The Cu plate was cut into 5mm ± 0.5mm in square and 1.5mm in thickness. As for the dimensions of the Ti plate, the thickness was 1mm and the square varied with different Ti contents, which were 1.8 mm ± 0.5 mm for 4 mass% Ti, 2.2 mm ± 0.5 mm for 6 mass% Ti and 3mm ± 0.5mm for 10 mass% Ti. The plates of Cu and Ti were weighted in designed proportion which the mass ratio of Cu/Ti were 96:4, 94:6 and 90:10, respectively, and the total mass was approximately 0.4 g in all cases. Before the wetting experiment, both the pre-alloyed Cu-Ti alloys and the metals of Cu and Ti were polished by emery papers from 400 to 2000 grit and cleaned with ethanol in order to prevent further oxidation.

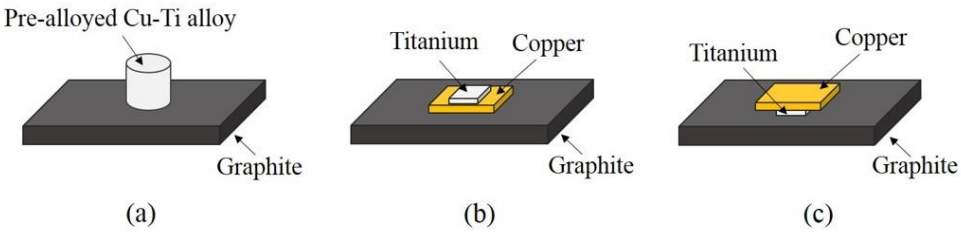

Figure 2.2.1 Schematic diagram of three kinds of placement states

The substrate used was high purity (99.99 mass %) graphite plates with a density of 1.88 g/cm³ and an ash content less than 5 ppm. These substrates were 12 mm in square and 2 mm in thickness. Due to both sides of substrate were different in surface roughness and wetting results can be strongly affected by the roughness of the substrate, the relatively smooth surface was chosen for this experiment and the average roughness Ra of this surface obtained from three-dimensional scanning electron microscopy (3D-SEM) was 0.9 μm ± 0.02 μm, indicating a highly polished surface. Before experiment, the substrates were ultrasonically cleaned in ethanol, then dried in air drying oven at least one week.

2.2.2 Experimental apparatus and procedure

The wetting experiments were carried out using the sessile drop method. The schematic diagram of sessile drop apparatus was shown in Figure 2.2.2, and this apparatus was mainly composed of three parts: a quartz tube furnace, two vacuum pumps (oil rotary pump and oil diffusion pump) and the image observation system. The metal samples were placed on the center of the graphite substrate and then adjusted horizontally. Two ceramic boats containing sponge titanium were used as the deoxidizing agent and placed at the

left and right sides, about 5 cm away from the sample respectively. The furnace was evacuated to a vacuum approximately 1.5 Pa at the room temperature and then heated to the experimental temperature of 1373 K. The wetting behavior of the sample was recorded using a Nikon D300s digital camera connected with a macro-lens by an extension bellows set placed in front of the observation window. The contact angle and the drop base diameter were recorded at intervals of 5 minutes at 1373 K and then measured from the drop profile using image analysis software. In order to obtain an average of the contact angle, both sides of droplet were measured.

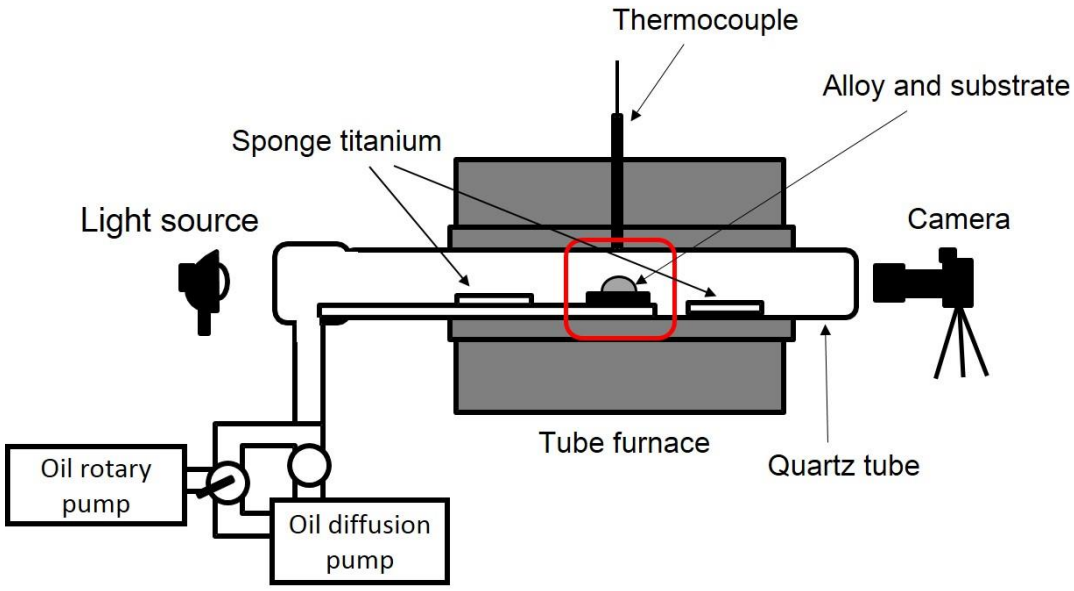

Figure 2.2.2 Schematic diagram of sessile drop apparatus

2.2.3 Analysis methods

After the sessile drop experiments, the selected samples were embedded in epoxy resin (Ollie, OMP-300, Japan), sectioned perpendicular to the interface by the wheel

diamond saw (Ollie, OL-150, Japan), grinded by emery papers from 400 to 1500 grit and polished using diamond pastes to examine the interfacial microstructures using an optical microscope (Keyence, VH-Z450, Japan) and an electron probe micro-analyzer (EPMA) (Jeol, JXA-8530F, Japan). And A X-ray diffraction analyzer (Jeol, JDX-3500K, Japan) was used to determine the phases of the interface.

2.3 Results

2.3.1 Contact angle phenomena

Figure 2.3.1 shows the time variation in the contact angle and the drop base diameter for the Cu-Ti alloys on the graphite substrates with different titanium contents in three placement states at 1373 K. For all the placement states, it was noticeable that the wettability improved with increasing titanium content from 4 mass% to 10 mass%. However, in the case of the placement state A (Figure 2.3.1(a)), the contact angles were barely varied with time in three kinds of titanium content. It could be find that the change from non-wetting to wetting behavior took place at somewhere between 6 mass% and 10 mass%, which seemed more close to 10 mass%, and the final contact angle of 10 mass% Ti was stabilized at approximately 81°. A different wetting phenomenon was obtained from the placement state B. As shown in Figure 2.3.1(b), the initial contact angles were much lower than that of the placement state A when the temperature reached at 1373 K, and then the contact angles decreased with time, except for the sample of 4 mass% Ti which the contact angle remained unchanged within 1 hour. Especially for the sample of 10 mass% Ti, the final contact angle reduced to approximately 16 ° continuously and the spreading of droplet occurred rapidly as compared with the sample of 4 mass% Ti.

Because the contact angle of 10 mass% Ti did not reach a stabilized value within 1 hour, the additional experiment were performed, and we found that the value of contact angle for this alloy stabilized at approximately 12 ° after 80 minutes, showing a remarkable wettability. A similar phenomenon was observed in the placement state C. According to Figure 2.3.1(c), a better wettability was obtained compared with the placement state B, as for the sample of 10 mass% Ti, the initial contact angle has already decreased to 17 ° when the temperature reached to 1373 K, and the final contact angle was stabilized at approximately 8 ° after 1 hour. In addition, from Figure 2.3.1, what was more noteworthy was the large difference of the contact angle between each of the placement states at the same Ti content, wherein the difference between the placement state A (pre-alloyed Cu-Ti alloys) and the placement states B or C (in situ alloyed Cu-Ti alloys) was much greater than that between the placement states B and C, and the best wettability was obtained from the placement state C, followed by the placement state B and the placement state A.

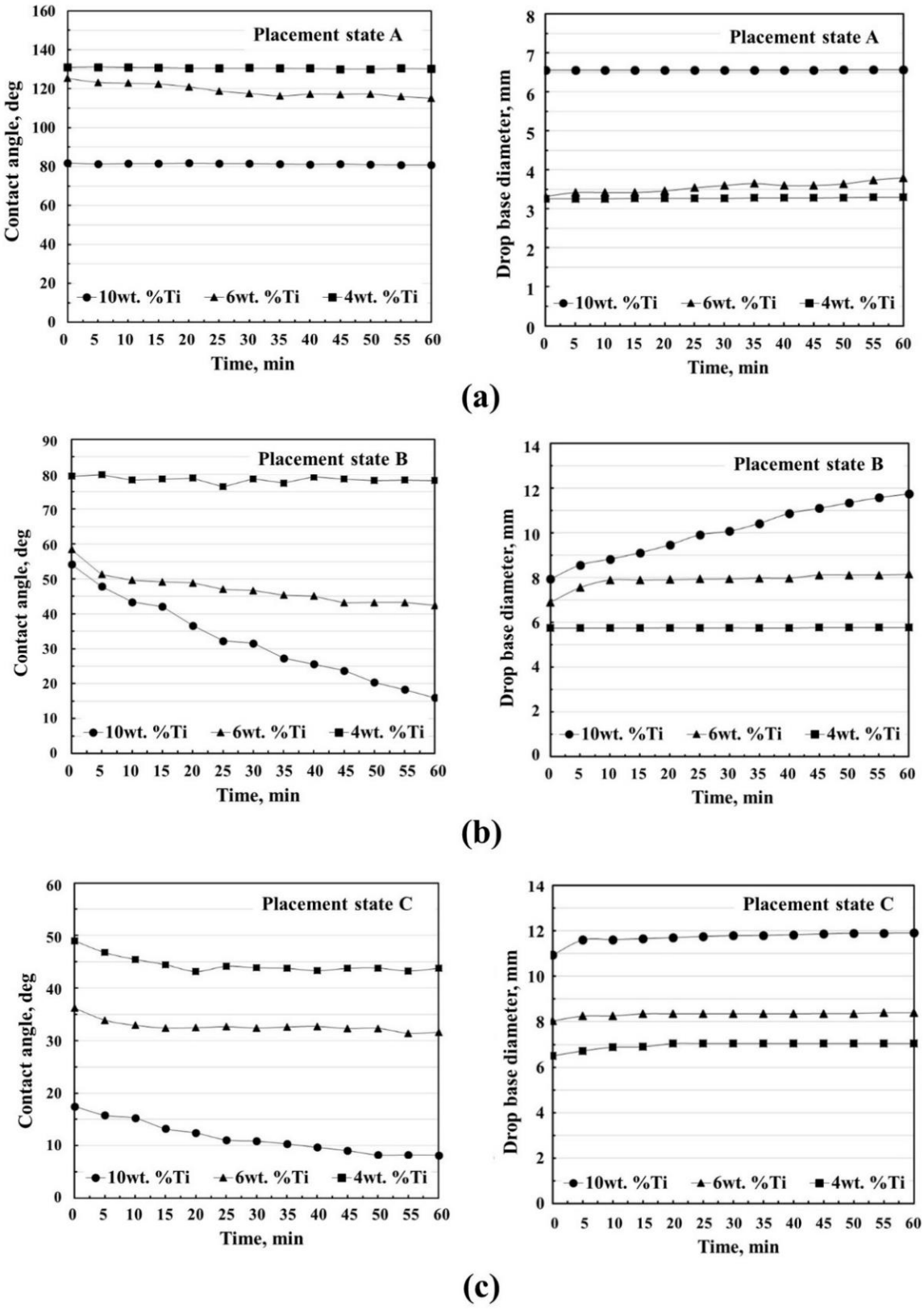

Figure 2.3.1 Variation in the contact angle and the drop base diameter for the Cu- Ti alloys on the graphite substrates with different titanium contents in three placement states at 1373 K: (a) placement state A; (b) placement state B;(c) placement state C

2.3.2 Reaction phenomena

Figure 2.3.2, Figure 2.3.3 and Figure 2.3.4 show the optical micrographs of the cross section of Cu-4 mass% Ti alloys/graphite, Cu-6 mass% Ti alloys/graphite and Cu-10 mass% Ti alloys/graphite systems in three kinds of placement states after the sessile drop experiments at 1373 K for 1 hour, respectively. A continuous reaction layer was formed at the interface between the Cu-Ti alloy and the graphite substrate in all cases (there was a gap appeared at the interface the Cu-4 mass% Ti alloys/graphite system in the placement state A and C, and it may occurred during when the samples were sectioned perpendicular to the interface). Figure 2.3.5 illustrates the influence of the Ti content in the Cu-Ti alloy on the thickness of the reaction layer in three kinds of placement states at 1373 K after 1 hour. It shows that the thickness of the reaction layer increased with the increase in Ti content, and the placement states B and C obtained much thicker layers than the placement state A at the same Ti content. It is considered that titanium has a strong affinity for carbon according to the following thermodynamic calculation:

Ti(l) + C(s) = TiC(s); $\Delta G^{\circ}_{(1373K)} = -173\text{kJ}$ [4]

$$\Delta G_{(1373K)} = \Delta G^{\circ}_{(1373K)} + RT \ln \frac{a_{(\text{TiC})}}{a_{(\text{Ti})} \cdot a_{(\text{C})}} = \begin{cases} -148\ \text{kJ} & \cdots\cdots \text{at 10mass\% Ti} \\ -143\ \text{kJ} & \cdots\cdots \text{at 6mass\% Ti} \\ -138\ \text{kJ} & \cdots\cdots \text{at 4mass\% Ti} \end{cases} \tag{2.3.1}$$

if the molten Cu-Ti alloy is considered to be an ideal solution, the value of the ΔG is calculated to be −148 kJ at 10 mass% (12.9 at. %) Ti, confirming great reactivity in this

system. What's more, when the Ti content is 6 mass % (7.81 at. %) or 4 mass % (5.24 at. %), the results of ΔG is －143 kJ or －138 kJ, respectively, also proving that the reaction can take place easily. By taking the Cu-10 mass % Ti/graphite system for instance, the backscattered electron composition (COMPO) image of the cross section and the elemental mapping in three kinds of placement states at 1373 K for 1 hour are presented in Figure 2.3.6. These figures show that the reaction layer consisted of quantities of fine granular phases in all cases (see the COMPO image), and the density of it in the placement states B and C was much higher than that in the placement state A, especially in the placement state C. The elemental mappings demonstrate that the elements of C and Ti were the main components of the interlayer in all cases. Quantitative determinations performed by spot analysis of EPMA at points 1~7 as shown in Table 2.3.1 revealed that the atomic ratio of Ti:C was approximately 1:1 in the placement state B and C, suggesting a TiC compound. But for the placement state A, the element of Ti, C and Cu existed at the interface with non-stoichiometric. This may be due to the reaction layer in this case was very thin and the fine granules was sparse, when the beam of electrons is fired at these fine granules, the surrounding substances (e.g. the Cu-Ti alloy or the graphite substrate) are also fired. Figure 2.3.7 shows the result of XRD for Cu-Ti alloy/graphite systems in three kinds of placement states after grinding the solidified Cu-Ti alloys away, the reaction layer was identified to be TiC layer in all cases. Meanwhile, many Cu-Ti intermetallic compounds, such as Cu_3Ti and Cu_4Ti_3, were also detected in the interlayer, and they existed above the TiC layers as coarse dendritic structures as shown in Figure 2.3.2, Figure 2.3.3 and Figure 2.3.4. On the other hand, it is clearly observed that the initially flat and smooth surface of graphite substrates became irregular after the experiments. For this phenomenon, many studies have documented that the growth of

TiC layers depend on the partial diffusion of carbon to the side of alloys, resulting in a considerably quantity of craters [5]. In addition, the diffusion of carbon at the interface seems to be more significant at placement states B and C, due to their more irregular surface than that of placement state A as shown in Figure 2.3.4.

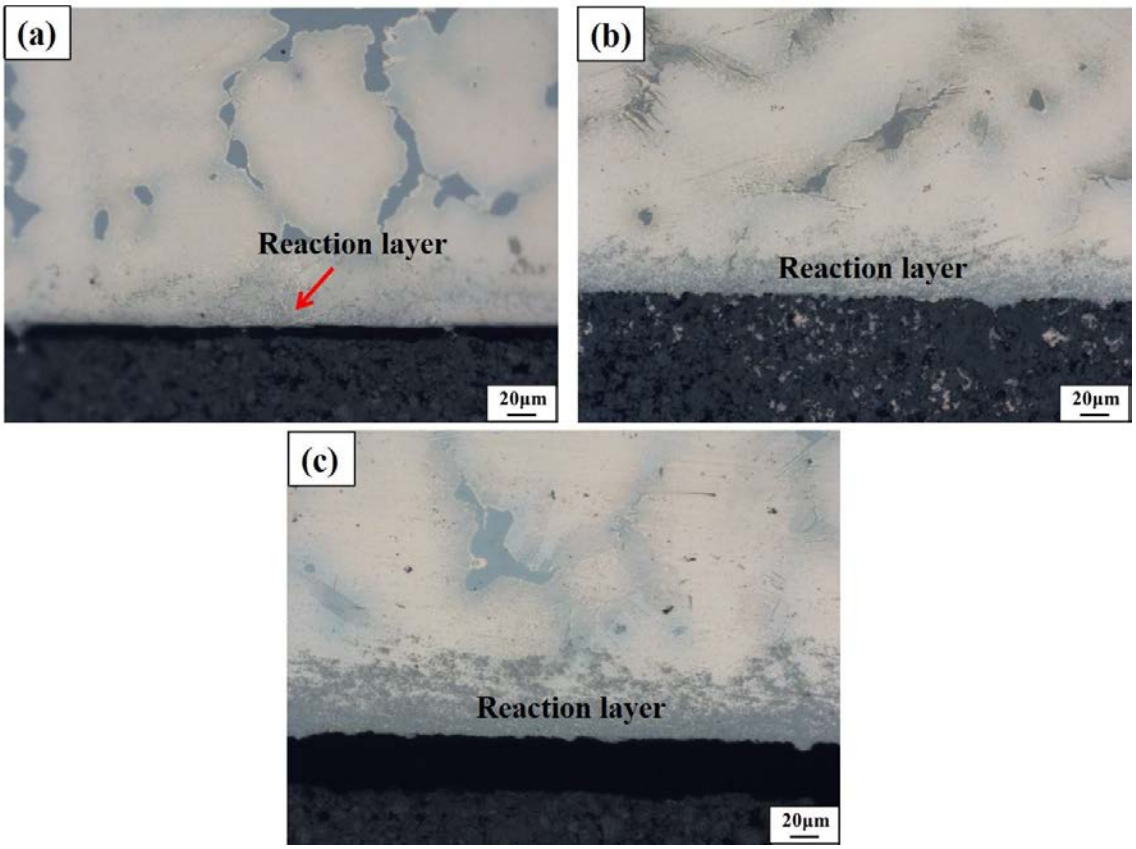

Figure 2.3.2 Optical micrographs of the cross section of Cu-4 mass% Ti alloys/graphite in three kinds of placement states after 1 hour at 1373 K (above was Cu-Ti alloy, below was graphite substrate): (a) placement state A; (b) placement state B; (c) placement state C

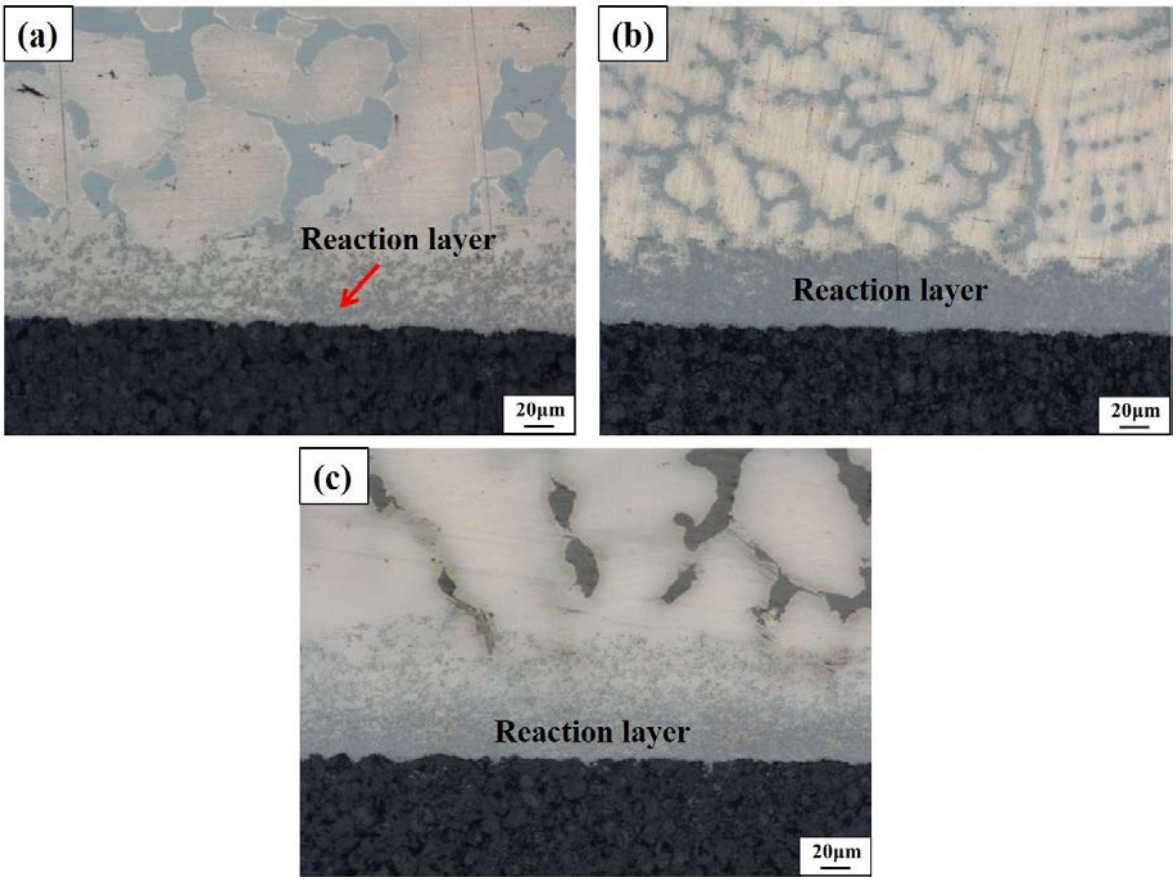

Figure 2.3.3 Optical micrographs of the cross section of Cu-6 mass% Ti alloys/graphite in three kinds of placement states after 1 hour at 1373 K (above was Cu-Ti alloy, below was graphite substrate): (a) placement state A; (b) placement state B; (c) placement state C

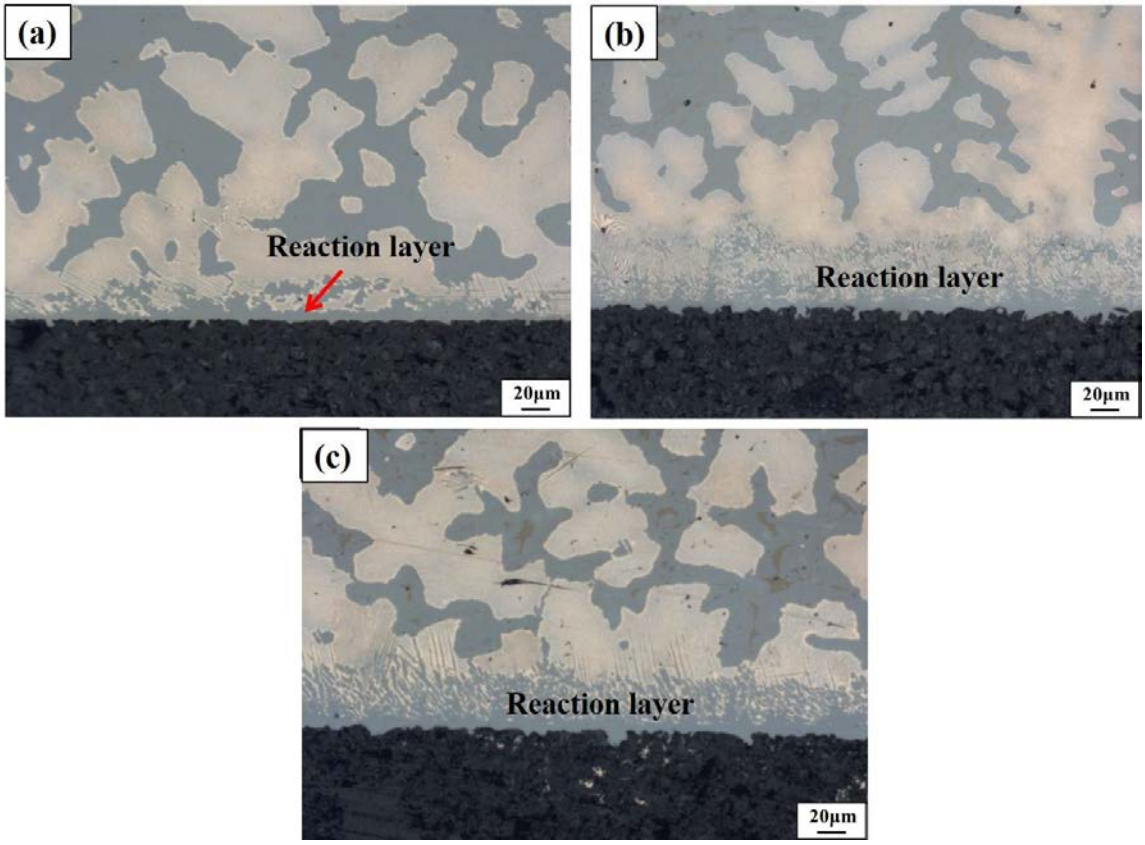

Figure 2.3.4 Optical micrographs of the cross section of Cu-10 mass% Ti alloys/graphite in three kinds of placement states after 1 hour at 1373 K (above was Cu-Ti alloy, below was graphite substrate): (a) placement state A; (b) placement state B; (c) placement state C

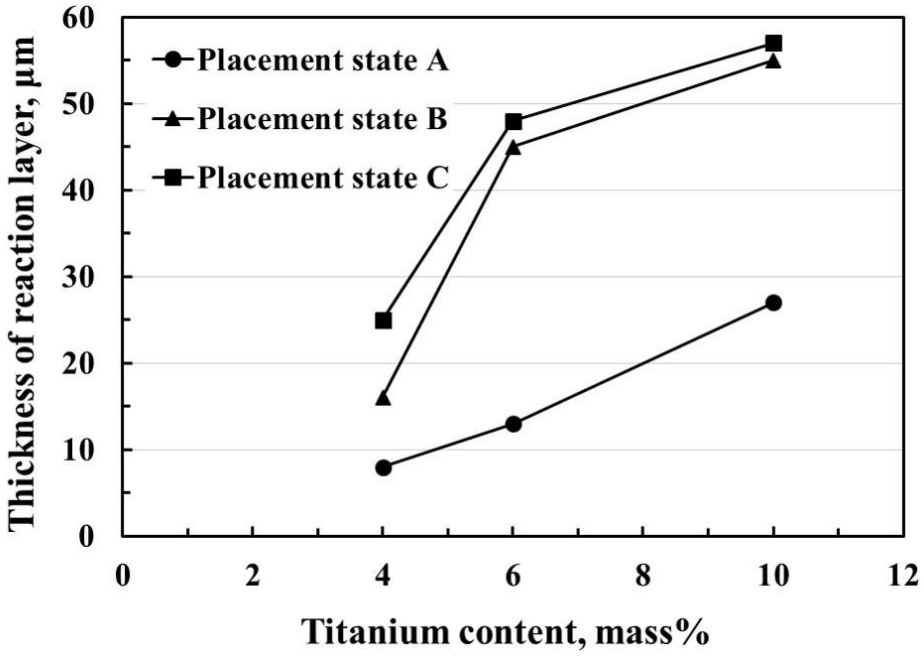

Figure 2.3.5 Influence of the Ti content in the Cu-Ti alloy on the thickness of the reaction layer in three kinds of placement states at 1373 K after 1 hour

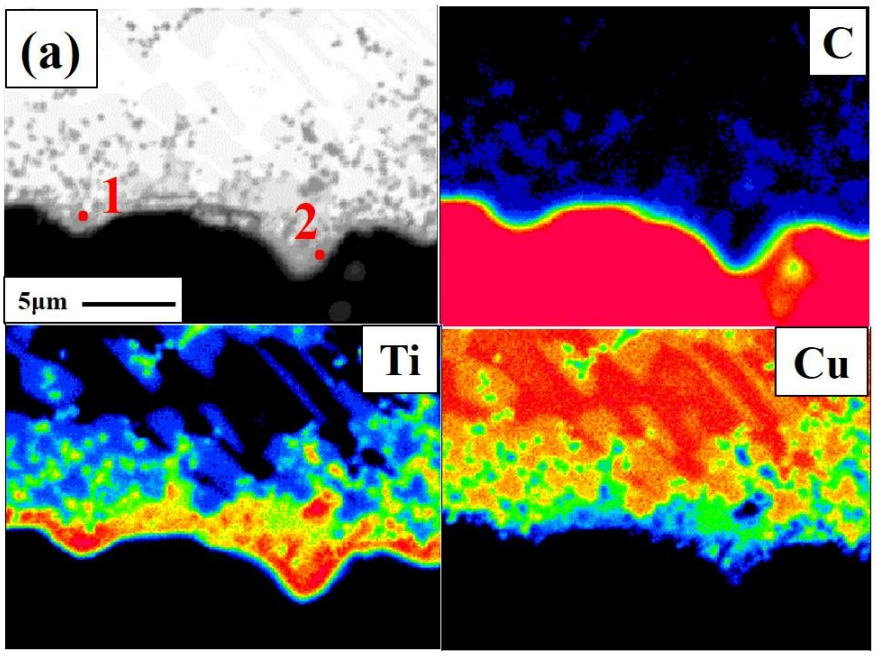

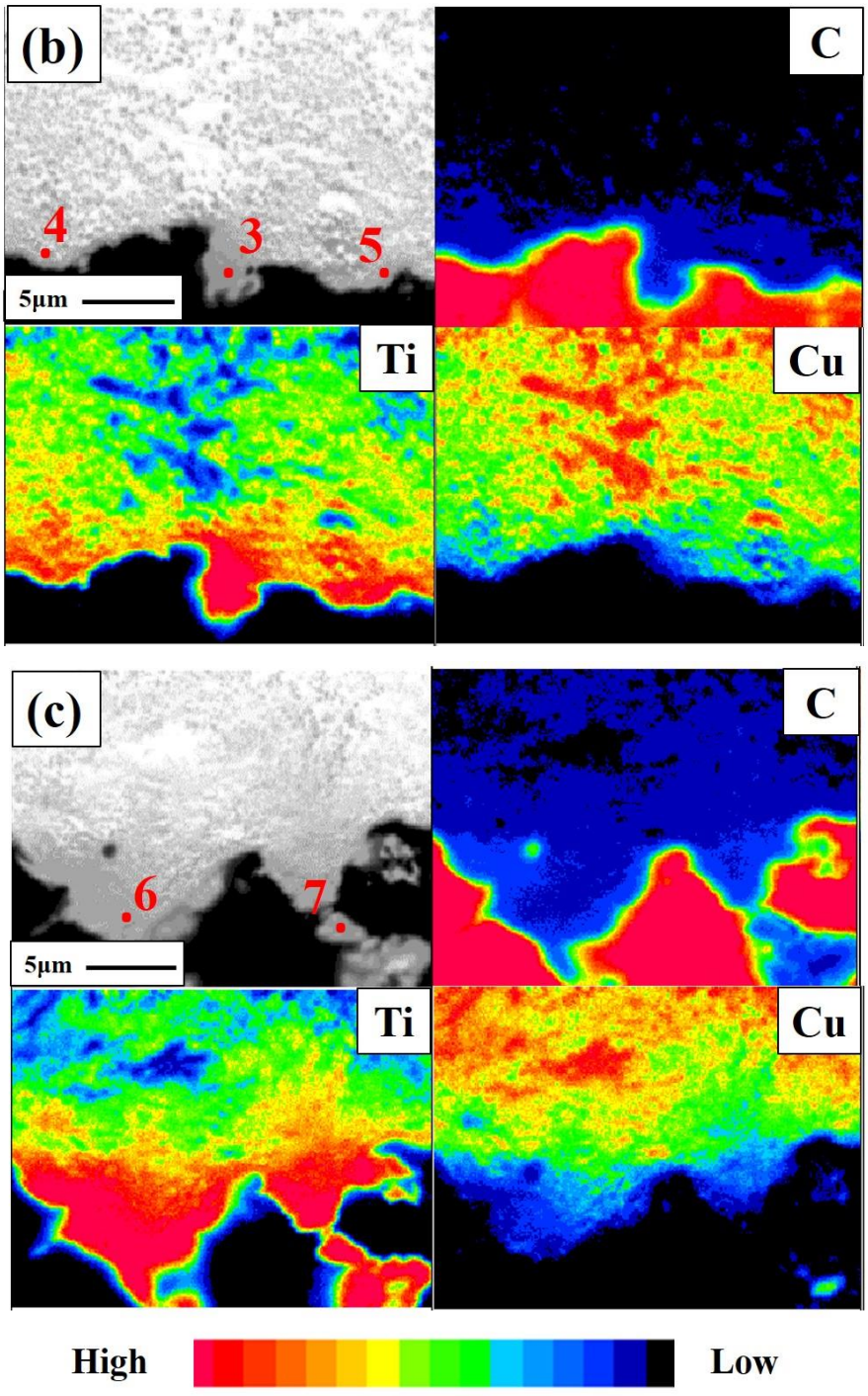

Figure 2.3.6 COMPO images of the cross section and elemental mapping of Cu-10 mass% Ti alloys/graphite in three kinds of placement state at 1373 K after 1 hour: (a) placement state A; (b) placement state B; (c) placement state C

Table 2.3.1. EPMA spot analysis results at the interface region of Cu-10 mass% Ti alloys/graphite system in three kinds of placement state

Placement state	Point	C (at. %)	Ti (at. %)	Cu (at. %)
A	1	42.9	39.2	17.9
	2	55.2	35.9	8.9
B	3	46.7	46.8	6.5
	4	45.6	44.6	9.8
	5	48.8	43.0	8.2
C	6	45.5	45.4	9.1
	7	46.7	46.8	6.5

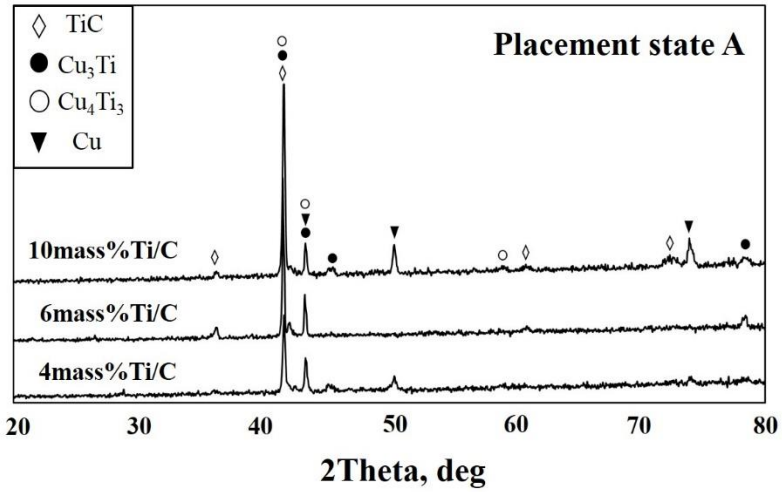

(a)

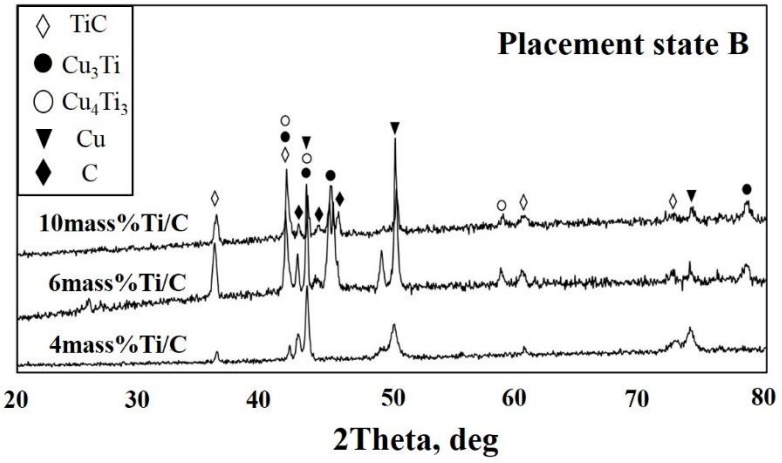

(b)

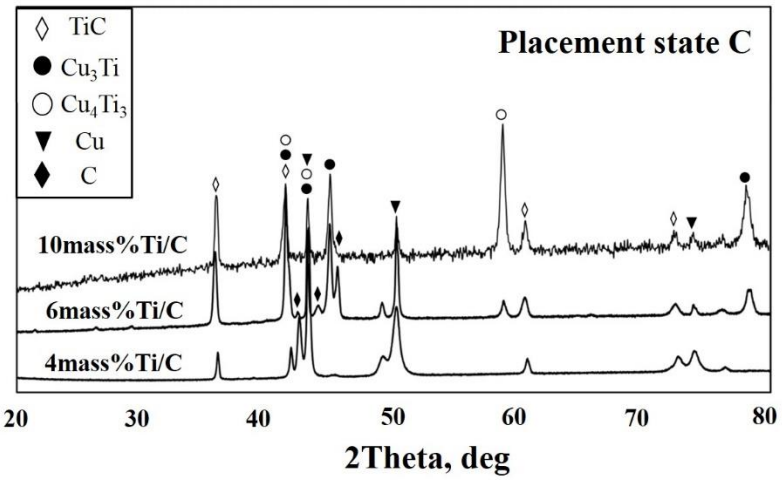

(c)

Figure 2.3.7 XRD patterns of the interface of Cu-Ti alloys/graphite system in in three kinds of placement state

2.4 Discussion

As mentioned above, with increasing titanium content from 4 to 10 mass %, the wettability of the Cu-Ti alloy/graphite systems improved, and the contact angles were markedly different across this range in this study. From the viewpoint of dynamics, the mechanism of wetting between Cu-Ti alloys and graphite substrates was confirmed by some researchers [1, 3], and it consisted of three stages: Firstly, Ti atoms diffused from the liquid Cu-Ti alloys and then moved to the interface; Secondly, Ti atoms were involved in the reaction and resulted in the formation of TiC; Finally, after forming a continuous reaction layer, the subsequent wetting was determined by the Cu-Ti melt on the TiC reaction layer. Here, the wettability between Cu-10 mass% Ti alloys and TiC substrates in the placement state A was investigated, and the result showed that once the liquid Cu-10 mass% Ti alloy occurred, it spread on the TiC substrate rapidly, and the contact angle was finally stabilized at 35°, revealing the great wetting between the Cu-10 mass% Ti alloy and TiC. Therefore, since the increase of the Ti content from 4 to 10 mass % increased the amount of TiC at the initial stage, the wettability of 10 mass % Ti alloys was better than that of 6 mass % Ti and 4 mass % Ti in subsequent wetting process, which led to markedly different contact angles.

However, the most puzzling aspect of this experiment was the different wetting behavior of the three kinds of placement states at the same titanium content, wherein the best wettability was obtained in the placement state C, followed by the placement state B, and the placement state A. It was considered that this phenomenon might relate to the different melting process of the Cu-Ti alloy by changing the placement state. Based on

the binary phase diagram of Cu-Ti [6] shown in Figure 2.4.1, we attempt to interpret the whole wetting process for each placement state by taking the Cu-10 mass % Ti/graphite system for instance. Figure 2.4.2 shows the supposed schematic wetting behavior of each placement state, which was drawn depending on the phenomenon during the experiments.

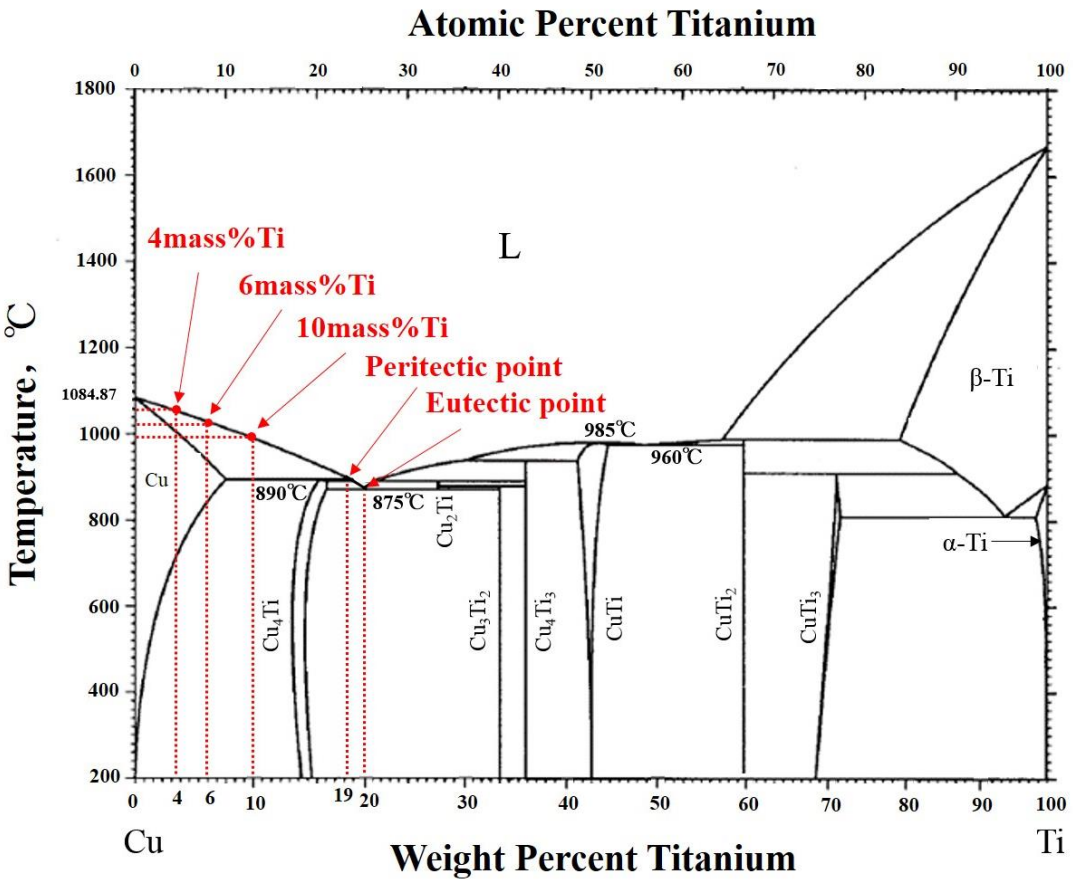

Figure 2.4.1 Binary phase diagram of Cu-Ti [6]

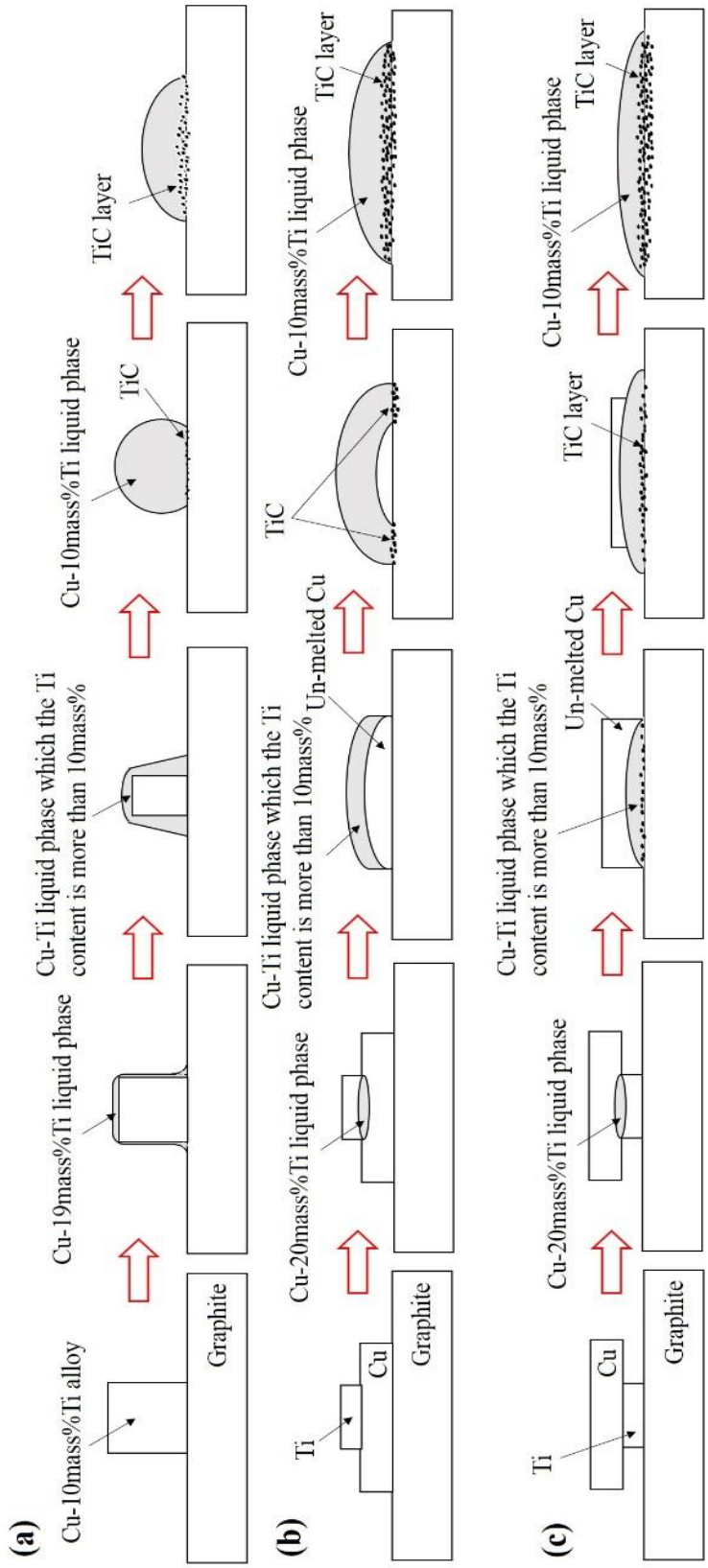

Figure 2.4.2 Schematic diagrams of wetting behavior of Cu-10mass%Ti alloys/graphite system: (a) placement state A; (b) placement state B; (c) placement state C

(1) For the wetting behavior of the placement state A shown in Figure 2.4.2 (a), when the heating temperature reached to the peritectic reaction temperature of 1163 K (890 ℃), the prior Cu-Ti liquid phase began to occur on the surface of the Cu-Ti alloy, and the content of molten Ti in this liquid phase was approximately 19 mass % which was equal to the Ti content at the right end of the 1163 K (890 ℃) isotherm. As the heating temperature was increased, the Cu-Ti liquid phase increased (much of it occurred around the Cu-Ti alloy and flowed toward the bottom), while the Ti content in the Cu-Ti liquid phase decreased along the liquidus and eventually became 10 mass % when the heating temperature reached above the liquidus of approximately 1273 K (1000 ℃). During this peritectic melting process, the Cu-Ti alloys melted incongruently, and the Ti content in the Cu-Ti liquid phase decreased from 19 to 10 mass %.

(2) For the wetting behavior of the placement state B shown in Figure 2.4.2 (b), with the increase in heating temperature, the inter-diffusion of atoms would take place at the contact surface between Cu and Ti, and it seems that the Ti atoms diffusing into the Cu side are faster than the Cu atoms diffusing into the Ti side according to Yoshiaki et al. [7] The total diffusion at the contact surface can be considered as the diffusion of Ti toward/in Cu. Therefore, the prior Cu-Ti liquid phase would occur at the eutectic point of 1148 K (875 ℃), which is close to pure Cu phase in the Cu-Ti phase diagram shown in Figure 2.3.1. When the heating temperature reached above 1148 K (875 ℃), the Cu-Ti liquid phase began to occur and the amount of it increased gradually by consuming the solid phase of Cu and Ti. The content of molten Ti in the Cu-Ti liquid phase remained at 20 mass % approximately which was equal to the Ti content of eutectic point in this stage. When all of the solid phase of Ti melted into the Cu-Ti liquid phase, part of unmelted solid phase of Cu still existed, and this part of Cu would be encircled and consumed by

the Cu-Ti liquid phase in the form of a droplet shape because of the surface tension effect of the Cu-Ti liquid phase. In this process, the contact area of the liquid phase with the graphite substrate increased continuously, and the content of Ti in the Cu-Ti liquid phase decreased along the liquidus, till all of the solid phase of Cu melted and formed a homogeneous Cu-Ti liquid phase with 10 mass % Ti. According to many studies, the increase of Ti content promotes the formation of more TiC and thus improves the wettability [9, 11, 16], so until the heating temperature reaching to 1373 K (1100 ℃), the molten Ti which was more than 10 mass % in the Cu-Ti liquid phase had begun to react with the graphite substrate to form the TiC layer at the interface. For this reason, the wettability of the placement state B was improved considerably as compared with the placement state A.

(3) For the wetting behavior of the placement state C shown in Figure 2.4.2 (c), the formation process of the Cu-Ti liquid phase was similar to that of the placement state B. However, since the solid phase of Cu was placed on the top, the generated Cu-Ti liquid would be affected by a certain pressure that came from the upper un-melted copper and spread on the surface of the graphite widely, leading to a larger contact area between the liquid phase and the graphite substrate as compared with that of the placement states A and B. Besides, the upper un-melted copper also provided protection of the molten Ti against the oxidation since it was difficult to avoid the oxidation of Ti even in a high vacuum or a well-controlled atmosphere. Thus, there were more molten Ti reacting with the graphite substrate, which contributed to the best wettability for the placement state C.

Additionally, in the placement states B and C, the melting processes of the Cu-4 mass % Ti and Cu-6 mass % Ti alloys were similar to that of the Cu-10 mass % Ti alloy. However, concerning to the placement state A, these alloys show different melting process with the

Cu-10 mass % Ti alloy. Heating of these alloys not only brought the Ti back into Cu solid solution, but melting of these alloys also resulted in lower content of Ti throughout the whole melting process, producing an even lower content of Ti compared to the placement states B and C. This was, at least in part, why the wetting results were so different for the Cu-4 mass % Ti and Cu-6 mass % Ti alloys in the placement state A compared to the placement states B and C.

Based on the above consideration, it was concluded that the difference of wetting behavior of the three kinds of the placement states was essentially attributed to the contact area of the generated Cu-Ti liquid phase with the graphite substrate, as well as the actual content of the molten Ti in the generated Cu-Ti liquid phase during the heating process.

Figure 2.4.3 presents the representative photographs of the wetting process of the Cu-10 mass % Ti alloy/graphite system for the three kinds of placement states, and the samples were immediately cooled to the room temperature when the temperature reached to 1273 K (1000 ℃) (the placement state A) and 1223 K (950 ℃) (the placement states B and C), respectively. It can be seen that for the placement state A (Figure 2.4.3(a)), the prior Cu-Ti liquid phase began to occur on the surface of the solid Cu-Ti alloy at approximately 1188 K (915 ℃) (because of the temperature differential between the inside and outside of the furnace, the liquid phase appearance temperature could not be ideally in agreement with the peritectic reaction temperature of 1163 K (890 ℃) as shown in the Cu-Ti binary phase diagram, and the real temperature of the sample was lower than the indicated temperature. The same goes for the placement states B and C), then melted toward the inside as the heating temperature continued to rise until a complete Cu-Ti droplet formed at approximately 1273 K (1000 ℃). For the placement state B (Figure 2.4.3(b)), the prior Cu-Ti liquid phase occurred at the contact surface between Cu

and Ti at approximately 1173 K (900 ℃), and the amount of it increased gradually by consuming the solid phase of Cu and Ti with the increase in temperature. When reaching to approximately 1223 K (950 ℃), the upper seemed to have melted completely and encircled the un-melted Cu in the form of a droplet shape. After sectioning this sample and observing the cross-sectional optical microstructure at the left edge (Figure 2.4.4(a)), all of the solid Ti have already melted into the Cu-Ti liquid phase, and the outer radii of the Cu-Ti liquid phase moved much faster than the inner area toward the side of Cu due to the surface tension effect. It was expected that this part of Cu-Ti liquid phase would be preferentially in contact with the graphite substrate and then reacts with the graphite substrate to form the TiC layer as the heating temperature continued to rise. The results of the EPMA qualitative line scans across the interface of this sample are shown in Figure 2.4.4(b). According to this, approximately 20 mass % Ti existing in the Cu-Ti liquid phase was equal to the Ti content of eutectic point, which corresponded to the presumption mentioned above. For the placement state C (Figure 2.4.3(c)), the Cu-Ti liquid phase in the placement state C began to occur at approximately 1173 K (900 ℃), similar to the placement state B, and then was rapidly weighed down by the un-melted Cu and spread on the surface of the graphite during the heating process. When the wetting sample was cooled from 1223 K (950 ℃) to the room temperature, the upper melt was not detached from the graphite substrate. By observing the cross-sectional optical microstructure close to the left edge of this sample (Figure 2.4.5(a)), the generated Cu-Ti alloy phase was covered with part of the upper Cu which had not melted yet. Additionally, a small amount of TiC particles distributed at the interface between the Cu-Ti liquid phase and the graphite substrate shown in the COMPO images of the cross section (Figure 2.4.5(b)). This phenomenon was consistent with the result of thermodynamic calculation which at

1223 K (950 ℃), the ΔG of TiC was approximately －148 kJ when the Ti content in the Cu-Ti liquid phase was assumed to be 10 mass % (the actual Ti content was more than 10 mass % at this temperature). It indicated that the wetting reaction occurred easily once the Cu-Ti liquid phase was formed and in contact with the graphite substrate.

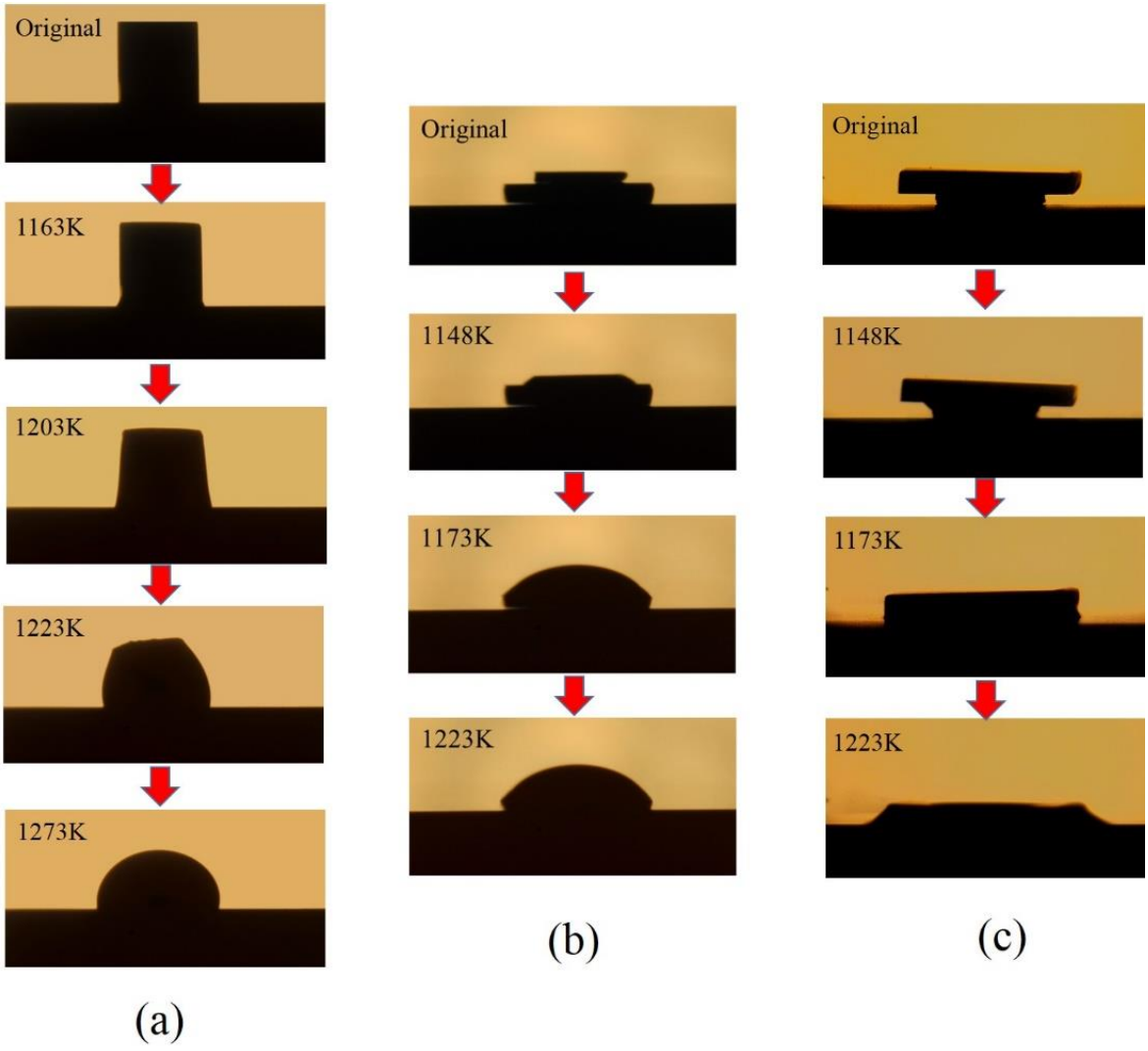

Figure 2.4.3 Representative photographs of the wetting process of the Cu-10 mass% Ti alloy/graphite system for three kinds of placement states: (a) placement state A; (b) placement state B; (c) placement state C

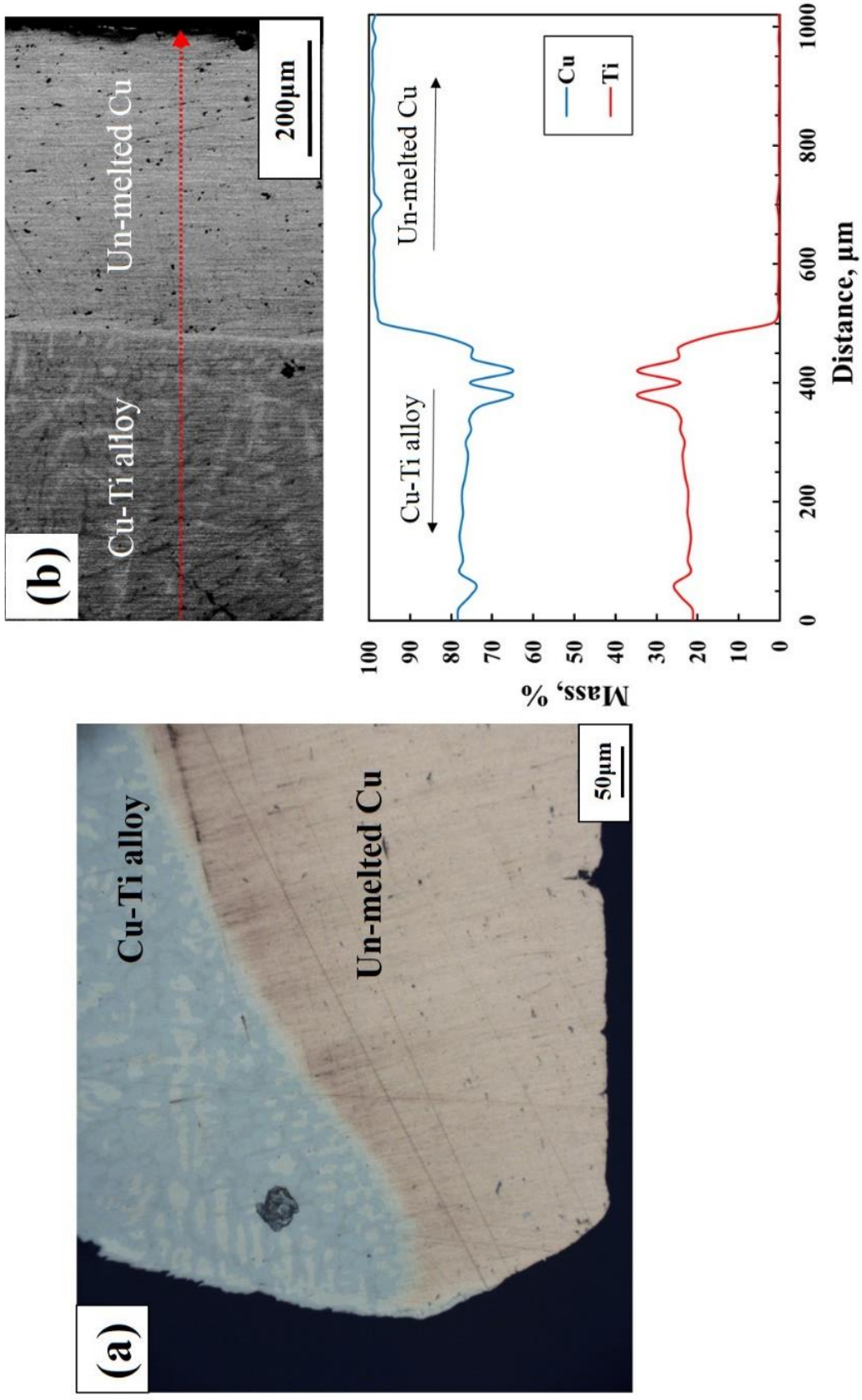

Figure 2.4.4 (a) Cross-sectional optical micrographs at the edge of the Cu-Ti alloy/un-melted Cu system and (b) EPMA qualitative line scans across the interface between the Cu-Ti alloy and the un-melted Cu in the placement state B at 1223 K with no holding time

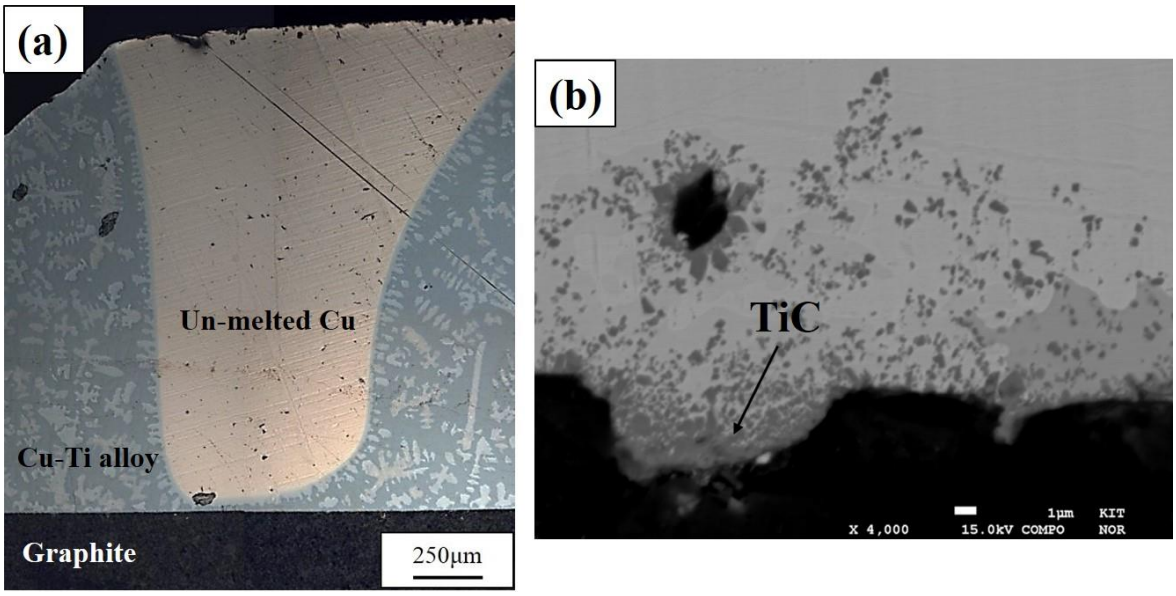

Figure 2.4.5 (a) Cross-sectional optical microstructure close to the left edge of the Cu-Ti alloy/graphite system and (b) COMPO images of the cross section of the interface between the Cu-Ti alloy and the graphite in the placement state C at 1223 K with no holding time

It is also noted that during the cooling process, some microcracks (at low Ti contents system) or even a cohesive fracture (at high Ti contents system) were often observed at the drop peripheries and propagated along the alloy-graphite interfaces shown in Figure 2.4.6, and Table 2.4.1 listed the crack forms of all nine configurations at 1373 K (1100 ℃) after 1 hour. As mentioned earlier, a mixed layer consisting of quantities of the fine TiC granules and the Cu-Ti alloy was formed at the interface in all cases. During the cooling process, due to the thermal expansion coefficient (CTE) of TiC (7.4×10^{-6} /K at room temperature [8]) and Cu-Ti alloy (16.5×10^{-6} /K and 8.4×10^{-6} /K at room temperature for Cu and Ti, respectively [9]) are larger than that of graphite substrate (2.0×10^{-6} /K at room temperature), the mixed layer would generate a much heavier degree of volume shrinkage than the graphite does. Therefore, a certain degree of thermal stress would be

generated which led to the occurrence of the microcracks at the drop peripheries. As shown in Figure 2.3.5, the thickness of the mixed layer increased with the increase in Ti content, and the placement states B and C obtained much thicker layers than the placement state A at the same Ti content. Especially for the Cu-10 mass % Ti alloys in the placement states B and C, the mixed layers were much thicker than that of other configurations, so it resulted in more volume shrinkage and thermal stress during the cooling process, which even led to a cohesive fracture. In any case, it is worth paying attention to this phenomenon in future work because these forms of cracks may seriously influence various properties of the material during the process of production and application. Using carbon fiber or granular graphite instead of the graphite substrate to reinforce the Cu-Ti alloy may be an effective way to avoid these forms of cracks.

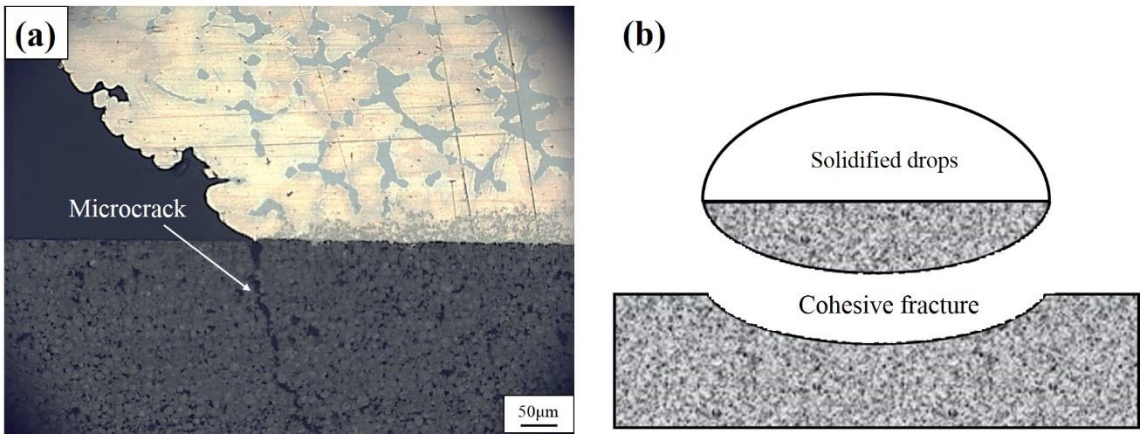

Figure 2.4.6 (a) Microcrack observed at the drop peripheries of the Cu-6 mass% Ti/graphite system in the placement state A and (b) typical cohesive fracture observed at 10 mass% Ti systems in placement states B and C at 1373 K

Table 2.4.1. The crack forms of all nine configurations at 1373K after 1 hour

Ti content	4 mass%			6 mass%			10 mass%		
Placement state	A	B	C	A	B	C	A	B	C
Crack form	M	M	M	M	M	M	M	C	C

M represents for microcrack, and C represents for cohesive fracture.

2.5 Conclusions

In this chapter, the wetting behavior of the Cu-Ti alloys with titanium contents of 4, 6, and 10 mass % on the graphite substrate was investigated at 1373 K using the sessile drop method in the three kinds of placement states which included (1) the Cu-Ti alloys were pre-alloyed from pure Cu and Ti by arc-melting before the wetting experiment and were settled on the graphite substrate (defined as the placement state A); (2) the Cu-Ti alloys were prepared in situ by directly melting the pure Ti and Cu, with the pure Ti being piled above the pure Cu on the graphite substrate during the experiment (defined as the placement state B), and (3) by directly melting the pure Cu and Ti, with the pure Cu being piled above the pure Ti on the substrate (defined as the placement state C). The following conclusions emerge from the present results:

(1) A TiC layer was formed at the interface between Cu-Ti alloy and graphite substrate in all cases. The wettability was considerably dependent on the titanium content, and it improved with increase in titanium contents from 4 to 10 mass % at the same placement state. Meanwhile, the best wettability was obtained from the placement state C in all the cases, followed by the placement state B and the placement state A.

(2) The different wetting behavior of the three kinds of placement states can be attributed to the contact area of the generated Cu-Ti liquid phase with the graphite substrate, as well as the actual content of molten Ti in the generated Cu-Ti liquid phase during the heating process.

(3) The difference in the thermal expansion coefficient between the mixed layer (consist of TiC granules and Cu-Ti alloy) and the graphite substrate would produce thermal stress, which often led to the occurrence of microcracks or even a cohesive fracture at the drop peripheries.

Figure 2.2.1, 2.3.1, 2.3.4, 2.3.5, 2.3.6, 2.4.1, 2.4.2, 2.4.3, 2.4.4, 2.4.5 and 2.4.6 used in this chapter have also been published in the following paper:

"Wettability of Cu-Ti Alloys on Graphite in Different Placement States of Copper and Titanium at 1373 K". Weiji Mao, Tomoko Yamaki, Noriko Miyoshi, Nobuya Shinozaki and Toshifumi Ogawa. Metallurgical and Materials Transactions A, 2015, 46(5): 2262-2272.

References

[1] Yang L, Shen P, Lin Q, Qiu F, Jiang Q. Wetting of porous graphite by Cu–Ti alloys at 1373K. Mater. Chem. Phys 2010; 124(1): 499-503.

[2] Mortimer D A, Nicholas M. The wetting of carbon and carbides by copper alloys. J. Mater. Sci 1973; 8(5): 640-648.

[3] Shinozaki N, Katayama Y, Umezawa Y, Wasai K. Reaction and wetting between molten Cu-Ti alloy and graphite. J. JRICu 2008; 47: 187-191.

[4] Barin I. Thermochemical Data of Pure Substances, Thermochemical Data of Pure Substances[M]. Wiley-VCH, 1997.

[5] Dahan I, Admon U, Frage N, Sariel J, Dariel M P. Diffusion in Ti/TiC multilayer coatings. Thin solid films 2000; 377: 687-693.

[6] Murray J L. The Cu− Ti (Copper-Titanium) system. Bull. Alloy Phase Diagrams 1983; 4(1): 81-95.

[7] Iijima Y, Hoshino K, Hirano K I. Diffusion of titanium in copper[J]. Metallurgical Transactions A, 1977, 8(6): 997-1001.

[8] Li X C, Stampfl J, Prinz F B. Mechanical and thermal expansion behavior of laser deposited metal matrix composites of Invar and TiC[J]. Materials Science and Engineering: A, 2000, 282(1): 86-90.

[9] Wang C, Li S, Zhang T, et al. The effect of silicon on the wettability and interfacial reaction in AlN/Cu alloy systems[J]. Materials Science and Engineering: B, 2011, 176(1): 53-59.

Chapter 3 Wettability and Interfacial Reaction between Al-Ti Alloys and Graphite

3.1 Introduction

Aluminium matrix composites reinforced by carbon materials are known as engineering materials for light-weight structural applications. However, liquid aluminum does not wet carbon materials at temperatures lower than 1173 K [1-3]. Although increasing temperature could improve it, harmful aluminum carbide would be formed at the interface simultaneously. Therefore, it is expected that alloying Al matrix with suitable reactive elements may promote favorable interfacial reactions with C, which could control the mechanical properties of the final product. Earlier investigations [4, 5] reported that addition of Ti in Al/C systems can effectively improves both the wettability and compatibility in the Al/C system because of the formation of more favorable TiC instead of undesirable Al_4C_3. However, S. Seal et al. [6, 7] questioned this view, since the formation of Al_4C_3 at the interface of Al-6mass%Ti alloy/graphite systems was observed by x-ray photoelectron spectroscopy and auger electron spectroscopy. For this inconsistent result, the effect of Ti addition into Al on wetting and interfacial reaction of Al/graphite systems at 1373 K by using sessile drop method was discussed in this chapter. At the same time, the study about the effect of the placement state of Al and Ti on wetting was also performed in order to explore one of the most favorable wetting schemes.

3.2 Experimental

3.2.1 Materials

High purity aluminium (99.99 wt. %) cubes and titanium (99.99 wt. %) foils were employed in this study and there were placed on the graphite substrates in three states which were separately defined as the placement state A (Figure 3.2.1(a)), B (Figure 3.2.1(b)) and C (Figure 3.2.1(c)). As shown in Figure 3.2.1(a), the placement of state A, from top to bottom, was settled as pre-alloyed Al-Ti/C. The pre-alloyed Al-Ti alloys with titanium content of 1 mass%, 3 mass% and 5 mass% were prepared from pure aluminium and titanium by arc-melting in a Ti (99.8 wt. %)-gettered argon (99.999% purity) atmosphere, and were machined into a small cubic sharp with 3 mm in side and weighting approximately 0.08 g for the experiment. The placement of state B and C, from top to bottom, was settled as Ti/Al/C and Al/Ti/C, respectively, shown as Figure 3.2.1(b) and 3.2.1(c). The drops of Al-Ti alloys were prepared in situ by melting the pure Ti foil and Al cube, which were directly piled on the graphite substrate. The Al cube was cut into a small cubic sharp with 3 mm in side. As for the dimensions of the Ti foil, the thickness was 0.4 mm and the square varied with different Ti contents, which were 2 mm ± 0.5 mm for 1 mass% Ti, 3.5 mm ± 0.5 mm for 3 mass% Ti and 4.8 mm ± 0.5mm for 5 mass% Ti. The Al cube and Ti foil were weighted in designed proportion which the mass ratio of Al/Ti were 99:1, 97:3 and 95:5, respectively, and the total mass was approximately 0.08 g in all cases. Before the wetting experiment, both the pre-alloyed Al-Ti alloys and the metals of Al and Ti were polished by emery papers from 400 to 2000 grit and cleaned with ethanol in order to prevent further oxidation.

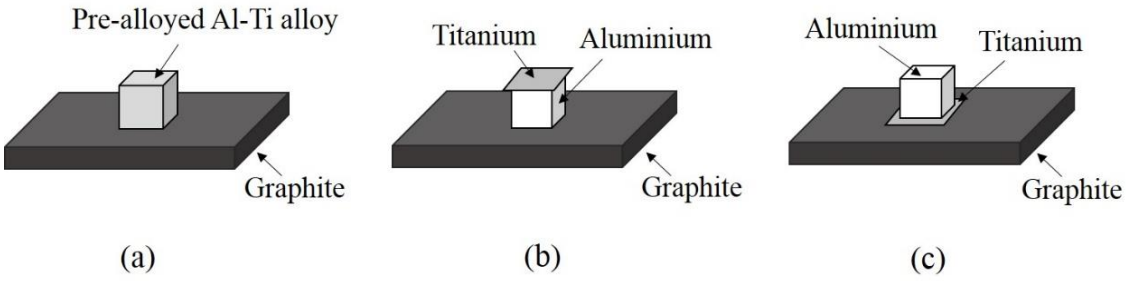

Figure 3.2.1 Schematic diagram of three kinds of placement states

3.2.2 Experimental apparatus and procedure

General experimental procedures are described in 2.2.2 section. The experimental temperature of the Al-Ti alloy/graphite systems was set to 1373 K and the holding time was 1 hour.

3.3 Results

3.3.1 Contact angle phenomena

Figure 3.3.1 shows the time variation in the contact angle for the Al-Ti alloys on the graphite substrates with different titanium contents in three placement states at 1373 K. It was note that with increasing the Ti content from 1 to 5 mass%, no apparent difference in the equilibrium contact angle was observed for all three kinds of the placement state. The values of the equilibrium contact angles at different Ti content were in the range of 17° ~ 19° for the placement state A, 18° ~ 22° for the placement state B and 14° ~17° for the placement state C, respectively. It also can be seen that at the same Ti content, the values of the equilibrium contact angle changed only slightly in different placement states,

which were in the range of 17° ~ 18° at 1 mass% Ti, 17° ~ 22° at 3 mass% Ti and 14° ~ 19° at 5 mass% Ti, respectively. In summary, good wettability in all nine configurations were observed, and their equilibrium contact angles showed no significant change. However, it did not mean that the wetting process in all nine configurations were also similar. For the placement states A and B, the values of the initial contact angle were in the range of 53° ~ 56° and 60° ~ 65° , respectively, and they decreased rapidly in the initial 10-15 minutes and then gradually stabilized in the subsequent wetting. But for the placement state C, the values of 30° ~ 40° in the initial contact angle were already small, and the decrease of the contact angle in the initial period was relatively slow.

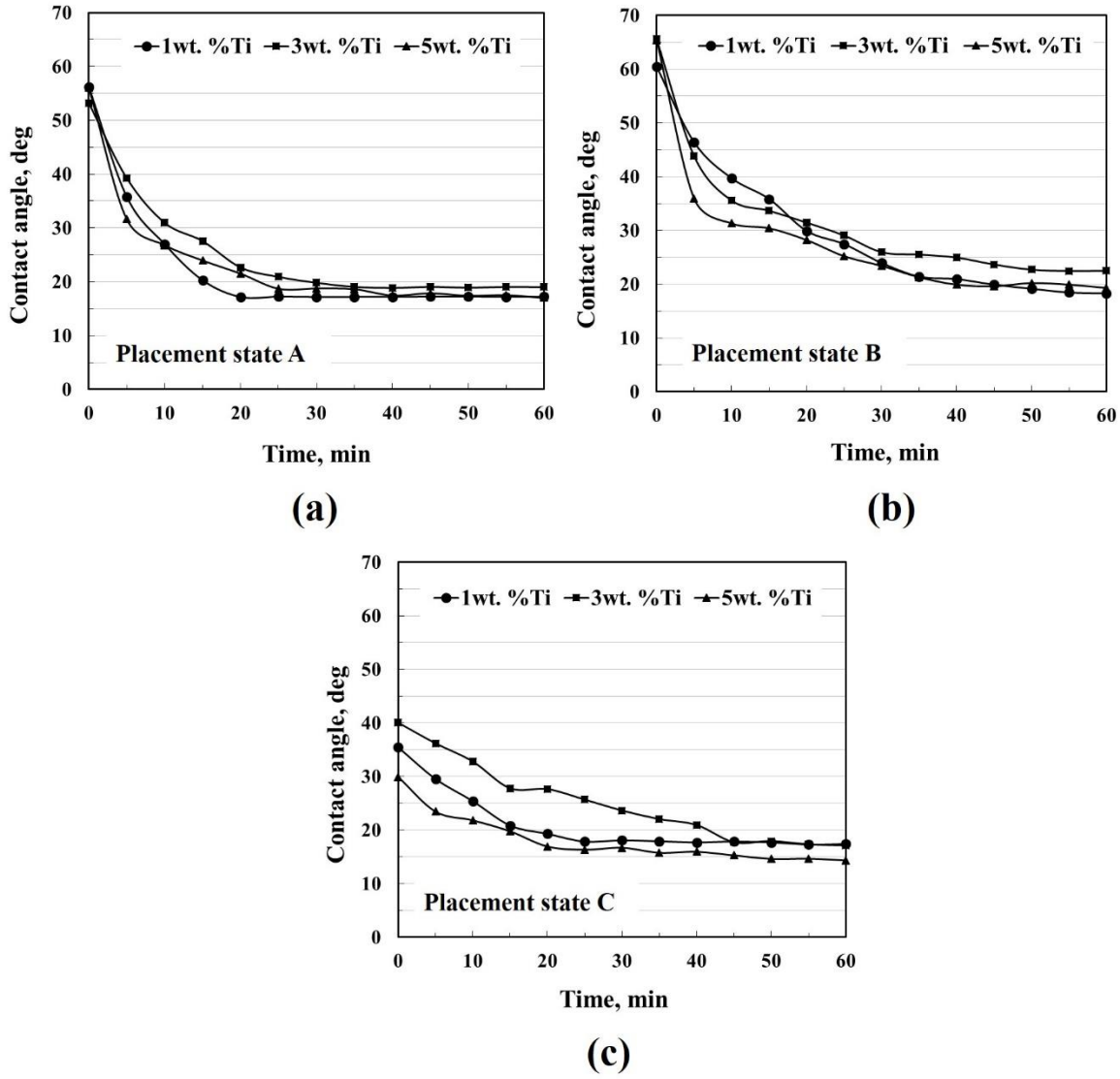

Figure 3.3.1 Variation in the contact angle for the Al-Ti alloys on the graphite substrates with different titanium contents in three placement states at 1373 K: (a) placement state A; (b) placement state B; (c) placement state C

3.3.2 Reaction phenomena

Figure 3.3.2, Figure 3.3.3 and Figure 3.3.4 show the optical micrographs of the cross section of Al-1 mass% Ti alloys/graphite, Al-3 mass% Ti alloys/graphite and Al-5 mass%

Ti alloys/graphite systems in three kinds of placement states after the experiments at 1373 K for 1 hour, respectively. In all the cases, two reaction layers were clearly observed at the interface between the graphite and the Al-Ti alloy near the center of the drop. The first layer near the Al-Ti alloy not only appeared at the interface, but also distributed into the Al-matrix. It was noted that the amount of the first layer extending into the Al-matrix increased with the increase of the Ti content, which suggested that the product in this layer was Ti-containing compound. Figure 3.3.5 presents the representative COMPO image of the cross section and the elemental mapping of the Al-1 mass % Ti alloy/graphite system in the placement state A. It was observed that the first layer consisted of massive fine granular phases, and the elements of Ti, Al and C all existed in this layer. For the second layer near the graphite, only the elements of Al and C was detected. Combined with the results of the spot analysis by EPMA at points 1, 2, 3, 4 (Table 3.3.1), the atomic ratio of Al:C at points 1 and 2 was approximately 4:3, which suggested that the second layer was Al_4C_3. Regarding to the points 3 and 4 at the first layer, the elements of Al, Ti and C existed with non-stoichiometry, but Ti and C were much richer than Al, suggesting a Ti-rich carbide layer. Due to the small thickness and density of this layer, it could not be determined whether the Al signal came from this layer or from the Al-matrix drop. Consequently, this layer could be either the coexistence of TiC and Al-matrix, or some Al, Ti ternary carbides [8]. Figure 3.3.6 shows the result of XRD for Al-Ti alloy/graphite systems in three kinds of placement states after grinding the solidified Al-Ti alloys away. Al_4C_3, and TiC were detected at the interface in all cases, and this result was consistent with the ternary phase diagram of Al-Ti-C [9]. However, by observing the COMPO image at the vicinity of the triple line (Figure 3.3.7), only Al_4C_3 layer existed in all cases.

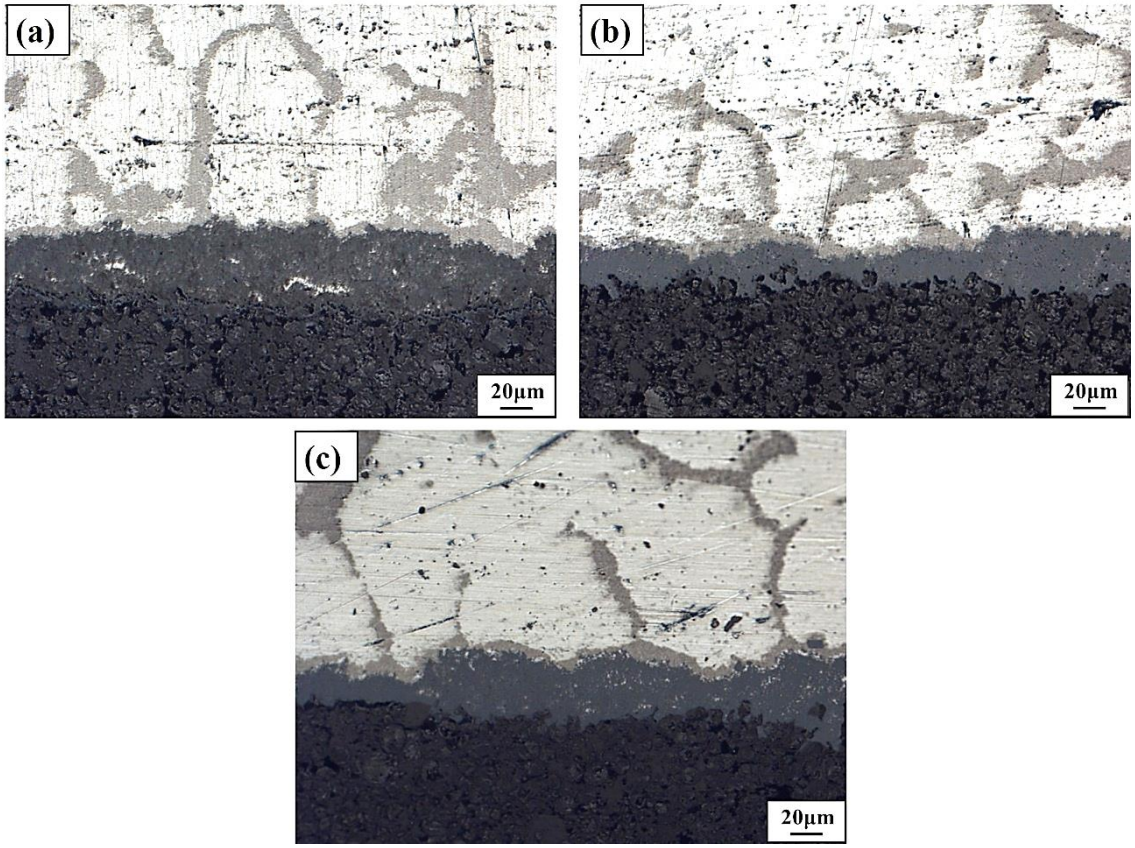

Figure 3.3.2 Optical micrographs of the cross section of Al-1 mass% Ti alloys/graphite in three kinds of placement states after 1 hour at 1373 K (above was Al-Ti alloy, below was graphite substrate): (a) placement state A; (b) placement state B; (c) placement state C

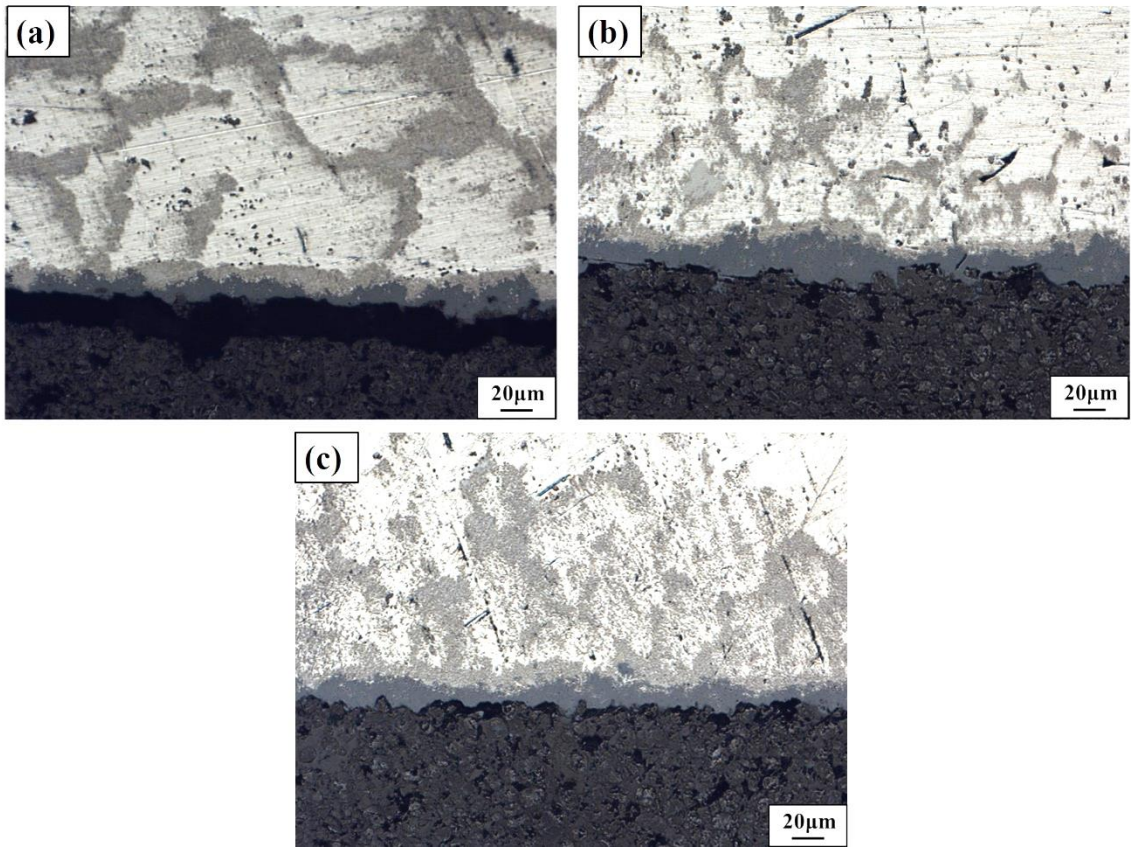

Figure 3.3.3 Optical micrographs of the cross section of Al-3 mass% Ti alloys/graphite in three kinds of placement states after 1 hour at 1373 K (above was Al-Ti alloy, below was graphite substrate): (a) placement state A; (b) placement state B; (c) placement state C

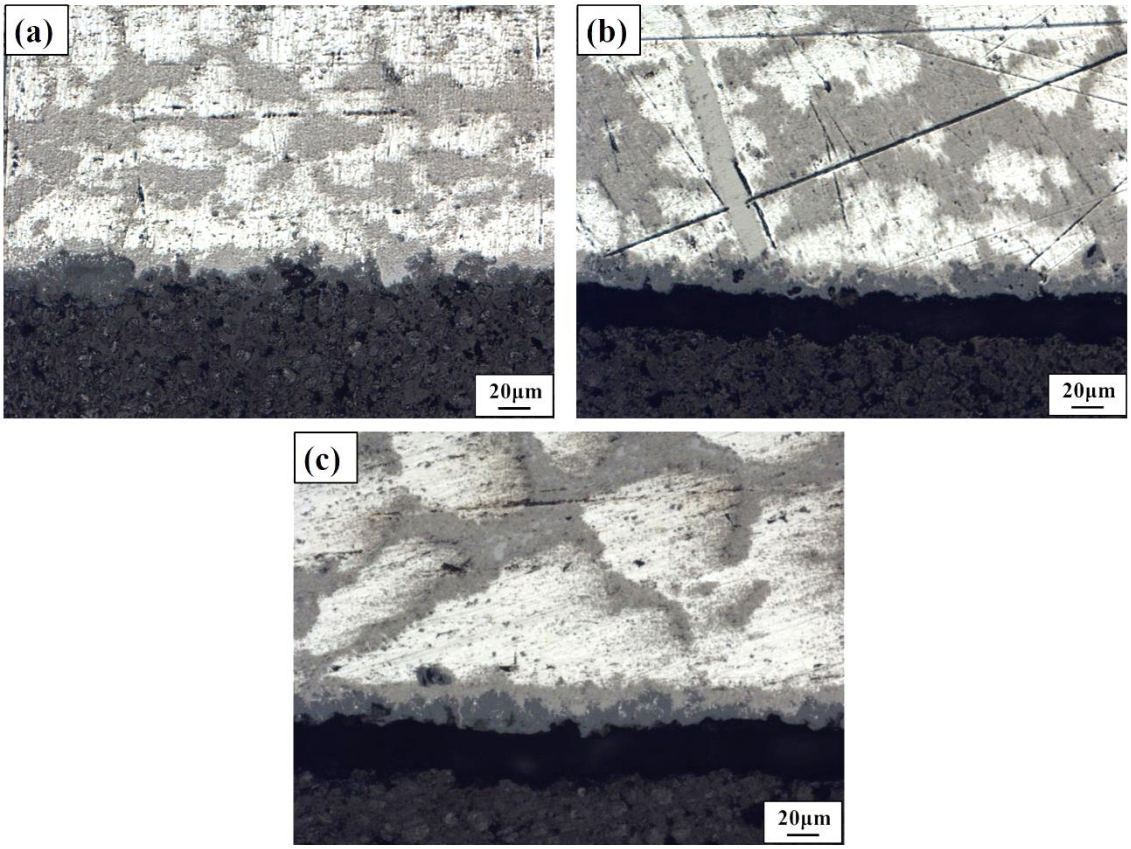

Figure 3.3.4 Optical micrographs of the cross section of Al-5 mass% Ti alloys/graphite in three kinds of placement states after 1 hour at 1373 K (above was Al-Ti alloy, below was graphite substrate): (a) placement state A; (b) placement state B; (c) placement state C

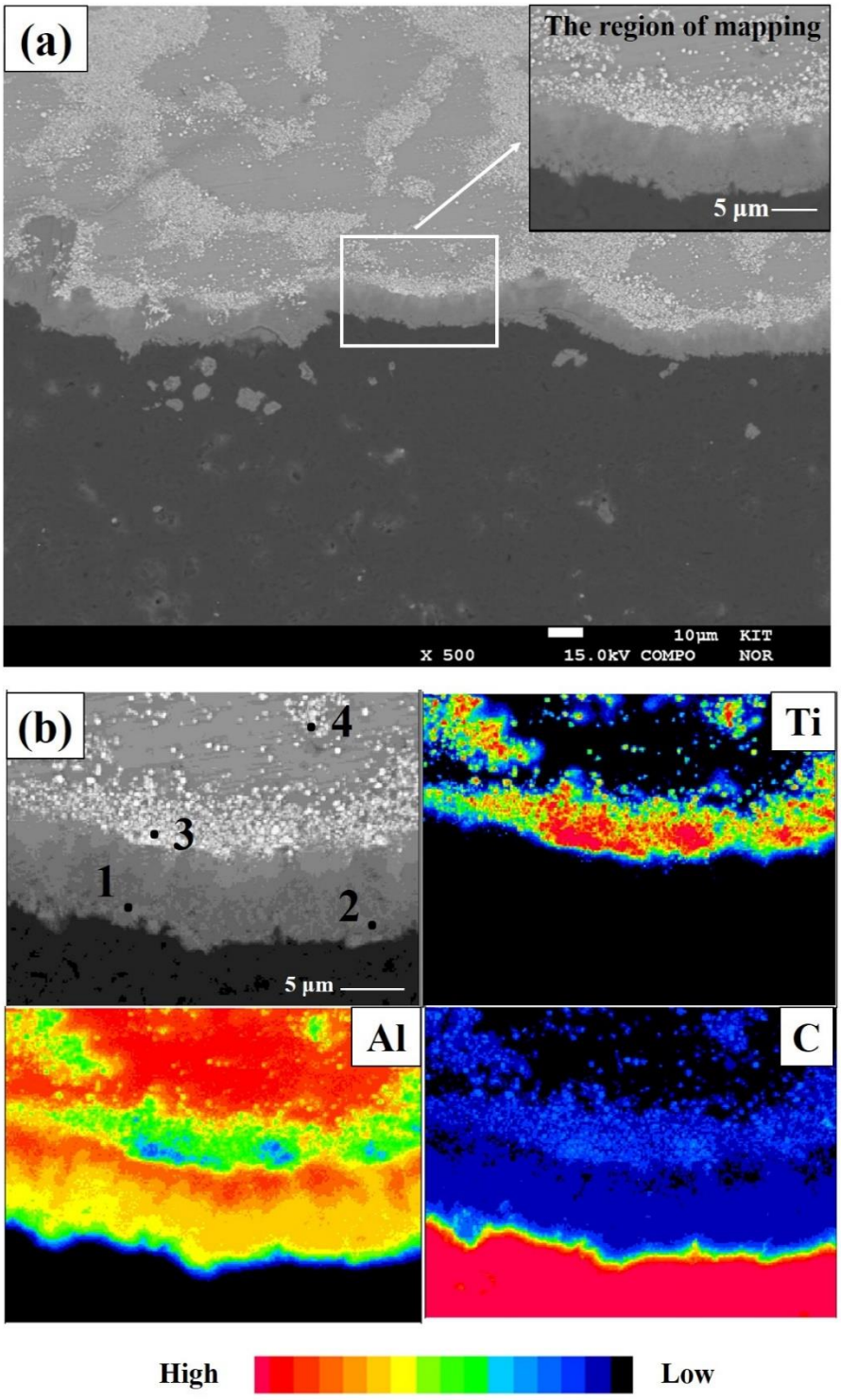

Figure 3.3.5 (a) COMPO image of the cross section and (b) elemental mapping of Al-1 mass % Ti alloy/graphite systems in the placement state A at 1373 K after 1 hour

Table 3.3.1. EPMA spot analysis results at the interface region of Al-1 mass% Ti alloys/graphite system in the placement state A

Points	C (at. %)	Ti (at. %)	Al (at. %)
1	41.9	0.2	57.9
2	43.5	—	56.5
3	47.4	41.8	10.8
4	50.0	42.7	7.3

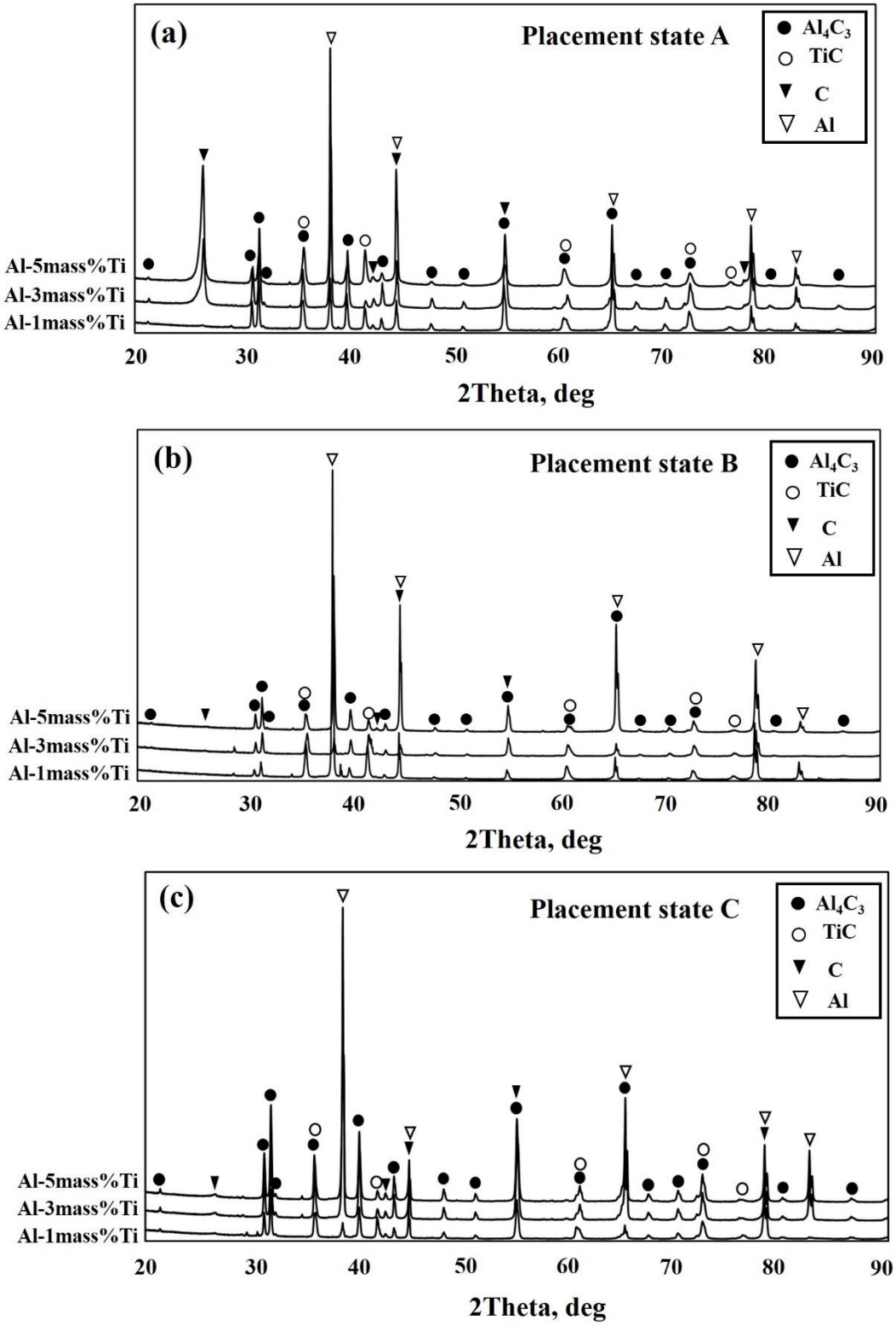

Figure 3.3.6 XRD patterns of the interface of Al-Ti alloys/graphite system in three kinds of placement state

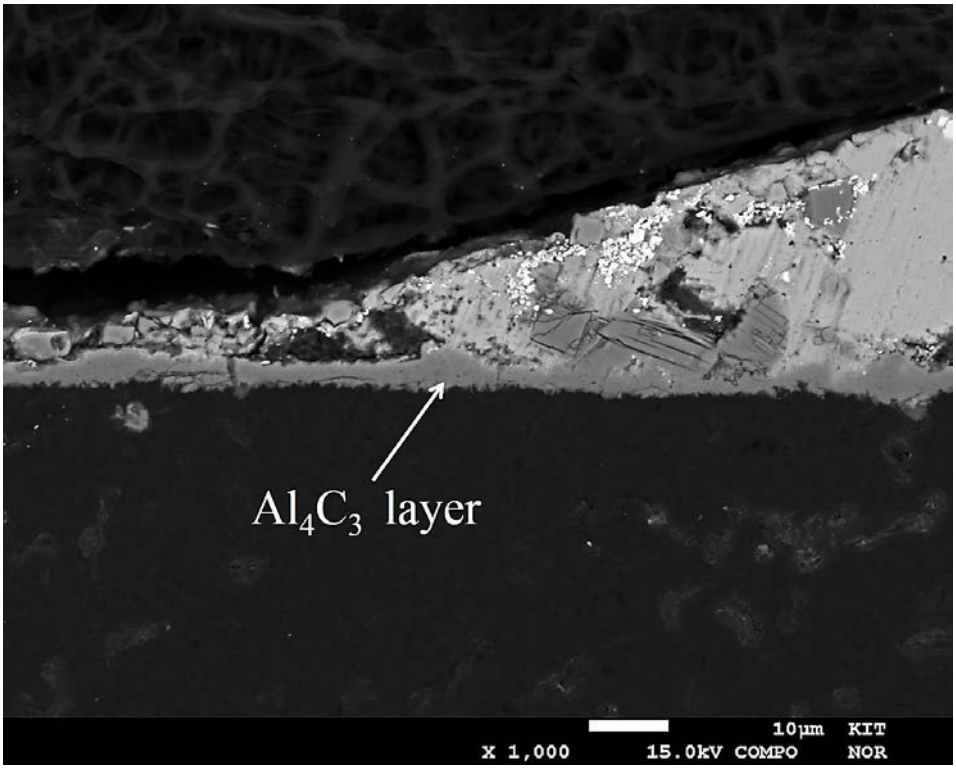

Figure 3.3.7 COMPO image of the cross section of Al-5mass%Ti alloys/graphite at the vicinity of the triple line in the placement state A after 1 hour at 1373 K (above was Al-Ti alloy, below was graphite substrate)

3.4 Discussion

3.4.1 Thermodynamic calculation

As mentioned previously, various reaction products were observed at the interface between the Al-Ti alloys and the graphite substrates in all cases. In fact, due to the complexity of the interfacial reaction in the Al-Ti alloy/C systems, the reaction products including several binary (Al_3Ti, AlTi, TiC and Al_4C_3) and ternary (Ti_2AlC and Ti_3AlC) carbides would be formed with various combinations, which primarily depended on several experimental parameters (e.g., temperature, holding time, atmosphere, and chemical composition of both the Al matrix and the alloy element) [10]. In this study, at

1373 K, Al and Ti would react with the graphite substrate to form Al_4C_3 and TiC, and the Gibbs free energy ΔG of each at different Ti content could be calculated as follows, provided that the liquid Al-Ti alloy is considered to be an ideal solution and thus the molar concentrations of Al and Ti were employed as their activities:

Ti(l) + C(s) = TiC(s) ; $\Delta G^{\circ}_{(1373K)} = -173$ kJ[11]

$$\Delta G_{(1373K)} = \Delta G^{\circ}_{(1373K)} + RT \ln \frac{a_{(\mathrm{TiC})}}{a_{(\mathrm{Ti})} \cdot a_{(\mathrm{C})}} = \begin{cases} -133 \text{ kJ} & \cdots\cdots \text{ at 5mass\% Ti} \\ -127 \text{ kJ} & \cdots\cdots \text{ at 3mass\% Ti} \\ -114 \text{ kJ} & \cdots\cdots \text{ at 1mass\% Ti} \end{cases}$$

(3.4.1)

$4Al(l) + 3C(s) = Al_4C_3(s)$; $\Delta G^{\circ}_{(1373K)} = -109$ kJ[11]

$$\Delta G_{(1373K)} = \Delta G^{\circ}_{(1373K)} + RT\, ln \frac{a_{(Al4C3)}}{a^4_{(Al)} \cdot a^3_{(C)}} = \begin{cases} -107 \text{ kJ} & \cdots\cdots \text{ at 5mass\% Ti} \\ -108 \text{ kJ} & \cdots\cdots \text{ at 3mass\% Ti} \\ -108 \text{ kJ} & \cdots\cdots \text{ at 1mass\% Ti} \end{cases}$$

(3.4.2)

It can be seen that ΔG in all cases was negative and its value for TiC was lower than that for Al_4C_3 at the same Ti content, which suggested that both TiC and Al_4C_3 could be formed at 1373 K, and TiC was readily formed at the interface than Al_4C_3. However, for the absence of AlTi and Al_3Ti at the Al matrix in this study, K.B. Lee et al. [12] and R. Mitra et al. [13] have suggested the following chemical reactions would occur in the Al-Ti-C system:

$$Al\ (l) + Ti\ (s) = AlTi\ (s) \qquad \Delta G^{\circ}_{(1373K)} = -59\ \text{kJ}^{[11]} \qquad (3.4.3)$$

$$3Al\ (l) + Ti\ (s) = Al_3Ti\ (s) \qquad \Delta G^{\circ}_{(1373K)} = -95\ \text{kJ}^{[11]} \qquad (3.4.4)$$

$$AlTi + C\ (s) = TiC(s) + Al(l) \qquad \Delta G^{\circ}_{(1373K)} = -114\ \text{kJ}^{[11]} \qquad (3.4.5)$$

$$Al_3Ti + C\ (s) = TiC(s) + 3Al(l) \qquad \Delta G^{\circ}_{(1373K)} = -78\ \text{kJ}^{[11]} \qquad (3.4.6)$$

$$3AlTi\ (s) + Al_4C_3(s) = 3TiC(s) + 7Al(l) \qquad \Delta G^{\circ}_{(1373K)} = -233\ \text{kJ}^{[11]} \qquad (3.4.7)$$

$$3Al_3Ti(s) + Al_4C_3(s) = 3TiC(s) + 13Al(l) \qquad \Delta G^{\circ}_{(1373K)} = -126\ \text{kJ}^{[11]} \qquad (3.4.8)$$

We can see that all the above reactions showed negative values of ΔG^{o} at 1373 K, which indicated once AlTi and Al_3Ti were formed in the Al matrix, they would react with C or Al_4C_3 and translated into TiC finally.

3.4.2 Effect of placement states and addition of Ti on wetting

In order to explain the different value of the initial contact angle in three kinds of placement state, the representative photographs of the wetting process of the Al-3 mass % Ti alloy/graphite system from room temperature to 1373 K for the three kinds of placement states is presented in Figure 3.4.1. The pre-alloys Al-Ti alloys in the placement state A (Figure 3.4.1(a)) melted into a spherical liquid drop completely when the heating temperature reached 1223 K. According to the binary phase diagram of Al-Ti [14] shown in Figure 3.4.2, a certain amount of Al_3Ti phase could exist in the Al-Ti liquid drop and the content of Ti in this liquid drop was less than 3 mass% at this temperature. Since both the Al and Ti were prone to be oxidized and an oxide film always formed on the liquid drop surface [15], the Al-Ti liquid phase could not react with the graphite substrate despite

of the reactivity of Al and Ti, which resulted in the non-wetting contact angle. As the heating temperature continued to increase to 1373 K, the liquid components would change along the liquidus, meanwhile the contact angle reduced by the reaction between Al or Ti and graphite, due to the de-oxidation of the liquid drop at high temperature [16]. Therefore, during the whole process till reaching 1373 K, the drop base diameter in the placement state A first decreased, then increased gradually. For the placement state B (Figure 3.4.1(b)), with increasing the heating temperature, the Al cube first melted according to the binary phase diagram of Al-Ti, then the Ti foil piled on the Al cube gradually melted into the Al liquid phase and the content of Ti in the liquid drop increased along the liquidus. At 1223 K, although all of the Ti foil did not melted into the liquid phase, a roughly spherical liquid drop was formed on the graphite, and the non-wetting contact angle, which also resulted from the formation of the oxide film, was similar to that in the placement state A. As the heating temperature continued to increase to 1373 K, all of the un-melted Ti foil, which might float on the drop surface, then melted into the liquid drop gradually, and the subsequent change of both the contact angle and the drop base diameter were nearly consistent with that in the placement state A. However, the melting process of the Al-Ti alloys in the placement state C was different from that in both the placement states A and B as shown in Figure 3.4.1(c). When the Ti foil placed under the Al cube began to melt into the generated Al liquid phase as the heating temperature was increased, it would be affected by a certain pressure that came from the upper liquid drop. Furthermore, the upper Al liquid phase also provided protection of the liquid Ti against the oxidation, which might lead to the formation of TiC and contribute to a lower contact angle in the early melting stage. Therefore, it was found that when the heating temperature reached 1223 K, unlike the change of the drop in the place states A

and B, the drop base diameter in the placement state C remained as previous length, and as the heating temperature continued to increase to 1373 K, the contact angle decreased to a lower value in comparison with the placement states A and B.

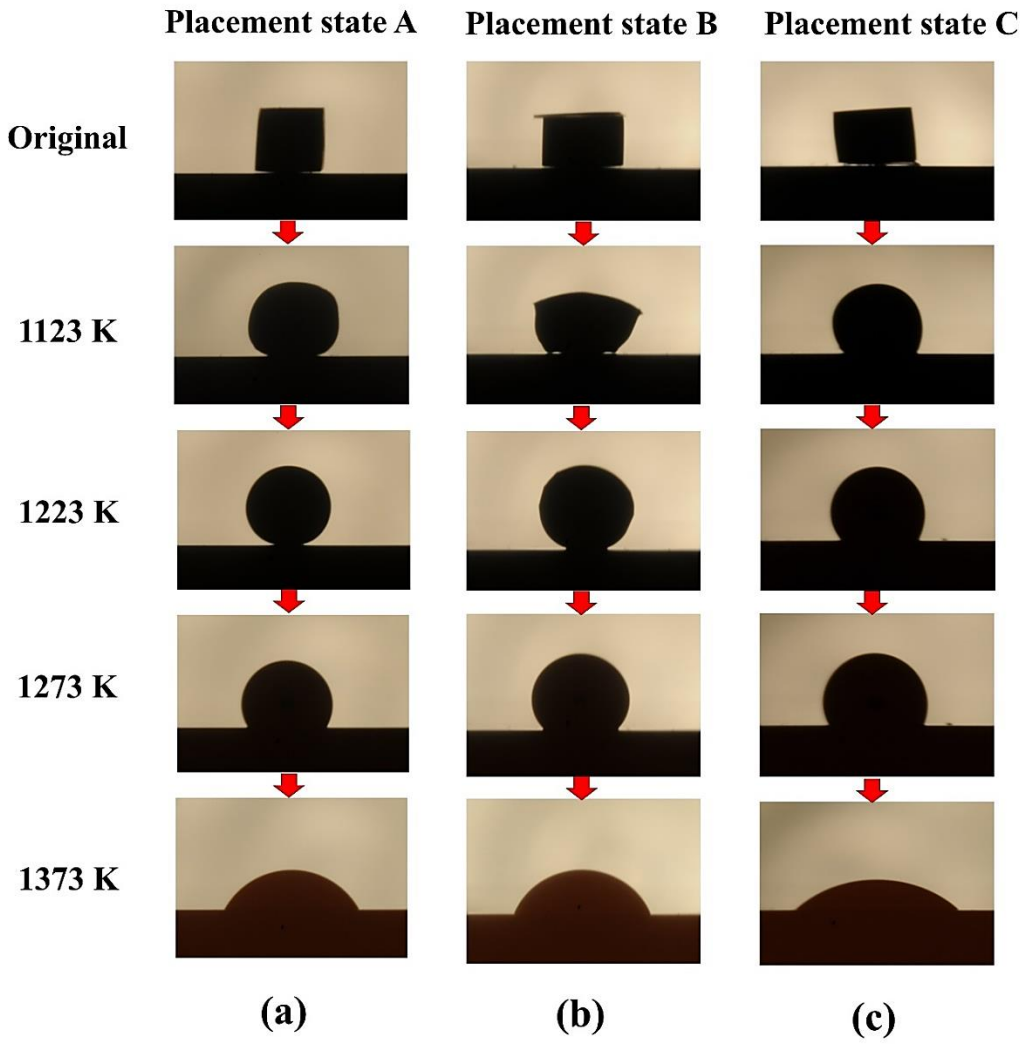

Figure 3.4.1 Representative photographs of the wetting process of the Al-3 mass % Ti alloy/graphite system from room temperature to 1373 K for the three kinds of placement states

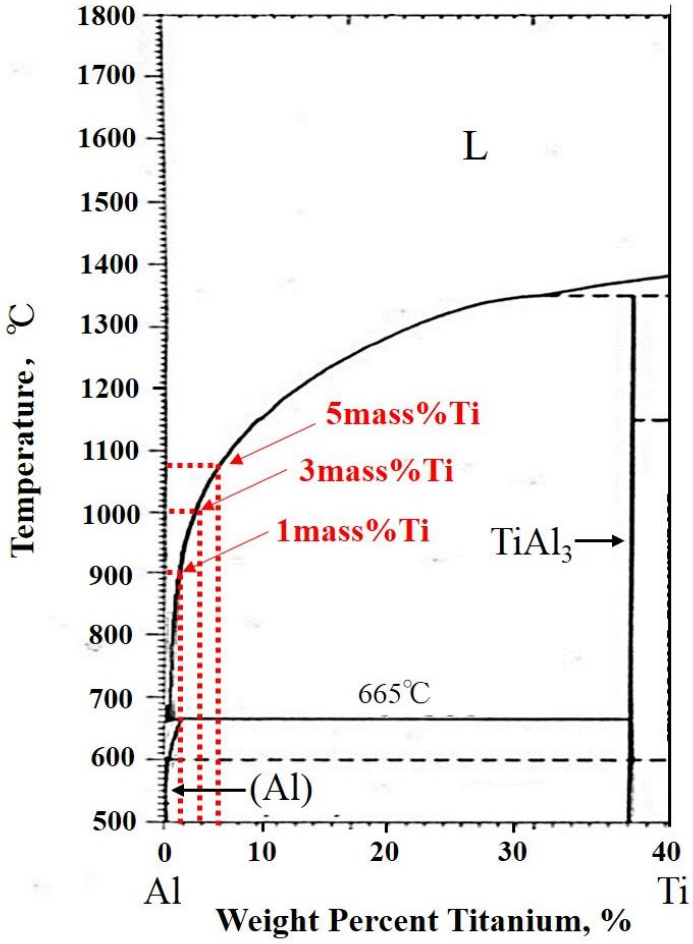

Figure 3.4.2 Binary phase diagram of Al-Ti [11]

Nevertheless, the values of the final contact angle were not significantly altered in all nine configurations in spite of the different values of the initial contact angle. For the Al-Ti-C system, it was expected that the addition of Ti on Al could result in the formation of metallic-like titanium carbide (e.g. TiC) at the interface, which appeared to be more wettable by liquid metal than covalent carbides (e.g. Al_4C_3)[17]. In this study, TiC was indeed detected at the interface for all the nine configurations, but at the same time, the formation of Al_4C_3 also occurred. Because only Al_4C_3 existed at the vicinity of the triple

line even at 5 mass %Ti, the wetting process was not affected by the formation of TiC in essence. A mass balance for Ti could clearly demonstrate that the absence of TiC at the triple line was simply attributed to the consumption of Ti during spreading for the formation of a TiC layer at the center of the drop. Therefore, it was suggested that the formation of TiC improved the wetting between the liquid drop and the graphite substrate only in the initial wetting stage, and after all of Ti was consumed, the rest of the wetting was dominated by the formation of Al_4C_3. In order to verify this assumption, the time variation in the contact angle for pure Al on the graphite substrates under the same condition was investigated and the result was shown in Figure 3.4.3. It was found that the decrease of the contact angle to the equilibrium state spent about 75 minutes, which was longer than that of Al-Ti/graphite systems. However, the equilibrium contact angle of approximately 25° showed no clear difference from that of Al-Ti/graphite systems. This result illustrated that the addition of less than 5 mass% Ti in Al could accelerate the spreading of the droplet, but had no measurable effect on the final contact angle. From this discussion, it was advocated that adding oversaturated amount of Ti on Al was advantageous to improve the wetting of the Al-Ti/graphite systems, which has been confirmed by Sobczak et al. [8] indeed.

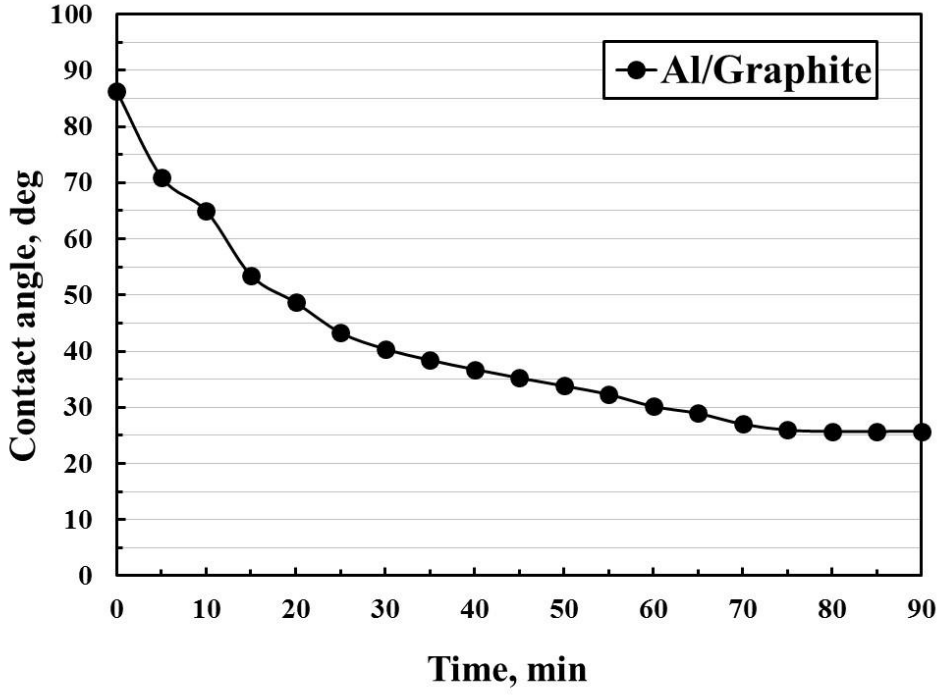

Figure 3.4.3 Variation in the contact angle for pure Al on the graphite substrates at 1373 K for 90 minutes

3.4.3 Harmfulness of formation of Al_4C_3

There was an instance that could prove the harmfulness of the formation of Al_4C_3 on the mechanical properties of materials. After the wetting experiment, if the samples, which have been embedded in epoxy resin and sectioned perpendicular to the interface, were exposed in the air at the room temperature for a period, the Al_4C_3 layer changed morphologically or even disappeared at the interface. Figure 3.4.4 shows the COMPO image of the cross section and the elemental mapping of the Al-1 mass % Ti alloy/graphite system in the placement state A, which was exposed in the air for two weeks. It was clearly observed that a number of cracks occurred in some places of the Al_4C_3 layer,

whereas the TiC layer remained unchanged. The elemental mapping revealed that only the elements of Al and oxygen existed at the vicinity of the region of these cracks, which meant that Al_4C_3 was attack by air moisture and translated into $Al(OH)_3$ and methane according to the following reaction [18]:

$$Al_4C_3\,(s) + 12H_2O = 4Al(OH)_3(s) + 3CH_4(g) \qquad (3.4.10)$$

Therefore, it was foreseeable that the whole Al_4C_3 layer would be corroded by air moisture if the samples was exposed in the air longer, which might result in the occurrence of the de-bonding between the alloy and the graphite substrate finally. This was why during the fabrication of Al-C related composites, preventing the development of Al_4C_3 at the interface has been increasingly emphasized by many researchers.

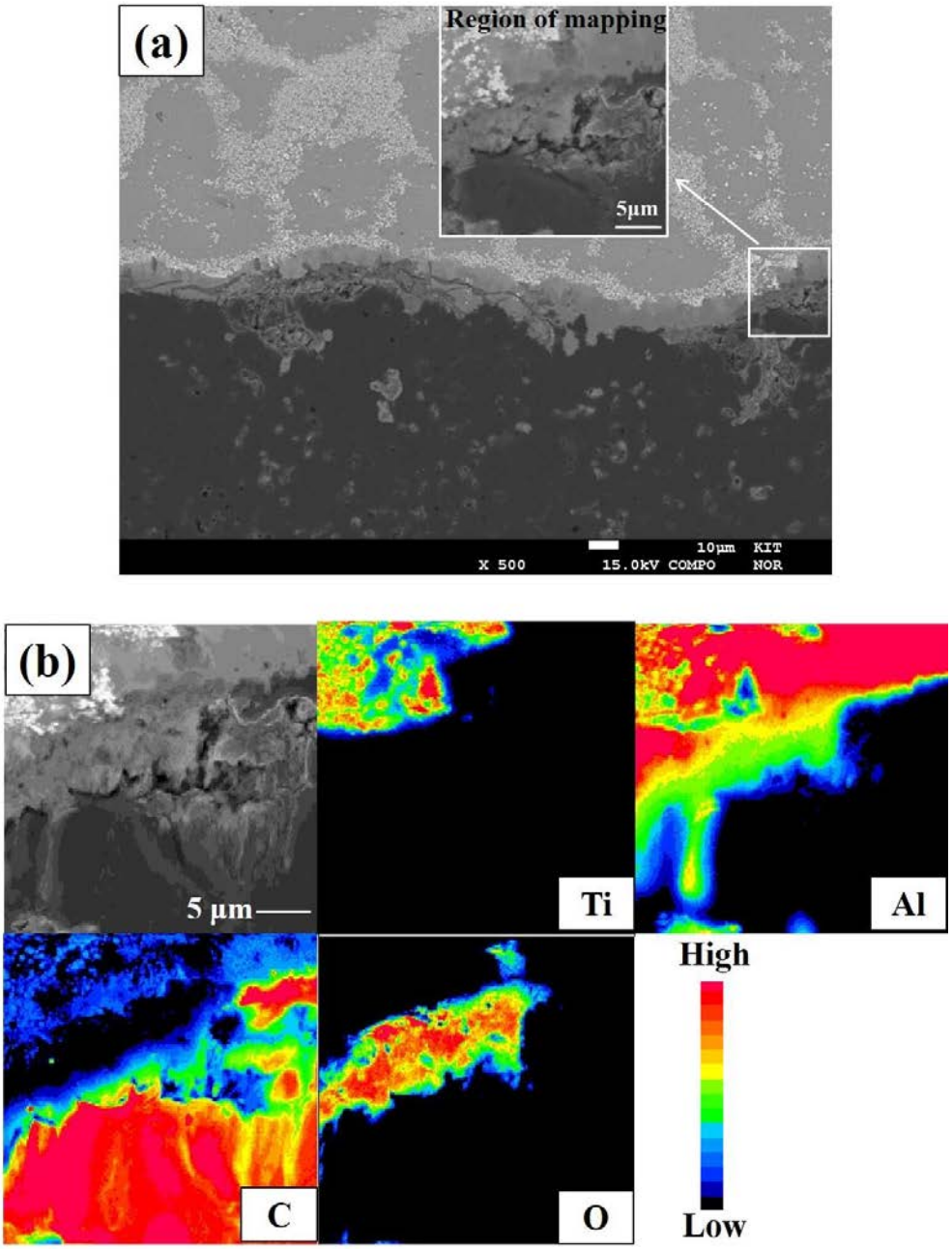

Figure 3.4.4 (a) COMPO image of the cross section and (b) elemental mapping of the Al-1 mass % Ti alloy/graphite system in the placement state A after the samples was exposed in the air at the room temperature for two weeks

3.5 Conclusions

In this chapter, the wettability of liquid aluminium-titanium alloys on graphite substrate with titanium content of 1, 3 and 5 mass % by changing the placement state of aluminium and titanium was investigated at 1373 K using sessile drop method under vacuum. The following conclusions have been drawn:

(1) Addition of less than 5mass% Ti in Al could accelerate the spreading of the droplet on the graphite, but had no measurable effect on the final contact angle. Furthermore, changing the placement state of the Al-Ti alloy on the graphite substrate only resulted in different values of the initial contact angle, the values of the equilibrium contact angle did not be affect by it.

(2) Addition of Ti in Al led to the formation of a bilayer of Al_4C_3 and TiC at the interface of the Al-Ti/ graphite systems. However, only Al_4C_3 layer existed at the vicinity of the triple line in all cases, thus the formation of TiC improved the wetting of the Al-Ti/ graphite systems only in the initial wetting stage, and after all of Ti was consumed, the rest of the wetting was dominated by the formation of Al_4C_3.

(3) Al_4C_3 layer was corroded by air moisture after the samples was exposed in the air at the room temperature for a period, which could lead to the occurrence of the de-bonding between the alloy and the graphite substrate and lower the mechanical properties of materials.

References

[1] MANNING C R, Gurganus T B. Wetting of Binary Aluminum Alloys in Contact with Be, B4C, and Graphite[J]. Journal of the American Ceramic Society, 1969, 52(3): 115-118.

[2] Seal S, Warwick T, Sobczak N, et al. A scanning photoemission microscope (SPEM) to study the interface chemistry of AlTi/C system[J]. Journal of materials science letters, 2000, 19(2): 123-126.

[3] Kimura Y, Mishima Y, Umekawa S, et al. Compatibility between carbon fibre and binary aluminium alloys[J]. Journal of materials science, 1984, 19(9): 3107-3114.

[4] Sobczak N. Effect of alloying elements on wettability and interfaces in aluminum-carbon system[C]//Proc. EMRS Conf. Light Alloys and Composites. 1999: 13-16.

[5] Sobczak N, Gorny Z, Ksiazek M, et al. Interaction between porous graphite substrate and liquid or semi-liquid aluminium alloys containing titanium[C]//Materials Science Forum. 1996, 217: 153-158.

[6] Seal S, Barr T L, Sobczak N, et al. Microscopy and electron spectroscopic study of the interfacial chemistry in Al–Ti alloy/graphite systems[J]. Journal of materials science, 1998, 33(16): 4147-4158.

[7] Seal S, Warwick T, Sobczak N, et al. A scanning photoemission microscope (SPEM) to study the interface chemistry of AlTi/C system[J]. Journal of materials science letters, 2000, 19(2): 123-126.

[8] Sobczak N, Gorny Z, Ksiazek M, et al. Interaction between porous graphite substrate and liquid or semi-liquid aluminium alloys containing titanium[C]//Materials Science Forum. 1996, 217: 153-158.

[9] Zhang M X, Chang Y A. Phase Diagrams of Ti-Al-C, Ti-YO, Nb-YO, and Nb-Al-O at 1100 C[J]. Journal of phase equilibria, 1994, 15(5): 470-472.

[10] Zhong W M, L'esperance G, Suery M. Interfacial reactions in Al-Mg (5083)/SiCp composites during fabrication and remelting[J]. Metallurgical and Materials Transactions A, 1995, 26(10): 2637-2649.

[11] Barin I. Thermochemical Data of Pure Substances, Thermochemical Data of Pure Substances[M]. Wiley-VCH, 1997.

[12] Lee K B, Sim H S, Kwon H. Reaction products of Al/TiC composites fabricated by the pressureless infiltration technique[J]. Metallurgical and Materials Transactions A, 2005, 36(9): 2517-2527.

[13] Mitra R, Fine M E, Weertman J R. Chemical reaction strengthening of Al/TiC metal matrix composites by isothermal heat treatment at 913 K[J]. Journal of materials research, 1993, 8(09): 2370-2379.

[14] Okamoto H. Al-Ti (aluminum-titanium)[J]. Journal of phase equilibria, 1993, 14(1): 120-121.

[15] Shinozaki N, Mukai K, Fujita T. Wettability of Al_2O_3-MgO substrates by molten aluminum[J]. Metallurgical and Materials Transactions B, 2002, 33(3): 506-509.

[16] Park S J, Fujii H, Nakae H. Wetting of boron nitride by molten Al-Si alloys[J]. Journal of The Japan Institute of Metals, 1994, 58(2): 208-214.

[17] Landry K, Rado C, Voitovich R, et al. Mechanisms of reactive wetting: the question of triple line configuration[J]. Acta materialia, 1997, 45(7): 3079-3085.

[18] Walter D, Karyasa I W. Solid State Reactions in the Al‐Si‐C System[J]. Journal of the Chinese Chemical Society, 2005, 52(5): 873-876.

Chapter 4 Wettability and Interfacial Reaction between Al-Si Alloys and Graphite

4.1 Introduction

In Al-Si-C systems, since both the aluminium and silicon can react with carbon at high temperature, the interfacial reaction becomes complex and in principle, it is expected that the addition of silicon on aluminium can not only suppress the formation of Al_4C_3 in Al/C systems because of the harmfulness of Al_4C_3 on the mechanical properties of materials [1, 2], but also improve the wetting of Al/C systems. However, although the wetting of carbon substrates by Al-Si alloys has been investigated by several researchers, the intrinsic wettability and the role of Si are still ambiguous [1, 3, 4]. For this reason, the wettability and interfacial reaction between liquid Al-Si alloys and graphite substrates with Si content of zero, 6, 10 and 20 mass % were investigated at 1273 K by using sessile drop method. In addition, the study about the effect of the placement state of Al and Si on wetting was also performed. The purpose of this study was to investigate the effect of the placement state of Al and Si on wetting results, and to explore an optimal addition amount of Si for wetting and interfacial reaction of Al/graphite systems.

4.2 Experimental

4.2.1 Materials

High purity aluminium (99.99 mass %) cubes and silicon (99.99 mass %) plates were employed in this study and they were placed on the graphite substrates in three states which were separately defined as the placement state A, B and C. As shown in Figure 4.2.1(a), the placement of state A, from top to bottom, was settled as pre-alloyed Al-Si/C. The pre-alloyed Al-Si alloys with silicon content of 6 mass%, 10 mass% and 20 mass% were prepared from pure Al and Si by arc melting in a Ti (99.8 mass%)-gettered argon atmosphere, and were machined into a small cuboid sharp with 3 mm ± 0.5mm in square and 5 mm ± 0.5mm in height and weighting approximately 0.13 g for the experiment. The placement of state B and C, from top to bottom, was settled as Si/Al/C and Al/Si/C, respectively, shown as Figure 4.2.1(b) and 4.2.1(c). The drops of Al-Si alloys were prepared in situ by melting the pure Si plate and Al cube, which were directly piled on the graphite substrate. The Al cube was cut into 3mm ± 0.5mm in square and 4mm ± 0.5mm in height. As for the dimensions of the Si plate, the thickness was 1.5 mm and the square varied with different Si contents, which were 1.5 mm ± 0.5 mm for 6 mass% Si, 1.8 mm ± 0.5 mm for 10 mass% Si and 3 mm ± 0.5mm for 20 mass% Ti. The metals of Al and Si were weighted in designed proportion which the mass ratio of Al/Si were 94:6, 90:10 and 80:20, respectively, and the total mass was approximately 0.13 g in all cases. Before the wetting experiment, both the pre-alloyed Al-Si alloys and the metals of Al and Si were polished by emery papers from 400 to 2000 grit and cleaned with ethanol in order to prevent further oxidation.

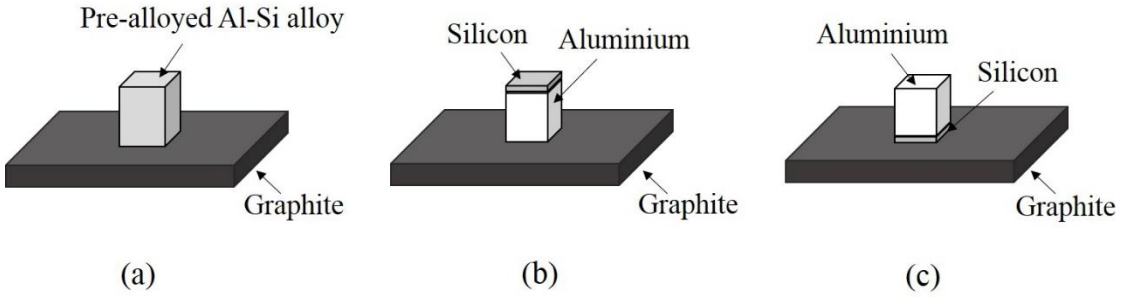

Figure 4.2.1 Schematic diagram of three kinds of placement states

4.2.2 Experimental apparatus and procedure

General experimental procedures are described in 2.2.2 section. The experimental temperature of the Al-Si alloy/graphite systems was set to 1273 K and the holding time was 1 hour.

4.3 Results and Discussion

4.3.1 Effect of placement states on wetting behavior

In chapter 2 and 3, we have reported that the wetting process was greatly affected by the placement state of Cu-Ti alloys or Al-Ti alloys on graphite substrates. Therefore, in this study, we firstly investigated the wetting process and the final contact angle between the Al-Si alloys and the graphite substrate in three different placement states. The representative photographs of the wetting process of the Al-6mass%Si/C system are shown in Figure 4.3.1. It can be seen that when the heating temperature reached approximately 1023 K, for the placement state A and B, a homogeneous and spherical liquid Al-Si drop was in situ formed on the graphite substrate without any interfacial

reaction by melting the pure Al cube and Si plate, while the pre-alloyed Al-Si alloys in the placement state C also melted completely into a spherical liquid Al-Si drop. These phenomena showed no difference in the forming process of liquid Al-Si drop regardless of the placement states. Figure 4.3.2 shows the time variation in the contact angle for the Al-6mass%Si alloys on the graphite substrates in three different placement states at 1273 K. It was found that the values of the initial contact angle were 123°, 125° and 128° and the equilibrium contact angle were 88°, 85° and 86° for the placement states A, B and C, respectively. The negligible difference in either the initial contact angle or the equilibrium contact angle for all three placement states suggested that the wetting result was not affected by the placement state of the Al-Si alloys on the graphite substrates.

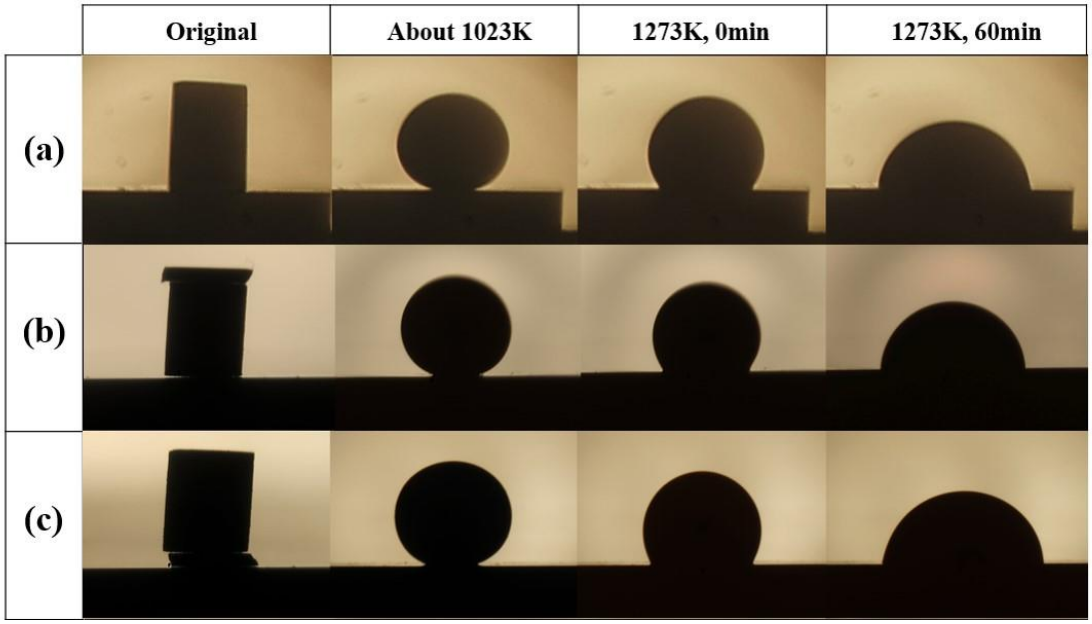

Figure 4.3.1 Representative photographs of the wetting process of the Al-6mass%Si/graphite system in three placement states: (a) the placement state A; (b) the placement state B; (C) the placement state C

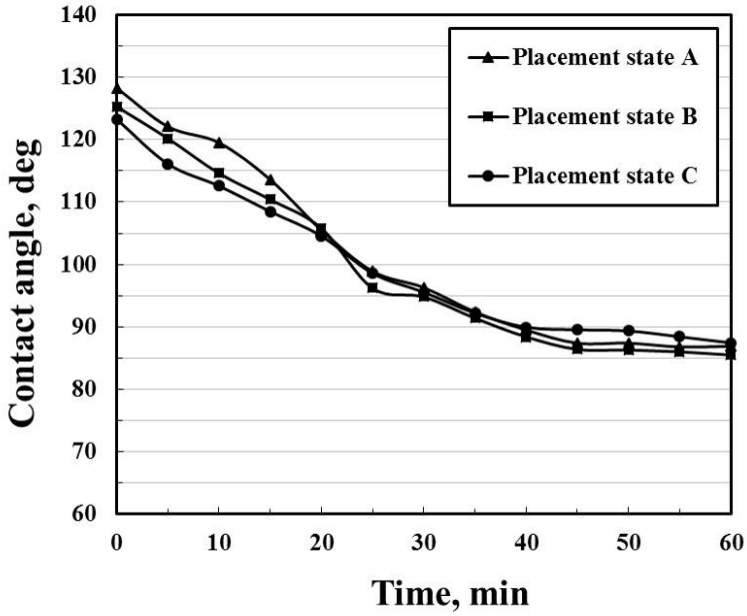

Figure 4.3.2 Time variation in the contact angle for the Al-6mass%Si alloys on the graphite substrates in three different placement states at 1273 K

Table 4.3.1 summarizes the melting point of nine kinds of alloys used in this thesis [5] and the heating time from room temperature to the melting point of each alloy by using the quartz tube furnace. It can be seen that among the Cu-Ti alloys and Al-Ti alloys provided, the melting point of the Al-1 mass% Ti alloy (about 910℃) was lowest, and it took at least 26 minutes when the temperature of the furnace was raised from room temperature to this melting point temperature. Therefore, in the placement states B or C (in situ alloyed Cu-Ti or Al-Ti alloys), the prior Cu-Ti or Al-Ti liquid phase formed during the heating process had adequate time to react with graphite, which could cause various wetting behaviors and results. However, since the melting point of three different of the Al-Si alloys were relatively lower, and heating from room temperature to the highest melting point (680 ℃ for the Al-20 mass% Si alloy) spent at most 13 minutes, the prior Al-Si liquid phase had no adequate time to react with graphite. On the other hand, it was

well known that Al was prone to be oxidized and the oxidation of the aluminum surface was generally unavoidable [6], so that once the prior Al-Si liquid phase occurred, the formed oxide film could greatly impede the reaction between it and the graphite substrate, till all of the solid phase of Al and Si melted and formed a homogeneous and spherical liquid Al-Si drop. Therefore, because there were no obvious difference by changing the placement state of Al and Si on the graphite substrate, in this study, the placement state C was selected for all systems.

Table 4.3.1 Melting point of each alloy [5] and heating time from room temperature (25℃) to melting point of these alloys

Alloys	Melting point (℃)	Heating time from 25℃ to melting point (min)
Cu-4mass%Ti	1050	46
Cu-6mass%Ti	1030	42
Cu-10mass%Ti	980	32
Al-1mass%Ti	910	26
Al-3mass%Ti	1010	37
Al-5mass%Ti	1070	53
Al-6mass%Si	620	10
Al-10mass%Si	600	9
Al-20mass%Si	680	13

4.3.2 Contact angle phenomena

The time dependence of the contact angle and the drop base diameter measured at 1273 K for molten Al-Si alloys on graphite substrates is shown in Figure 4.3.3. As stated previously, a spherical liquid Al-Si drop was formed on the graphite substrate in the placement state C when the heating temperature reached to approximately 1023 K. At this time, the contact angle in all cases was approximately 160° as shown in Figure 4.3.3(a), which was large and non-wetting. The large contact angle resulted from the formation of the aluminium oxide film on the molten drop surface, which could greatly impede the movement of the triple line [2]. However, as the heating temperature continued to rise, the contact angle decreased remarkably, and finally reached to approximately 124° for the Al/C, Al-6 mass %Si/C and Al-10 mass %Si/C systems, and 109° for the Al-20 mass %Si/C system when the heating temperature reached to 1273K. In addition, the molten drop spread rapidly over the graphite substrate in all cases as shown in Figure 4.3.3(b). This period could be characterized as stage I, and it mainly occurred in the heating process from the melting point of the samples to 1273 K. The subsequent wetting can be distinguished as stage II and stage III. The stage II began to take place at the time when the heating temperature reached to 1273 K, and finished within approximately 45 minutes in all cases. Obviously, the contact angle in this stage continued to decrease but at a slower rate in comparison with the stage I, and the wettability improved with increasing silicon content, which the contact angle after holding for 45 minutes decreased from 124° to 91° , 86° and 83° for the Al/C, Al-6 mass %Si/C and Al-10 mass %Si/C systems, respectively, and decreased from 109° to 64° for the Al-20 mass %Si/C system. In the final stage, both the contact angle and the drop base diameter remained unchanged

nearly, and the final contact angle after holding 1 hour was stabilized at 91° , 86° , 83° and 61° for the Al/C, Al-6 mass %Si/C, Al-10 mass %Si/C and Al-20 mass %Si/C systems, respectively.

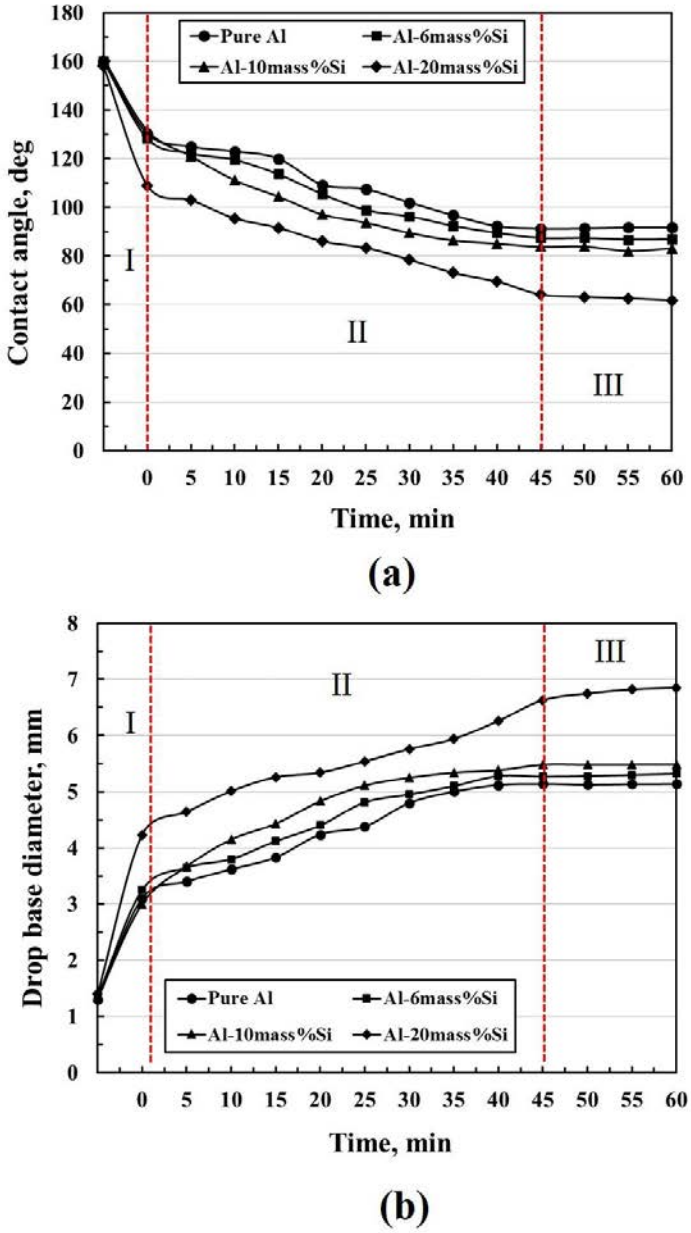

Figure 4.3.3 Variation in the contact angle (a) and the drop base diameter (b) with time for the Al-Si alloys on the graphite substrates at 1273 K

4.3.3 Wetting kinetics of Al-Si/C systems

From the viewpoint of wetting kinetics of Al-Si/C systems, the three successive stages mentioned above was discussed:

(1) Stage I—Removal of oxide film

Many literatures [3, 7, 8] have documented that the reduction of the contact angle in the stage I can be attributed to the deoxidation of the oxide film on the surface of the molten drop at high temperature, as expressed by the reaction (4.3.1):

$$\frac{4}{3}\mathrm{Al(l)} + \frac{1}{3}\mathrm{Al_2O_3(s)} = \mathrm{Al_2O(g)} \qquad \Delta G^{\circ}_{(1273K)} = +189\ \mathrm{kJ}\ [9] \qquad (4.3.1)$$

According to this reaction, the equilibrium partial pressure of Al_2O at 1273 K was calculated to be approximately 1.7×10^{-3} Pa, which was only 0.1 percent of the total pressure in the furnace. Therefore, the oxide film was most probably disrupted when the furnace was ceaselessly evacuated to the vacuum of 1.5 Pa during the whole experiment. This reaction enabled the subsequent wetting to proceed between the molten Al-Si drop and the graphite substrate.

(2) Stage II—Interfacial reaction between the Al-Si drop and the graphite substrate

BAO Sarina et al. [7] and Nakae et al. [10] suggested that the reduction of the contact angle in the stage II was controlled by the interfacial reaction between the Al-Si alloys and the graphite substrate. For the Al/C system, the Gibbs free energy ΔG of Al_4C_3 at 1273 K was -134 kJ according to the following reaction (4.3.2), confirming great reactivity between Al and graphite.

$$4Al(l) + 3C(s) = Al_4C_3(s); \qquad \Delta G^{\circ}_{(1273K)} = -134 \text{ kJ} \ [9] \qquad (4.3.2)$$

However, for the Al-Si/C systems, due to the addition of Si, it is necessary to consider both the formation of Al_4C_3 and SiC. The stability of Al_4C_3 and SiC were described by the following reaction (4.3.3), and the calculation of the Gibbs free energy ΔG of this reaction was derived from the method given by Isaikin et al. [11], as expressed by equation (4.3.4):

$$Al_4C_3(s) + 3Si(l) = 3SiC(s) + 4Al(l) \qquad (4.3.3)$$

$$\Delta G = -113900 + 12.05T\text{In}T - 8.91 \times 10^{-3}T^2 - 7.53 \times 10^{4}T^{-1} - 21.5T + RT \ln \frac{a_{SiC}^3 \cdot a_{Al}^4}{a_{Al4C3} \cdot a_{Si}^3} \qquad (4.3.4)$$

The critical condition for the formation of Al_4C_3 in the reaction (4.3.3) was investigated by T. Iseki et al. [12]. They adopted the value of ΔG calculated from the equation (4.3.4) using the activity of Si and hypothesizing that the activities of SiC, Al and Al_4C_3 were set equal to unity. However, due to the addition of Si, the activities of Si and Al should be considered simultaneously. Here, by referring to the values of Al and Si activity reported from Ref. [13], the value of ΔG for the Al-6 mass %Si/C, Al-10 mass %Si/C and Al-20 mass %Si/C systems was calculated to be 36 kJ, 12 kJ and -26 kJ, respectively. Thermodynamically, these results suggested that the formation of SiC would be observed at 20 mass %Si, whereas Al_4C_3 was formed at 6 mass %Si and 10 mass %Si. Furthermore, assuming the value of ΔG = 0, the content of Si in the Al-Si alloys was found to be approximately 13 mass %. Figure 4.3.4 shows the optical micrographs of the cross section of the interface between the alloy drops and the graphite substrate in all cases at 1273 K

for 1 hour. It was found that a continuous reaction layer was formed at the interface for the Al/C, Al-6 mass %Si/C and Al-10 mass %Si/C systems, while a very thin or even discontinuous reaction layer was formed at the interface of the Al-20 mass %Si/C system. Figure 4.3.5, Figure 4.3.6 and Figure 4.3.7 present the COMPO image of the cross section and the elemental mapping for the Al-6 mass %Si/C, Al-10 mass %Si/C and Al-20 mass %Si/C systems at 1273 K after 1 hour, respectively. It can be seen that the morphology of the reaction layer formed at the Al-6 mass %Si/C and Al-10 mass %Si/C systems was different than that formed at the Al-20 mass %Si/C systems. The element mapping revealed that the elements of C and Al were the main components of the reaction layer at the Al-6 mass %Si/C and Al-10 mass %Si/C systems, whereas only C and Si existed at the interface of the Al-20 mass %Si/C systems. Quantitative determinations performed by spot analysis of EPMA at points 1~6 (Table 4.3.2) indicated that the atomic ratio of Al:C at the interface for the Al-6 mass %Si/C and Al-10 mass %Si/C systems was approximately 4:3, suggesting an Al_4C_3 compound. And for the Al-20 mass %Si/C system, the element of Si and C existed at the reaction layer with the atomic ratio of approximately 1:1, which illustrated that it might be composed of SiC. Combined with the result of XRD (Figure 4.3.8) after grinding the solidified alloy drops away, the reaction layer was identified to be Al_4C_3 layer in the case of the Al/C, Al-6 mass %Si/C and Al-10 mass %Si/C systems, which agreed with the result of spot analysis of EPMA. Meanwhile, SiC, rather than Al_4C_3, was detected at the interface of the Al-20 mass %Si/C system. This observation supported the above thermodynamic calculation and indicated that the interfacial reaction product would transform from Al_4C_3 into SiC, provided that the addition of sufficient amount of Si (at least larger than 13 mass %) to Al.

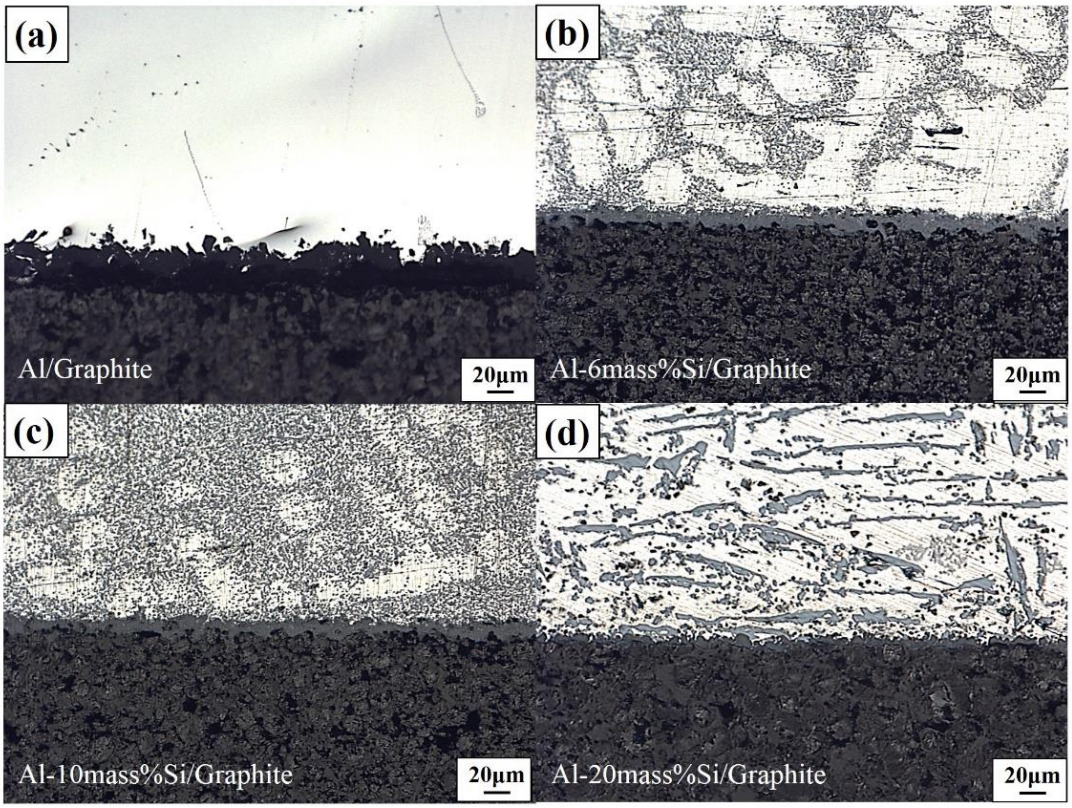

Figure 4.3.4 Optical micrographs of the cross section of the interface between the alloy drops and the graphite substrate at 1273 K after 1 hour (above was Al-Si alloy, below was graphite substrate): (a) Al/C; (b) Al-6 mass %Si/C; (c) Al-10 mass %Si/C; (d) Al-20 mass %Si/C

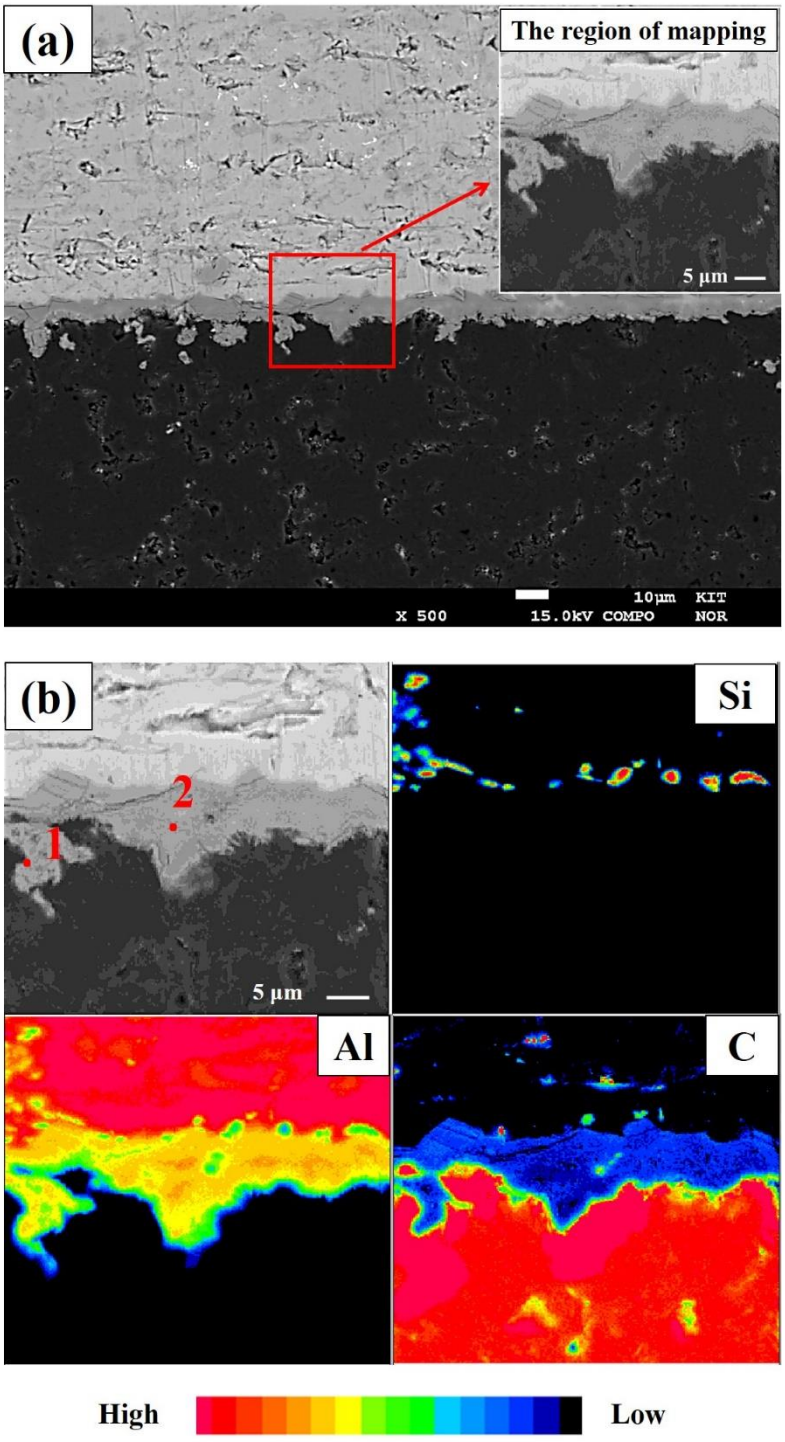

Figure 4.3.5 (a) COMPO image of the cross section and (b) elemental mapping for the Al-6 mass %Si/C at 1273 K after 1 hour

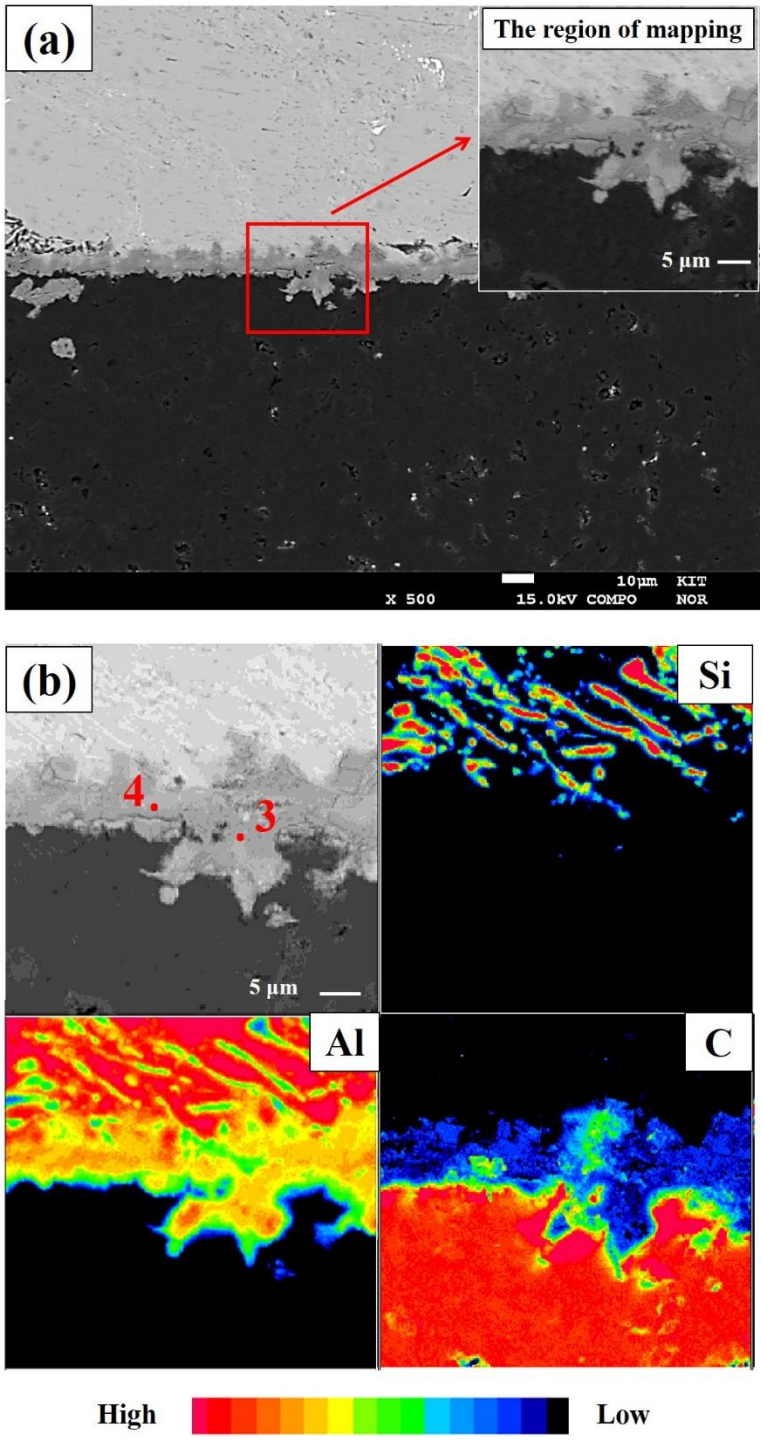

Figure 4.3.6 (a) COMPO image of the cross section and (b) elemental mapping for the Al-10 mass %Si/C at 1273 K after 1 hour

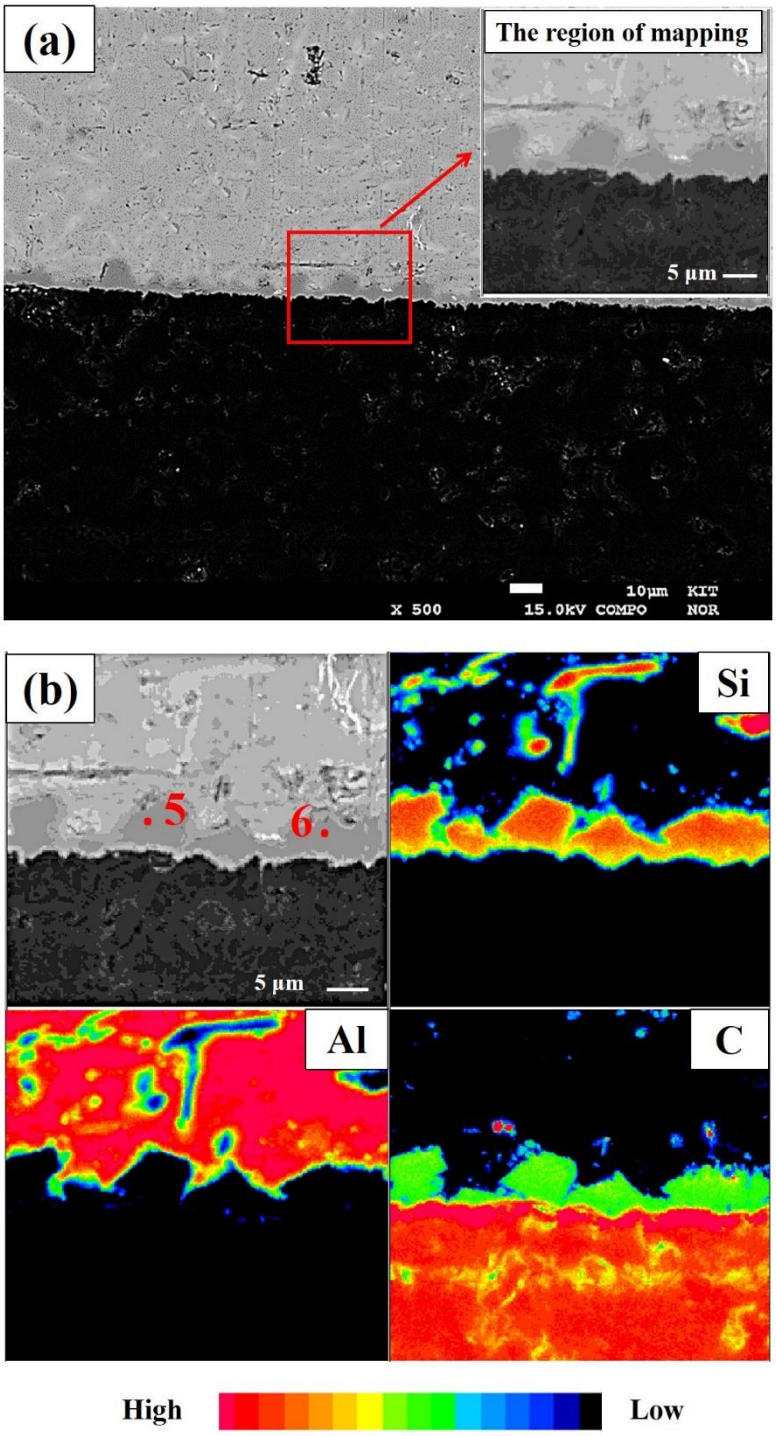

Figure 4.3.7 (a) COMPO image of the cross section and (b) elemental mapping for the Al-20 mass %Si/C at 1273 K after 1 hour

Table 4.3.2. EPMA spot analysis results at the interface region of Al-Si alloys/graphite system with different silicon contents

Alloy	Point	C (at. %)	Si (at. %)	Al (at. %)
Al-6mass%Si	1	44.0	0.7	55.3
	2	42.8	0.4	56.9
Al-10mass%Si	3	42.4	0.8	56.8
	4	45.6	0.6	53.8
Al-20mass%Si	5	50.3	49.0	0.7
	6	51.6	47.4	1.0

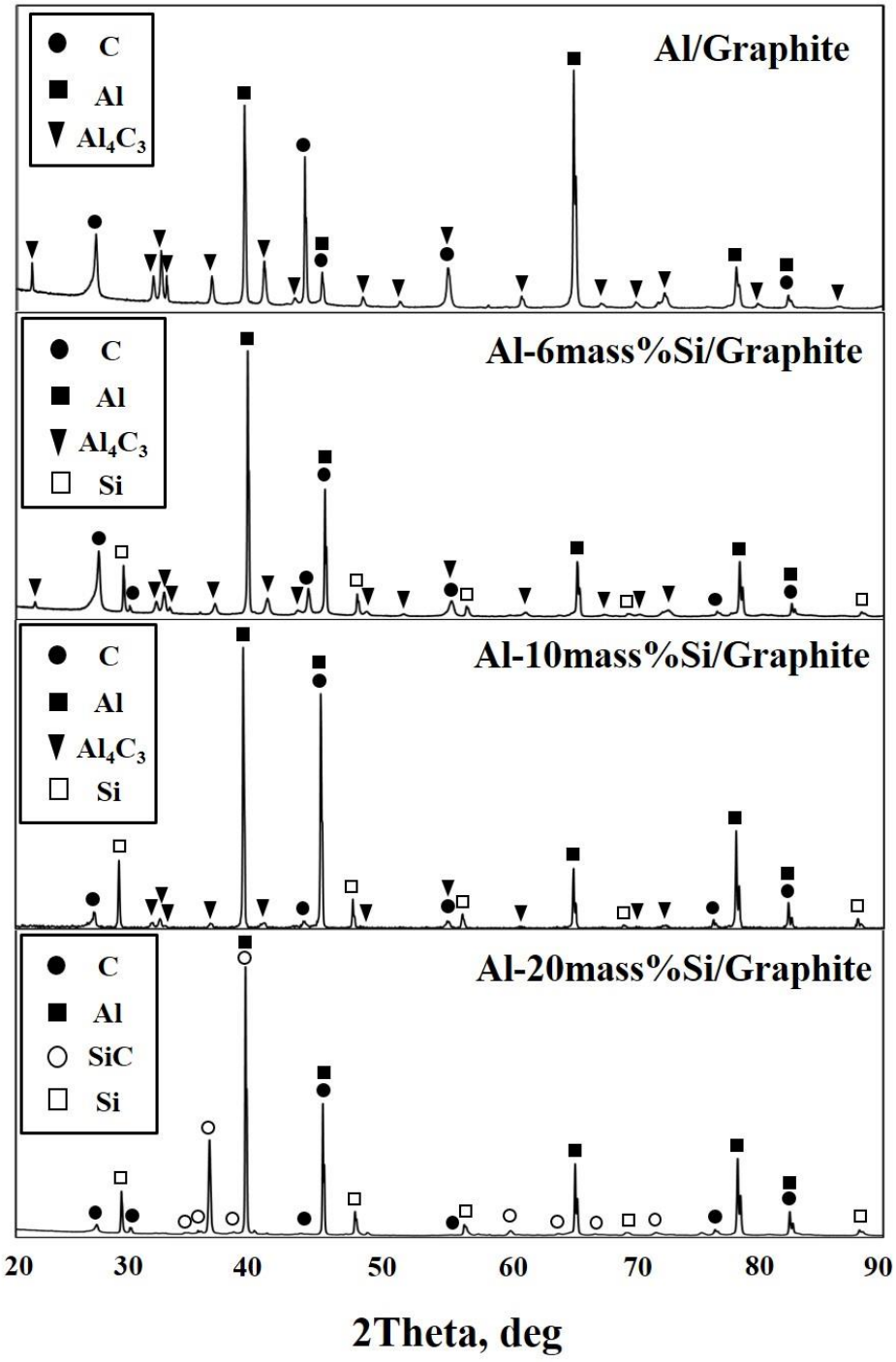

Figure 4.3.8 XRD patterns of the interface between the alloy drops and the graphite substrate

(3) Stage III—Equilibrium contact angle

After the stage II of the interfacial reaction, the melt/Al_4C_3 interface was formed in the Al/C, Al-6 mass %Si/C and Al-10 mass %Si/C systems, and the melt/SiC interface was formed in the Al-20mass%Si/C system. An equilibrium contact angle was obtained in all cases. It was found that the wettability did not show a significant improvement as increasing the Si content from zero to 10 mass %, and the observed difference of 8° in the contact angle was slight. But as adding the Si content from 10 mass % to 20 mass %, a relatively notable decrease of 22° in the contact angle appeared. In order to understand this phenomenon, we investigated the wettability between Al-Si alloys and SiC substrates at the same experiment condition and the result is shown in Figure 4.3.9. Regarding to the Al-Si alloys with same composition, the equilibrium contact angles on SiC substrates were lower than that on graphite substrate correspondingly. The contact angle of all the Al-Si/SiC systems decreased fast in the early wetting stage as compared with the Al-Si/C systems, especially for the Al-20mass%Si/SiC systems, the contact angle after holding for 10 minutes reached to about 15° , indicating a remarkable wettability. Thereafter, the contact angle in the Al/SiC, Al-6 mass %Si/SiC and Al-10 mass %Si/SiC systems continued to decrease slightly while that in the Al-20 mass %Si/SiC system remained unchanged nearly. Figure 4.3.10 presents the representative backscattered electron composition (COMPO) images of the cross section of the interface for the Al-10 mass %Si/SiC and Al-20 mass %Si/SiC systems at 1273 K for 1 hour. A reaction layer that was identified as Al_4C_3 by means of the spot analysis of EPMA was formed at the interface of the Al-10 mass %Si/SiC system, whereas no any reaction product was observed at the interface of the Al-20 mass %Si/SiC system. This difference was attributed to the fact that the addition of sufficient amount of Si to Al completely

suppressed the formation of Al_4C_3, thus as for the Al-20 mass %Si/SiC system, the triple line could move rapidly up to the equilibrium state in the initial 10 minutes, which led to the unchanged contact angle in the subsequent holding time. But for the Al/SiC, Al-6 mass %Si/SiC and Al-10 mass %Si/SiC systems, it was suggested that the Al_4C_3 particles was formed from the early wetting stage in fact since the decrease of the contact angle in this stage was slower than that in the Al-20 mass %Si/SiC system, and the formation of these Al_4C_3 particles resulted in a rough interface (see the interface shown in Figure 4.3.10(a)), which would delay or even impede the spreading of the triple line [1, 10]. From this discussion, we inferred that liquid Al can wet SiC very well in nature. Therefore, due to the formation of a thin SiC layer at the interface of the Al-20 mass %Si/C system, the contact angle decreased considerably as compared with other systems.

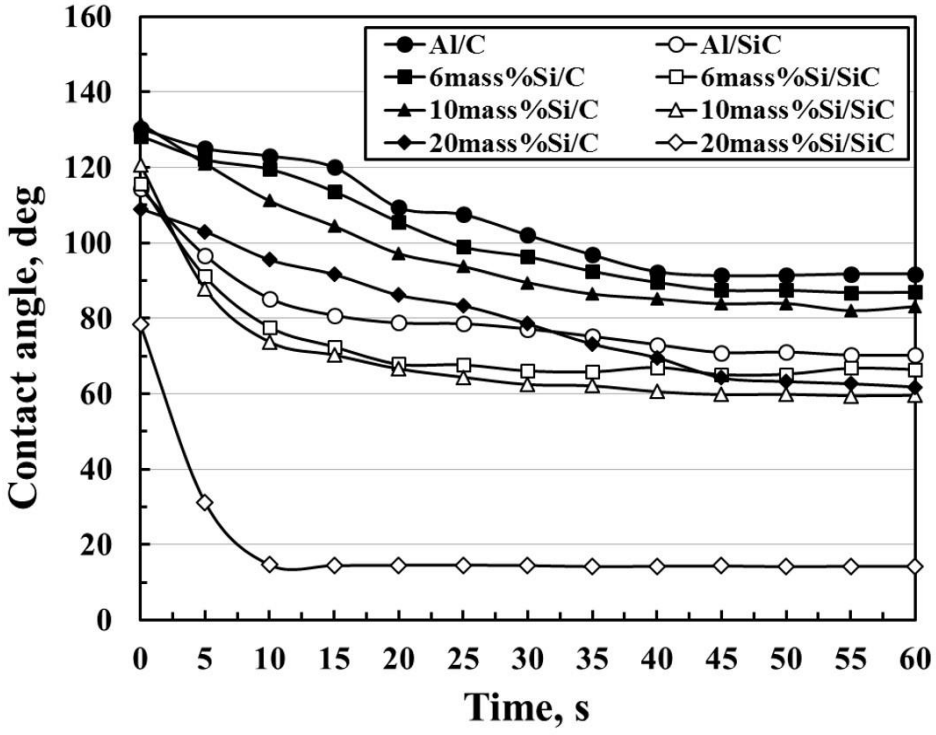

Figure 4.3.9 Comparison of the variations in the contact angles for Al-Si alloys on the graphite and SiC substrates at 1273 K

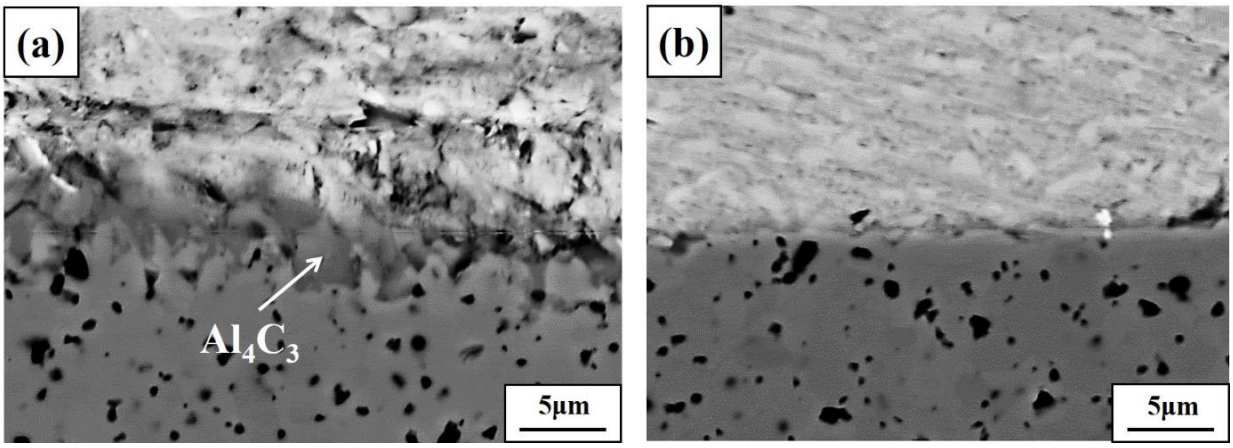

Figure 4.3.10 COMPO images of the cross section of the interface between the alloy drops and the SiC substrate at 1273 K (above was Al-Si alloy, below was SiC substrate): (a) Al-10 mass %Si/SiC; (b) Al-20 mass %Si/SiC

4.4 Conclusions

In this chapter, the wettability of molten aluminium-silicon alloys on graphite substrate with silicon content of zero, 6, 10 and 20 mass % by changing the placement state of aluminium and silicon were investigated at 1273 K using sessile drop method under vacuum. The following conclusions emerge from the present results:

(1) The wetting result was not affected by the placement state of the Al-Si alloys on the graphite substrate.

(2) The equilibrium contact angle was 91° , 86° , 83° and 61° for the Al/C, Al-6 mass %Si/C, Al-10 mass %Si/C and Al-20 mass %Si/C systems, respectively. The difference of 8° in the contact angle indicated that the wettability did not be improved significantly as increasing Si content from zero to 10 mass %, whereas a relatively notable decrease of 22° in the contact angle was observed as adding Si content from 10 mass % to 20 mass %. This was attributed to the transformation of the interfacial reaction product

from Al_4C_3 into SiC, provided that the addition of sufficient amount of Si (at least larger than 13 mass %) to Al. It was verified that the liquid Al can wet the SiC substrate very well in nature, which might explain why the occurrence of SiC would improve the wettability of the Al-20 mass %Si alloy on graphite substrate.

References

[1] Cong X S, Shen P, Wang Y, et al. Wetting of polycrystalline SiC by molten Al and Al− Si alloys[J]. Applied Surface Science, 2014, 317: 140-146.

[2] Eustathopoulos N, Joud J C, Desre P, et al. The wetting of carbon by aluminium and aluminium alloys[J]. Journal of Materials Science, 1974, 9(8): 1233-1242.

[3] Laurent V, Chatain D, Eustathopoulos N. Wettability of SiC by aluminium and Al-Si alloys[J]. Journal of materials science, 1987, 22(1): 244-250.

[4] Kimura Y, Mishima Y, Umekawa S, et al. Compatibility between carbon fibre and binary aluminium alloys[J]. Journal of materials science, 1984, 19(9): 3107-3114.

[5] Okamoto H. Phase diagrams for binary alloys. Desk handbook[J]. ASM International, Member/Customer Service Center, Materials Park, OH 44073-0002, USA, 2000. 828, 2000.

[6] Shinozaki N, Mukai K, Fujita T. Wettability of Al 2 O 3-MgO substrates by molten aluminum[J]. Metallurgical and Materials Transactions B, 2002, 33(3): 506-509.

[7] Bao S, Tang K, Kvithyld A, et al. Wetting of pure aluminium on graphite, SiC and Al2O3 in aluminium filtration[J]. Trans. Nonferrous Met. Soc. China, 2012, 22(8): 1930-1938.

[8] Park S J, Fujii H, Nakae H. Wetting of Boron Nitride by Molten Al-Si Alloys[J]. Journal of the Japan Institute of Metals-Nihon Kinzoku Gakkaishi, 1994, 58(2): 208-214.

[9] Barin I. Thermochemical Data of Pure Substances, Thermochemical Data of Pure Substances[M]. Wiley-VCH, 1997.

[10] Nakae H, Yamamoto K, Sato K. Measurement of Wetting of Graphite by Al and Al–

Si Alloys Using Meniscography[J]. Materials Transactions, JIM, 1991, 32(6): 531-538.

[11] Isaikin A S, Chubarov V M, Trefilov B F, et al. Compatibility of carbon filaments with a carbide coating and an aluminum matrix[J]. Metal Science and Heat Treatment, 1980, 22(11): 815-817.

[12] Iseki T, Kameda T, Maruyama T. Interfacial reactions between SiC and aluminium during joining[J]. Journal of Materials Science, 1984, 19(5): 1692-1698.

[13] Kozuka Z, Yasugi S, Nakajima W, et al. A study on the fire smelting of aluminium[J]. Denki Kagaku, 1966, 34(1): 35-39.

Chapter 5 Composite of Carbon Fiber and Cu-Ti, Al-Ti and Al-Si Alloys

5.1 Introduction

In chapter 2, the occurrence of microcracks or even a cohesive fracture at the drop peripheries was observed in all the Cu-Ti alloy/graphite systems. In fact, not only in the Cu-Ti alloy/graphite system, these defects occurred in the Al-Ti alloy/graphite and Al-Si/graphite systems as well, and it mainly resulted from the difference in the thermal expansion coefficient between the reaction layer and the graphite substrate, and would seriously influence various properties of the material during the process of production and application. Furthermore, since the graphite is very soft and brittle, and it is difficult to uniformly disperse in the metal matrix without dispersants, the use of graphite as the reinforcement phase shows a certain limitation. Using carbon fiber instead of the graphite substrate may be an effective way to avoid these forms of cracks. Generally, carbon fiber can be an equally satisfactory reinforcement material in metal, polymer as well as ceramic matrices because it not only possesses most of the advantages of graphite, but also has some excellent properties that are not available with graphite, such as higher specific strength than graphite, high specific modulus, light weight, good fatigue resistance and low CTE (the CTE of carbon fiber material in fiber direction is almost zero at room temperature) [1-3]. The composites reinforced by carbon fiber have been more widely used in aerospace, civil engineering, military, and motorsports, along with other competition

sports [4]. For this reason, the composite of Cu-Ti, Al-Ti and Al-Si alloys and carbon fiber felt was investigated by using the sessile drop method in this chapter, and this work aims to establish a basic concept about copper/aluminium-matrix composites reinforced by carbon fiber.

5.2 Composite of Carbon Fiber and Cu-Ti Alloys

5.2.1 Experimental

The carbon fiber felt with 15 mm in square and 4 mm in thickness was used as the substrate, and the XRD result shown in Figure 5.2.1 illustrated that its main component included graphite and octacarbon (C_8).We note that the lack of sharp peaks appeared at the main characteristic peaks of graphite, and this might be attributed to a variation in the lattice constant of graphite, which results in some angle deviations. The purity of the carbon fiber felt was 99.98 mass % examined by the quantitative determination of the X-ray fluorescence (XRF) and the density of it was 0.089 g/cm³, which indicated a porous structure in comparison with the graphite substrate used in previous chapters (the density of the graphite substrate was 1.88 g/cm³). The Cu-10 mass% Ti alloy in the placement state C was selected as the alloy material since it resulted in the best wetting on the graphite substrate. The experimental apparatus, procedure and condition were all consistent with that in the Cu-Ti/graphite system.

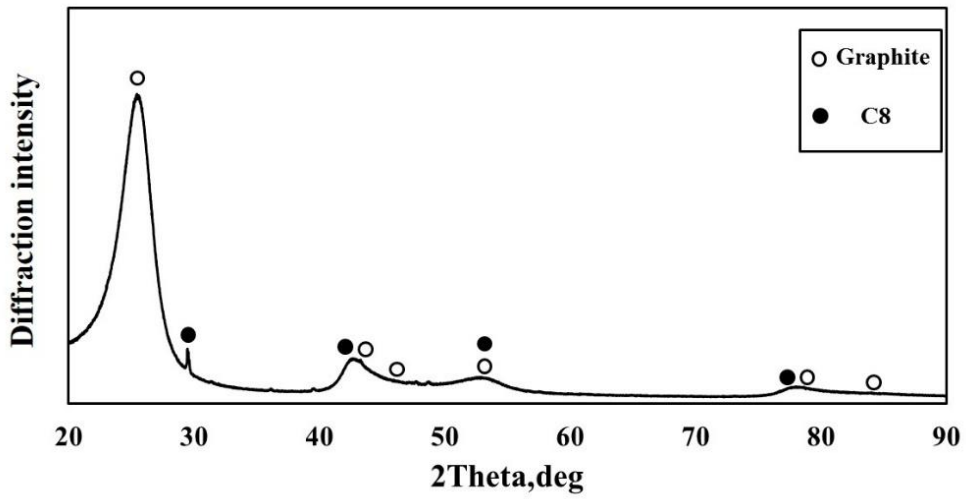

Figure 5.2.1 XRD patterns of carbon fiber felt

5.2.2 Results and Discussion

Figure 5.2.2 shows the representative photographs of the wetting process of the Cu-10 mass % Ti alloy on the carbon fiber felt in the placement state C with increasing the heating temperature. As indicated, the droplet of liquid Cu-Ti alloys was formed at approximately 1292 K. As the heating temperature continued to rise, the droplet base diameter of the liquid Cu-Ti alloys remained unchanged but the height of the droplet reduced gradually. When the droplet disappeared completely at approximately 1361 K, the sample were immediately cooled to the room temperature and taken out from the quartz tube. It was found that only a golden layer remained on the center of the surface of the carbon fiber felt (Figure 5.2.3). To identify the internal changes of the carbon fiber felt, this sample was embedded into resin and sectioned perpendicular to the interface, and it was observed that all of the Cu-Ti alloy have penetrated into the carbon fiber felt without the spreading of the droplet base diameter as shown in Figure 5.2.4(a). By

observing the cross-sectional optical microstructure (Figure 5.2.4(b) and Figure 5.2.4(c)), we found that a lot of oblate black particles or even sticks distributed not only at the interface of the Cu-Ti alloy/carbon fiber felt system, but also at the side of the Cu-Ti alloy far away from the interface. It was suggested that these oblate black particles or sticks were the cross-section of the carbon fibers which have run throughout the entire interior of the Cu-Ti alloys and been sectioned by the wheel diamond saw. Figure 5.2.5 presents the COMPO image of the cross section and the elemental mapping at the side of the alloy far away from the interface of Cu-10 mass % Ti alloy/carbon fiber felt system. The COMPO image shows that numerous fine granular phases were formed around these oblate black particles. The elemental mapping indicated that the oblate black particles indeed was the cross-section of the carbon fibers and the elements of C and Ti were the main components of fine granular phases. The result of the spot analysis by EPMA as shown in Table 5.2.1 indicated that the atomic ratio of Ti:C at points 1, 2 was approximately 1:1, suggesting a TiC compound. Furthermore, combined with the XRD result of the cross section of the Cu-10 mass%Ti alloy/carbon fiber felt system (Figure 5.2.7), these fine granules was identified to be TiC phase.

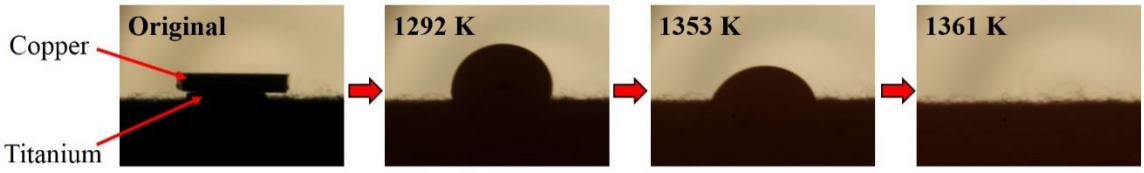

Figure 5.2.2 Representative photographs of wetting process of Cu-10 mass % Ti alloy on carbon fiber felt in the placement state C with increasing the heating temperature

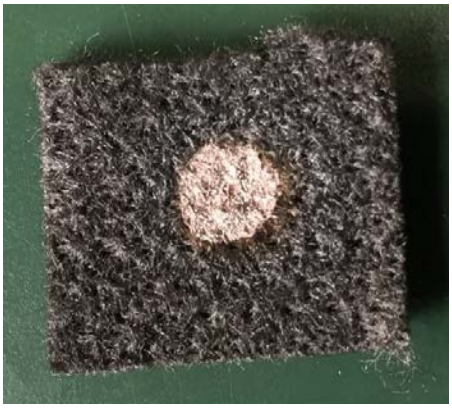

Figure 5.2.3 Photographs of Cu-10 mass % Ti alloy on carbon fiber felt after wetting experiment (frontal view)

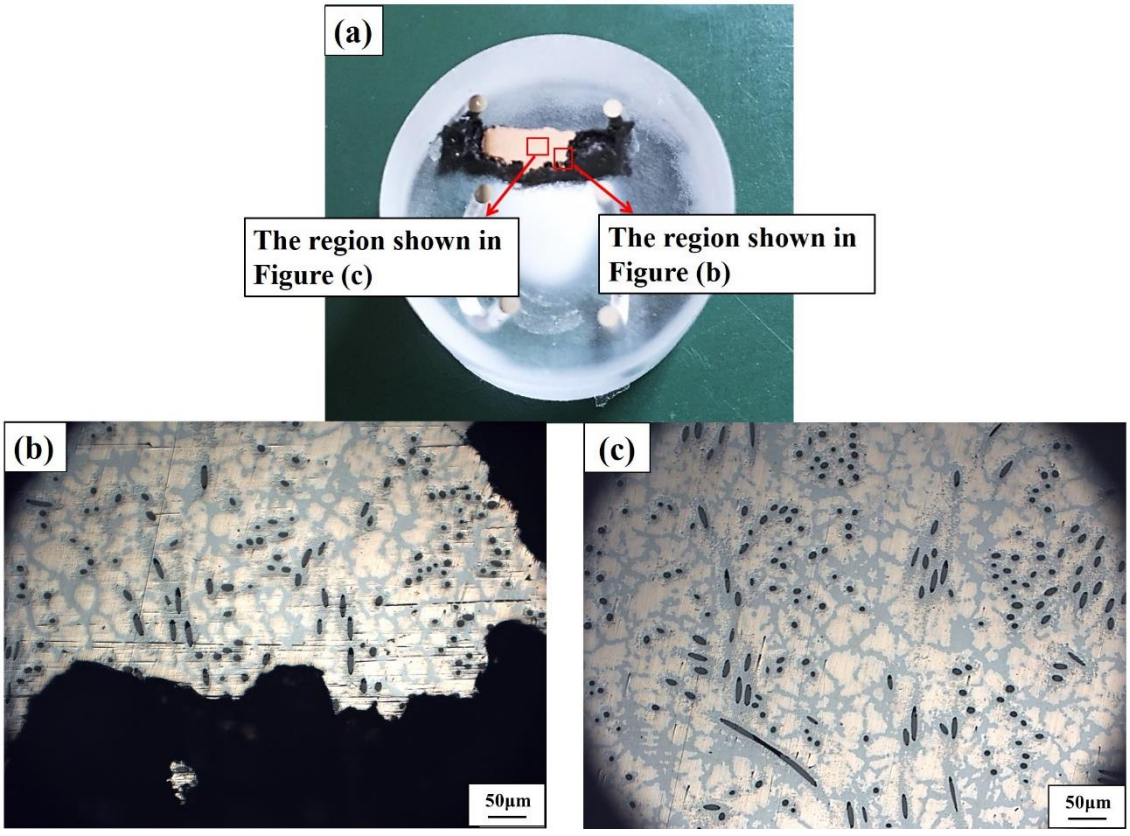

Figure 5.2.4 (a) Photographs of cross section of Cu-10 mass % Ti alloy on carbon fiber felt after being embedded into resin and sectioned perpendicular to the interface. (b) Cross-sectional optical microstructure at the interface of the Cu-10 mass %Ti alloy/carbon fiber felt system and (c) at the side of the Cu-Ti alloy far away from the interface

As mentioned earlier, Ti is very reactive with carbon, and in this case, once the prior Cu-Ti liquid phase with 20 mass % Ti began to occur with the increase of the heating temperature, according to the mechanism of wetting between liquid Cu-Ti alloys and carbon, Ti atoms would be firstly react with the outermost surface of the carbon fiber and TiC phase was formed at the interface between the Cu-Ti liquid phase and numerous carbon fibers. The subsequent wetting, whereupon, would occur after forming this TiC phase. However, unlike the graphite substrate, since the carbon fiber felt that was porous had many small pores, the liquid Cu–Ti alloy could penetrate through these fine open channels to contact the fresh surface of the carbon fiber, instead of spreading along the outermost surface of the carbon fiber felt. When new TiC phase was formed at the surface of the inside carbon fibers, the liquid Cu–Ti alloy would continue to penetrate down until all submerged into the carbon fiber felt. Therefore, the wetting process in this case can be considered as an in-situ reactive penetration of the Cu–Ti alloy into the carbon fiber felt, and the fact that the great penetrability of liquid Cu-Ti alloy in the carbon fiber felt without external pressure and the uniform distribution of the carbon fiber in the Cu-Ti alloy without dispersant illustrated that using the carbon fiber instead of the graphite substrate was an ideal way during the process of production and application.

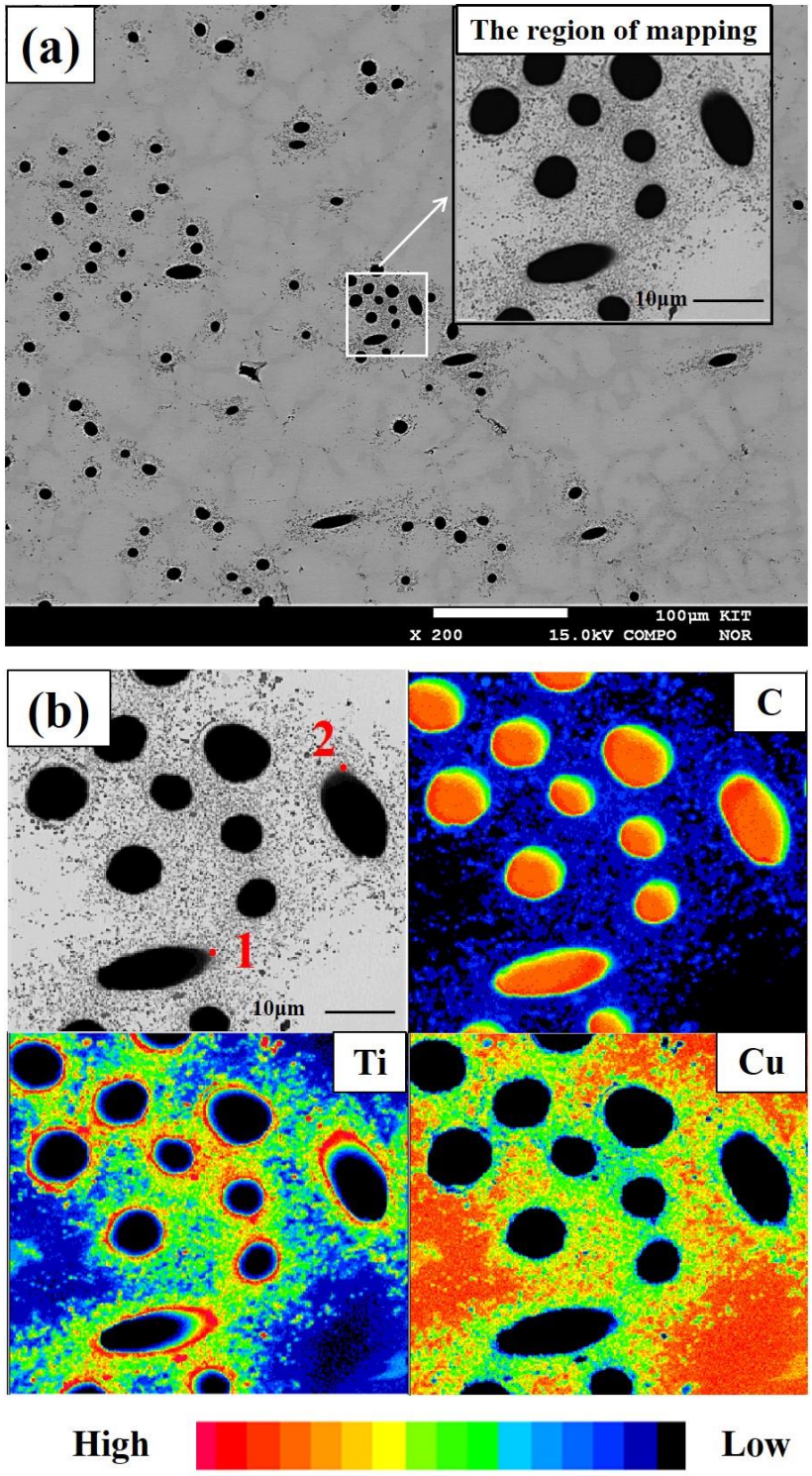

Figure 5.2.5 (a) COMPO image of the cross section and (b) elemental mapping at the side of the alloy far away from the interface of Cu-10 mass % Ti alloy/carbon fiber felt system

Table 5.2.1 EPMA spot analysis results at the interface region of Cu-10 mass% Ti/carbon fiber systems

Points	C (at. %)	Ti (at. %)	Cu (at. %)
1	42.8	47.0	10.2
2	43.2	44.8	12.0

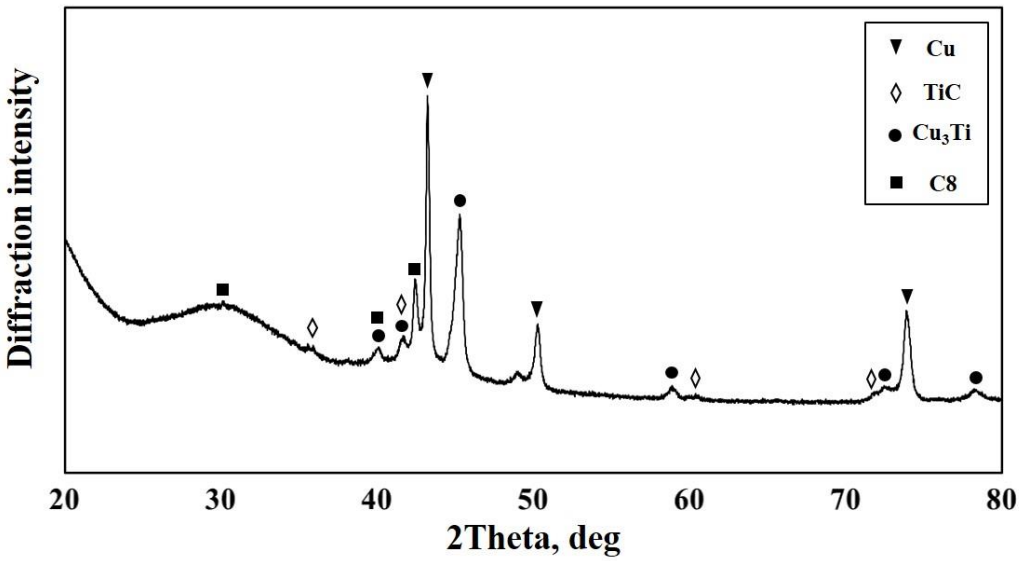

Figure 5.2.6 XRD patterns of Cu-10 mass% Ti alloy/carbon fiber felt system

5.3 Composite of Carbon Fiber and Al-Ti Alloys

5.3.1 Experimental

The details of the carbon fiber felt used are described in the 5.2.1 section. We selected the Al-5mass%Ti alloy in the placement state A as the alloy material since the wetting between the Al-Ti alloy and the graphite substrate did not vary with the change of not only the Ti content but slao the placement state of Al and Ti on the graphite based on the results in the chapter 3. The experimental apparatus, procedure and condition were all consistent with that in the Al-Ti/graphite system.

5.3.2 Results and Discussion

Figure 5.3.1 shows the representative photographs of wetting process of Al-5 mass % Ti alloys on carbon fiber felt in the placement state A with increasing the heating temperature. It can be seen that the alloy sample melted into a liquid droplet at 1273 K and as the heating temperature continued to rise, the height of the droplet reduced gradually. When the heating temperature exceeded 1353 K, this reduction began to accelerate and finally the liquid droplet disappeared on the carbon fiber felt at 1368 K. After the experiment, these two samples were embedded into resin and sectioned perpendicular to the interface, it was found that all of the liquid droplet has penetrated into the carbon fiber felt (Figure 5.3.2a), and a number of the cross-section of the carbon fibers existed in the Al matrix by observing the COMPO images (Figure 5.3.2b). The high-magnification COMPO image shows that all of these carbon fibers were surrounded by two new reaction layers, which from inside to outside, were the gray layer and the

white layer, respectively. The white layer was found to be composed of numerous white fine granular phases, which even extended into the Al matrix and slightly mixed with the gray layer. Figure 5.3.3 shows the elemental mapping image for the Al-5mass%Ti/carbon fiber system at the vicinity of the cross-section of the carbon fiber. This figure indicated that the elements of Al and C were mainly detected at the gray layer, and a small quantity of Ti also existed in this layer. But for the white layer, only the elements of Ti and C were the main components, Al appeared to be absent. To define the exact composition of these two layer, spot analysis of EPMA was conducted at points 1 and 2, and the results were listed in Table 5.3.1. The atomic ratio of Ti:C at points 1 was approximately 1:1, which indicated that the white layer was composed of numerous TiC fine granular phases. For the gray layer, the elements of Al, Ti and C existed with non-stoichiometry at point 2, and the amount of Al and C were much richer than that of Ti. Since the gray layer was doped with a small quantity of the white layer, the Ti signal might come from TiC phase, and it was suggested that this layer was composed of massive Al_4C_3 and little TiC phases. Moreover, the results of XRD (Figure 5.3.4) indeed demonstrated the existence of both Al_4C_3 and TiC phases.

As similar with the in-situ reactive penetration of the Cu-Ti/carbon fiber felt system, all the liquid Al-Ti droplet also penetrated into the carbon fiber felt before the heating temperature reached 1373 K. Therefore, it could be suggested that in this case, the significant penetration of liquid Al-Ti droplets into the carbon fiber felt was also attributed to the addition of Ti, which was very reactive with C and formed wettable TiC layer at the interface. In fact, TiC layer was indeed formed around the carbon fiber in this study, but the formation of Al_4C_3 layer occurred at the same time, and the fact that this Al_4C_3 layer was sandwiched between TiC layer and the carbon fiber seemed to prove that

the penetration was caused by the formation of Al_4C_3 layer, not TiC layer. Therefore, the formation mechanism of the two layers in Al-Ti/graphite or carbon fiber system needed to be figured out. Generally, TiC was readily formed at the interface than Al_4C_3 according to the thermodynamic calculation in the chapter 3. After TiC layer grew to a particular size, it would fracture from the carbon fiber due to residual stresses introduced owing to volume changes upon carbide formation by re-precipitation process. As a result, liquid Al matrix began to infiltrate and reacted with the carbon fiber to form Al_4C_3. This mechanism have been confirmed by S. Seal et al. [5]. Therefore, in the Al-Ti/carbon fiber system, although Al_4C_3 layer finally lay between TiC layer and the carbon fiber, the penetration was determined by TiC layer which was formed at first.

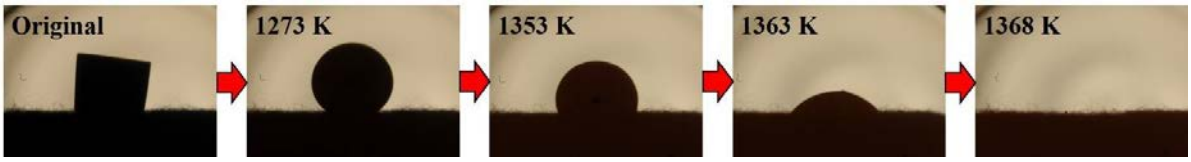

Figure 5.3.1 Representative photographs of wetting process of Al-5 mass % Ti alloy on carbon fiber felt with increasing the heating temperature

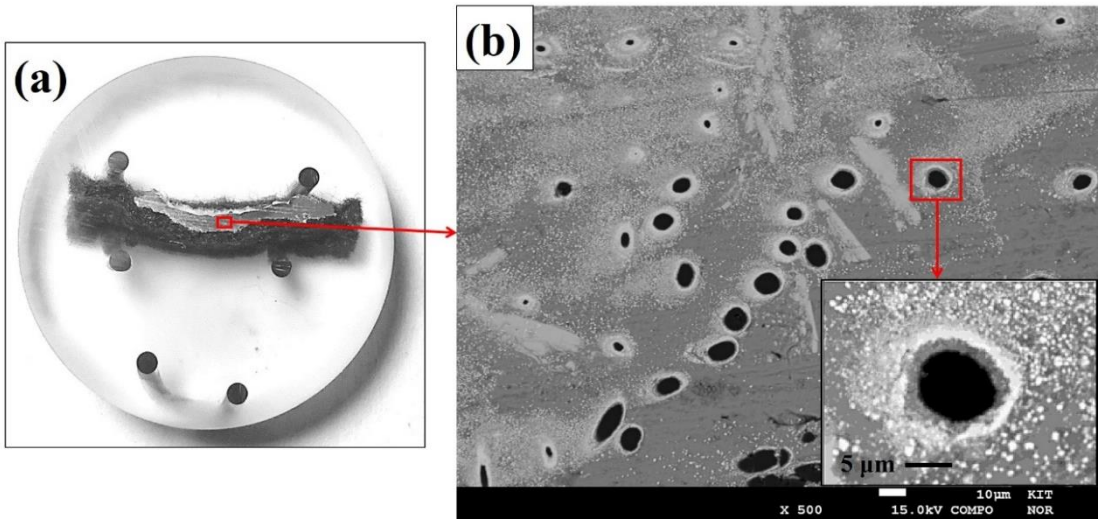

Figure 5.3.2 (a) Photographs of cross section of Al-5 mass % Ti alloy on carbon fiber felt after being embedded into resin and sectioned perpendicular to the interface. (b) Cross-sectional COMPO image at the side of the Al-Ti alloy far away from the interface

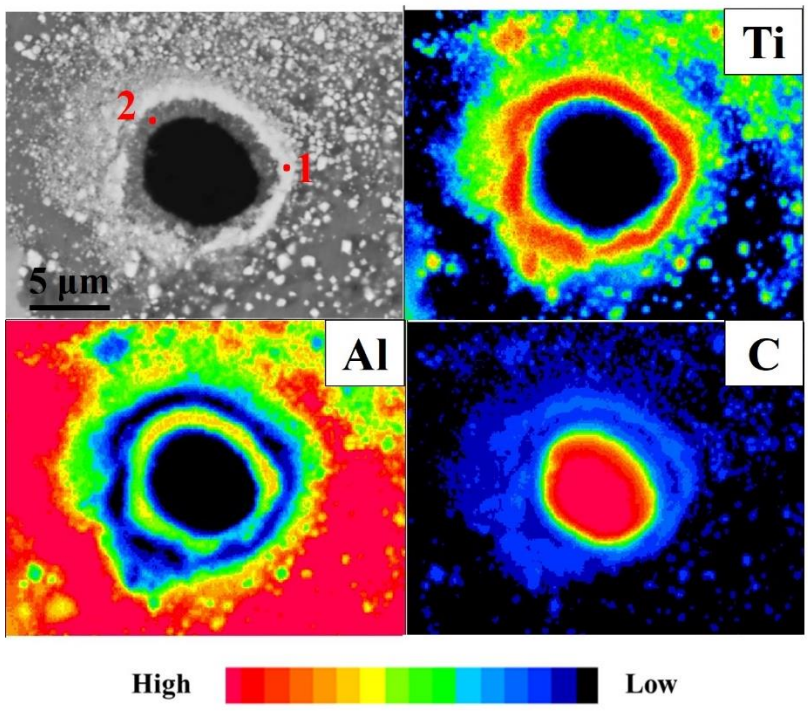

Figure 5.3.3 Elemental mapping at the vicinity of the cross-section of the carbon fiber for Al-5 mass % Ti alloy/carbon fiber felt systems

Table 5.3.1 EPMA spot analysis results at the interface region of Al-5 mass% Ti/carbon fiber systems

Points	C (at. %)	Ti (at. %)	Al (at. %)
1	47.5	48.0	4.5
2	41.2	11.2	47.6

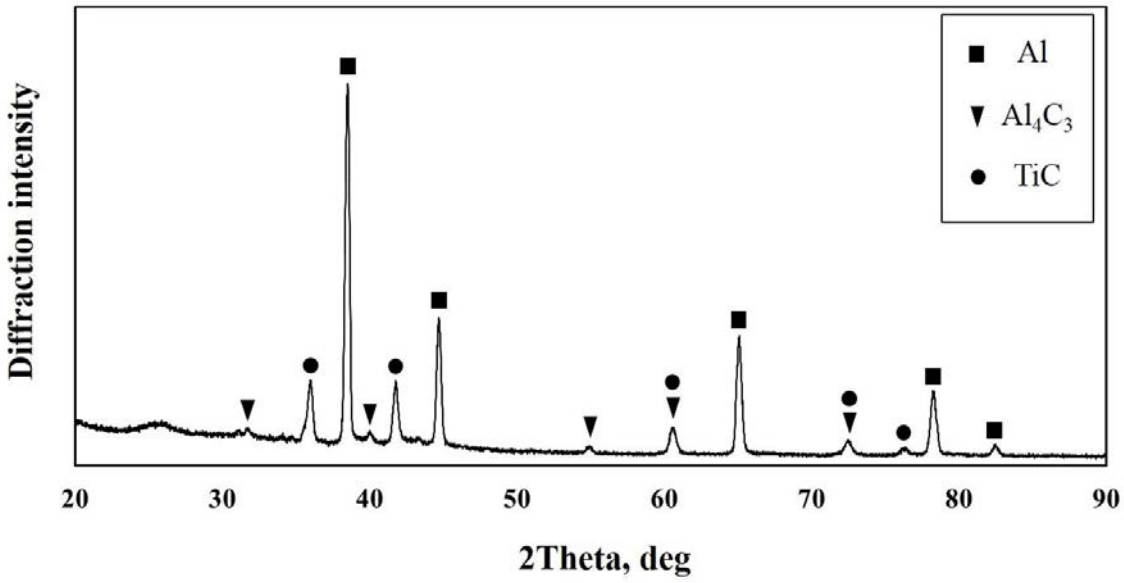

Figure 5.3.4 XRD patterns of Al-5 mass% Ti alloy/carbon fiber felt system

5.4 Composite of Carbon Fiber and Al-Si alloys

5.4.1 Experimental

The details of the carbon fiber felt used are described in the 5.2.1 section. Based on the result of the chapter 4, Al_4C_3 was formed at the interface of the Al-Si/graphite system when the addition of Si was less than 10 mass%, whereas the formation of SiC was observed at 20 mass% Si. Therefore, the Al-Si alloys containing 10 mass% Si and 20 mass% Si were selected as the alloy material in order to investigate the effect of the interfacial reaction product on the wetting. The experimental apparatus, procedure and condition were all consistent with that in the Al-Si/graphite system.

5.4.2 Results and Discussion

Figure 5.4.1 shows the representative photographs of the wetting process of the Al-10 mass % Si (Figure 5.4.1a) and Al-20 mass% Si (Figure 5.4.1b) alloys on the carbon fiber felt at 1273 K. Two totally different wetting behaviors were observed. For the Al-10mass%Si/carbon fiber system, the contact angle of the liquid droplet appeared to have no significant decrease, which the value of it decreased from 131° to 120° after holding 1 hour at 1273 K. But for the Al-20mass%Si/carbon fiber system, it was found that the height of the liquid droplet reduced rapidly and ultimately disappeared on the carbon fiber felt in only 50 seconds. After the experiments, these two samples were embedded into resin and sectioned perpendicular to the interface, it can be seen that the base of the liquid droplet slightly penetrated into the carbon fiber felt in the Al-10mass%Si/carbon fiber system (Figure 5.4.2a). The COMPO images (Figure 5.4.2b) revealed that a number of

the cross-section of the carbon fibers was observed only at the interface between the Al-10mass%Si alloy and the carbon fiber felt, and a new reaction product was formed around these cross-section of the carbon fibers. On the other hand, all of the liquid droplet penetrated into the carbon fiber felt in the Al-20mass%Si/carbon fiber system (Figure 5.4.3a), and it was found that the cross-section of the carbon fibers uniformly distributed not only at the interface of the Al-Si alloy/carbon fiber system, but also at the side of the Al-Si alloy far away from the interface (Figure 5.4.3b). In addition, the formation of a new reaction product also occurred around these cross-section of the carbon fibers. Figure 5.4.4 shows the elemental mapping images for the Al-10mass%Si/carbon fiber (Figure 5.4.4a) and Al-20mass%Si/carbon fiber (Figure 5.4.4b) systems at the vicinity of the cross-section of the carbon fiber. The elements of Al and C were the main components of the reaction product for the Al-10mass%Si/carbon fiber system, whereas only the elements of Si and C existed in the reaction product for the Al-20mass%Si/carbon fiber system. Combined with the results of spot analysis conducted at points 1~4 shown in Table 5.4.1, the atomic ratio of Al:C in the Al-10mass%Si/carbon fiber system and Si:C in the Al-20mass%Si/carbon fiber system were almost 4:3 and 1:1, respectively, suggesting Al_4C_3 and SiC compounds. The XRD results (Figure 5.4.5) conducted at the cross section of specimens revealed that SiC was indeed detected in the Al-20mass%Si/carbon fiber system. The absence of Al_4C_3 in the Al-10mass%Si/carbon fiber system was attributed to the fact that the thickness of the penetrated liquid alloy was too thin to be detected probably. Therefore, it was concluded that the reaction product around the carbon fibers were consistent with the results obtained in the Al-Si/graphite systems.

According to the results given in the chapter 4, both the Al-10mass%Si/graphite and Al-20mass%Si alloys/graphite couples were verified as reactive wetting systems, and the

final contact angle of the liquid droplet on the graphite was actually governed by that of the liquid droplet on the interfacial reaction layer, which for the Al-10mass%Si/graphite couple, was Al_4C_3 layer, and for the Al-20mass%Si/graphite couple, was SiC layer. The contact angle of the Al-20%Si alloys on SiC layer have been reported to be 15° at 1273 K in chapter 4, indicating a remarkably good wetting. Therefore, in this study, once the formation of SiC occurred at the interface between the melt and the outermost surface of the carbon fiber felt, all of the liquid Al-Si droplet would then penetrated into the pores of carbon fiber felt rapidly. For the contact angle of Al-10mass%Si alloys on Al_4C_3 layer, Ferro et al. [6] have reported that the contact angle of Al-5.1mass%Si on Al_4C_3 substrate was approximately 60° at 1273 K. Although the addition amount of Si was lower than 10mass% added in this work, we can roughly consider that 60° of the contact angle was equal to that of Al-10mass%Si alloy on Al_4C_3, since adding less than 13mass% of Si in Al did not affect the reaction product and wetting of Al/Al_4C_3 systems. However, the relatively large contact angle did not appear to be the reason of that the penetration almost did not occur in the Al-10mass%Si/graphite system, because 60° of the contact angle also indicated a wetting system. Therefore, other theories were required to explain this phenomenon. G. Kaptay et al. [7] have proposed a penetration mode for liquid melt/porous material systems, which the porous material was built from closely packed spherical particles. They concluded that the penetration should link with the contact angle of liquid melt on the solid material, and it occurred spontaneously only when the contact angle was less than 50.7°. Although this penetration mode did not fully fit the liquid melt/carbon fiber felt systems in this work, it qualitatively illustrated that a critical contact angle was required for penetration. From this discussion, it was clear that the contact angle of the Al-10mass%Si/Al_4C_3 system was higher than the critical contact angle, so that after an

Al_4C_3 layer was formed on the outermost surface of the carbon fiber felt, the liquid droplet did not continue to penetrate.

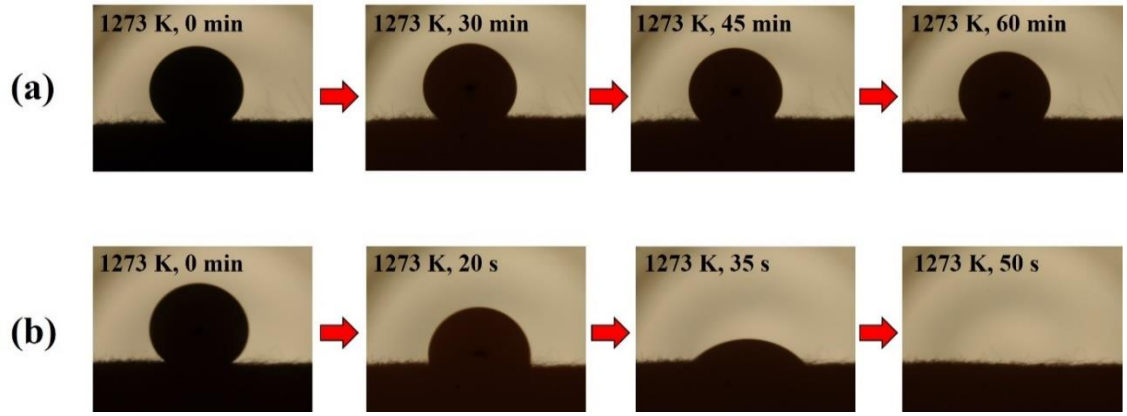

Figure 5.4.1 Representative photographs of the wetting process of (a) Al-10 mass % Si and (b) Al-20 mass% Si alloys on carbon fiber felt at 1273 K

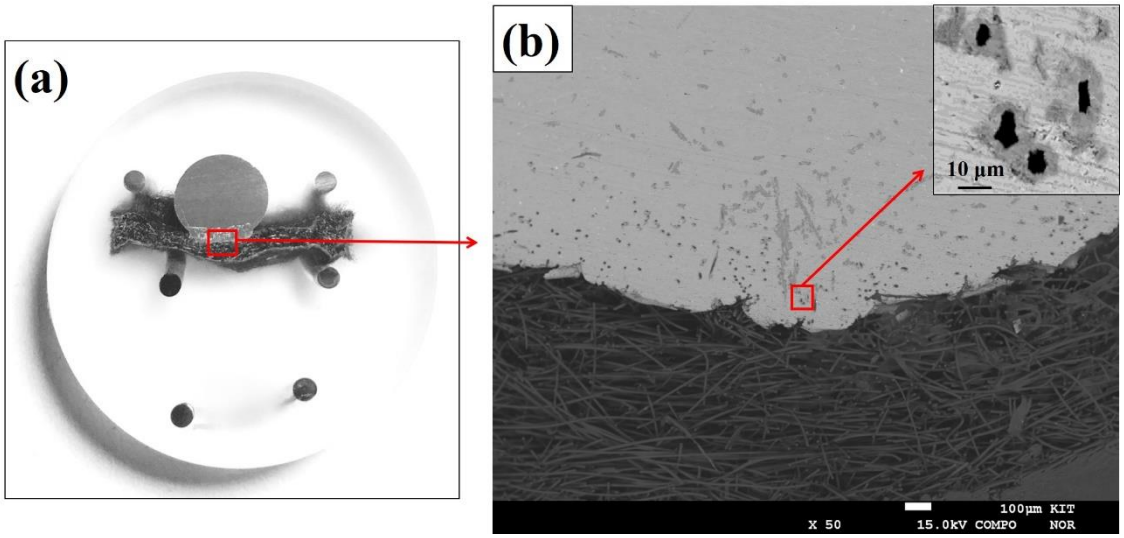

Figure 5.4.2 (a) Photographs of cross section of Al-10 mass % Si alloys on carbon fiber felt after being embedded into resin and sectioned perpendicular to the interface. (b) Cross-sectional COMPO image at the interface of the Al-10 mass %Si alloy/carbon fiber felt system

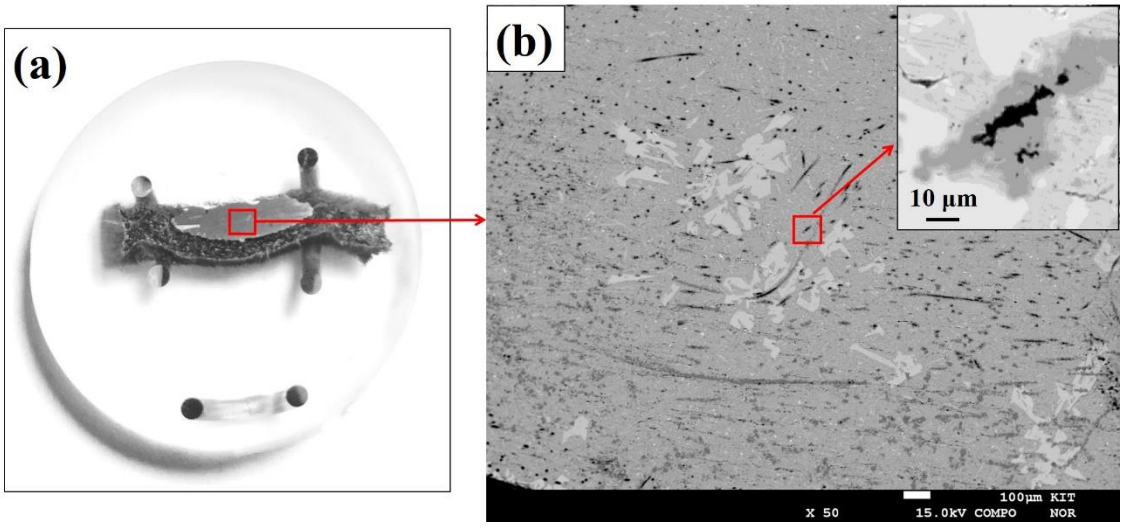

Figure 5.4.3 (a) Photographs of cross section of Al-20 mass % Si alloys on carbon fiber felt after being embedded into resin and sectioned perpendicular to the interface. (b) Cross-sectional COMPO image at the side of the Al-Si alloy far away from the interface

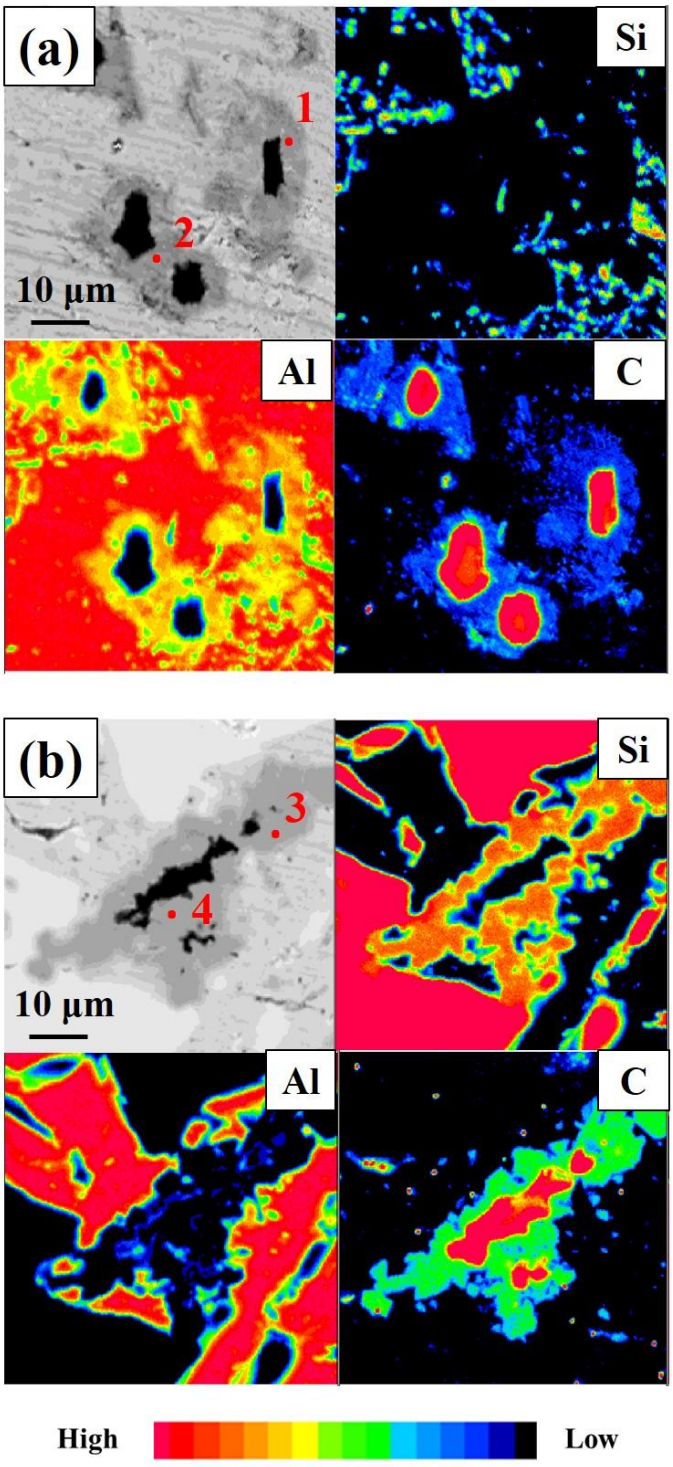

Figure 5.4.4 Elemental mapping at the vicinity of the cross-section of the carbon fiber: (a) Al-10 mass % Si alloy/carbon fiber felt system; (b) Al-20 mass % Si alloy/carbon fiber felt system.

Table 5.4.1 EPMA spot analysis results at the interface region of Al-Si/carbon fiber systems

Alloy	Points	C (at. %)	Si (at. %)	Al (at. %)
Al-10mass%Si	1	44.0	0.7	55.3
	2	42.8	0.4	56.9
Al-20mass%Si	3	50.5	47.8	1.7
	4	47.5	49.6	2.9

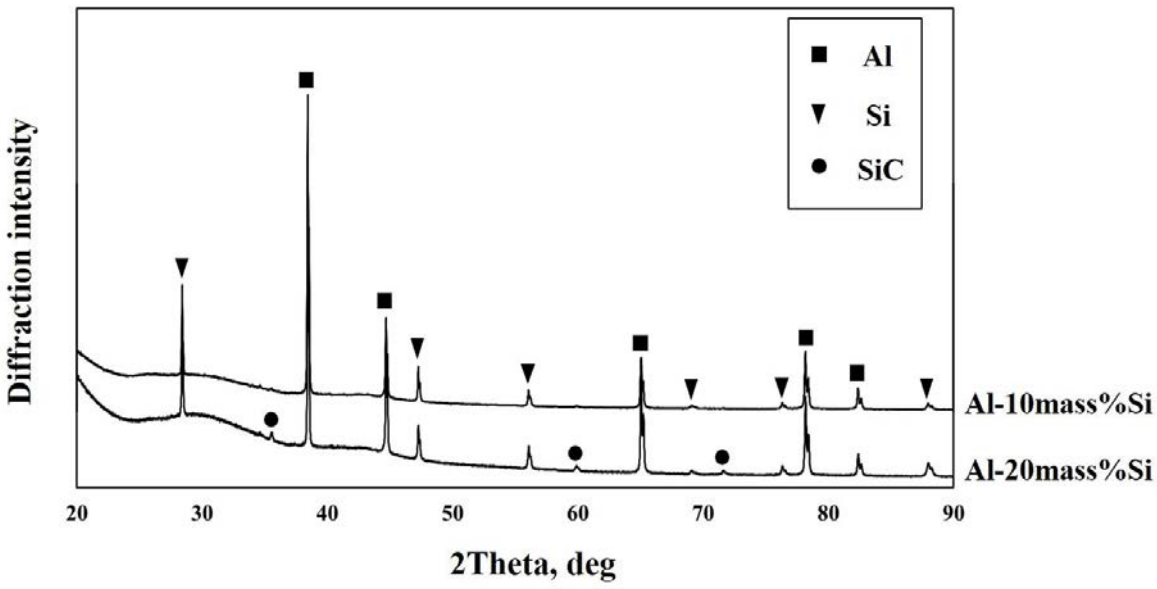

Figure 5.4.5 XRD patterns of Al- Si alloy/carbon fiber felt systems

5.5 Conclusions

In this chapter, the composite of Cu-Ti (10 mass% Ti), Al-Ti (5 mass% Ti), Al-Si (10 and 20 mass% Si) alloys and carbon fiber was investigated by using the sessile drop

method under vacuum. The results showed that the reaction product formed at the interface of each alloys/carbon fiber systems was consistent with that formed at the interface of each alloys/graphite systems, correspondingly. For the Cu-10mass%Ti/carbon fiber and Al-5mass%Ti/carbon fiber systems, the liquid alloy droplet completely penetrated into the carbon fiber felt spontaneously before the heating temperature reached 1373 K, due to the porous structure of the carbon fiber felt and the formation of wettable TiC at the interface between liquid alloys and the carbon fiber. For the Al-Si/carbon fiber systems, spontaneous penetration of the liquid droplet only occurred at 20mass%Si, and it was attributed to that the reaction product of the Al-Si/carbon fiber systems was SiC at 20mass%Si and Al_4C_3 at 10mass%Si, respectively, and the contact angle of liquid Al-Si droplet on SiC layer was lower than the critical contact angle of penetration, whereas that on Al_4C_3 layer was higher than the critical contact angle of penetration. The great penetrability of liquid alloy in the carbon fiber without external pressure and the uniform distribution of the carbon fiber in the alloy matrix without dispersant illustrated that using the carbon fiber instead of the graphite was an ideal way during the process of production and application.

References

[1] Dong S R, Tu J P, Zhang X B. An investigation of the sliding wear behavior of Cu-matrix composite reinforced by carbon nanotubes[J]. Materials Science and Engineering: A, 2001, 313(1): 83-87.

[2] Kuzumaki T, Miyazawa K, Ichinose H, et al. Processing of carbon nanotube reinforced aluminum composite[J]. Journal of Materials Research, 1998, 13(09): 2445-2449.

[3] Feng Y, Yuan H L, Zhang M. Fabrication and properties of silver-matrix composites reinforced by carbon nanotubes[J]. Materials Characterization, 2005, 55(3): 211-218.

[4] Bakshi S R, Lahiri D, Agarwal A. Carbon nanotube reinforced metal matrix composites-a review[J]. International Materials Reviews, 2010, 55(1): 41-64.

[5] Seal S, Warwick T, Sobczak N, et al. A scanning photoemission microscope (SPEM) to study the interface chemistry of AlTi/C system[J]. Journal of materials science letters, 2000, 19(2): 123-126.

[6] Ferro A C, Derby B. Wetting behaviour in the Al-Si/SiC system: interface reactions and solubility effects[J]. Acta metallurgica et materialia, 1995, 43(8): 3061-3073.

[7] Kapthy G, Stefanescu D M. Theoretical Analysis of the Effect of Oxygen on the Penetration Factor in the Iron/Silica System[J]. AFS Transactions, vol 100, 1992 (1992).

Chapter 6 Surface Tension of Liquid Cu-Ti, Al-Ti and Al-Si Alloys

6.1 Introduction

A precise knowledge of the surface tension of liquid metals and alloys is increasingly important as progress is made in numerical simulations of complex processes [1], such as casting, welding, crystal growth and surface treatment. Especially, for a full analysis of capillary systems, the knowledge of adhesion characteristics (e.g. work of adhesion and adhesion tension) is required, and the surface tension value is necessary for these calculations according to the Young–Dupre equation [2].

The surface tension of most liquid metals and alloys have been determined experimentally. In general, the measurement method of the surface tension mainly includes sessile drop or pendant drop method, capillary height method, wilhelmy plate method and maximum bubble pressure method. Among these, the sessile drop method have been extensively used to measure the surface tension of liquid metals because of its easy-operating and the accuracy of the measuring results at high temperature [3]. However, due to the difficulty of maintaining uncontaminated liquid alloys surfaces, and the strong reaction proneness between liquid alloys and contacting substrates at high temperatures, the accurate measurement of the surface tension of liquid alloys with high melting point in sessile drop method is a very challenging task by using the sessile drop method, and this is also an important reason that the earlier measured data of the surface tension exhibits considerable scatter [4]. Therefore, as a factor that can be selected artificially,

using a contacting substrate with chemical inertness is effective way to obtain relatively accurate values of the surface tension of liquid alloys. In this chapter, Yttria Partially-Stabilized Zirconia (Y-PSZ, ZrO_2 stabilized with 3 mol% Y_2O_3) was selected as the contacting substrate to investigate the surface tension of liquid Cu-Ti, Al-Ti and Al-Si alloys as a function of composition by using the sessile drop method, and this study contributes to providing useful and reliable data for any metallurgical and materials-related process.

6.2 Experimental

6.2.1 Alloys materials

Three different alloys were used for the measurement of the surface tension: Cu-Ti, Al-Ti and Al-Si alloys. The composition of each alloys were consistent with that used for the wetting experiment, which included the Cu-Ti alloys with Ti content of 4, 6 and 10mass%, the Al-Ti alloys with Ti content of 1, 3 and 5mass%, and the Al-Si alloys with Si content of 0, 6, 10 and 20mass%. All kinds of alloys was placed on the substrate in the placement state A and the details of this placement state are described in the relevant chapter. Before experiments, the samples were polished by emery papers from 400 to 2000 grit and cleaned with ethanol in order to prevent further oxidation.

6.2.2 Substrate for surface tension

The measurement of the surface tension using the sessile drop method is determined by the profile of the molten drop placed on a flat and non-wetting substrate [5]. Therefore,

the final result of the surface tension will be affected by the sharp of the molten drop, and a perfect spherical profile of the drop is desirable in order to obtain a higher accuracy of the value of the surface tension. Since graphite could react with the alloys containing the element of Ti, Al and Si at high temperature, the initially flat and smooth surface of graphite substrate would be destroyed, which might result in the deformation of the drop and affect the measurement. Therefore, in this study, we use the Yttria Partially-Stabilized Zirconia (Y-PSZ, ZrO2 stabilized with 3 mol% Y_2O_3) instead of the graphite because the Y-PSZ with high chemical inertness and stability is very difficult to react with Ti, Al or Si in a wide temperature range [6]. Here, it is necessary to discuss the possibility of the reaction between these three element and Y-PSZ substrate. For the Ti element, due to there are many kinds of titanium oxide, such as TiO_2 (ANATASE), TiO_2 (RUTILE), Ti_4O_7(s), Ti_3O_5(s), Ti_2O_3(s) and TiO(s), we should calculate the standard Gibbs free energy ΔG° when titanium oxide is formed in all cases. Based on the following thermodynamic calculation:

$Ti(l) + ZrO_2(s) = TiO_2(s) + Zr(s)$ $\Delta G^{\circ}_{(1373K)} = +144$ kJ (ANATASE) [7]

$\Delta G^{\circ}_{(1373K)} = +138$ kJ (RUTILE) [7]

$\frac{8}{7}Ti(l) + ZrO_2(s) = \frac{2}{7}Ti_4O_7(s) + Zr(s)$ $\Delta G^{\circ}_{(1373K)} = +105$ kJ [7]

$\frac{6}{5}Ti(l) + ZrO_2(s) = \frac{2}{5}Ti_3O_5(s) + Zr(s)$ $\Delta G^{\circ}_{(1373K)} = +93$ kJ [7]

$\frac{4}{3}Ti(l) + ZrO_2(s) = \frac{3}{2}Ti2O3(s) + Zr(s)$ $\Delta G^{\circ}_{(1373K)} = +70$ kJ [7]

$2Ti(l) + ZrO_2(s) = 2TiO(s) + Zr(s)$ $\Delta G^{\circ}_{(1373K)} = +6$ kJ [7]

$Ti(l) + \frac{2}{3}Y_2O_3(s) = TiO_2(s) + \frac{4}{3}Y(s)$ $\Delta G^{\circ}_{(1373K)} = +312$ kJ(ANATASE) [7]

$\Delta G^{\circ}_{(1373K)} = +306$ kJ (RUTILE) [7]

$\frac{8}{7}Ti(l) + \frac{2}{3}Y_2O_3(s) = \frac{2}{7}Ti_4O_7(s) + \frac{4}{3}Y(s)$ $\Delta G^{\circ}_{(1373K)} = +272$ kJ[7]

$\frac{6}{5}Ti(l) + \frac{2}{3}Y_2O_3(s) = \frac{2}{5}Ti_3O_5(s) + \frac{4}{3}Y(s)$ $\Delta G^{\circ}_{(1373K)} = +260$ kJ[7]

$\frac{4}{3}Ti(l) + \frac{2}{3}Y_2O_3(s) = \frac{2}{3}Ti_2O_3(s) + \frac{4}{3}Y(s)$ $\Delta G^{\circ}_{(1373K)} = +238$ kJ[7]

$2Ti(l) + \frac{2}{3}Y_2O_3(s) = 2TiO(s) + \frac{4}{3}Y(s)$ $\Delta G^{\circ}_{(1373K)} = +173$ kJ[7]

All above the standard Gibbs free energy are positive values, which means that these reactions can hardly occur at 1373K and the surface of the Y-PSZ substrate can remain flat and smooth. For the element of Al and Si, the positive values of the ΔG^{o} can also be obtained, as expressed in the following thermodynamic calculation:

$2Al (l) + \frac{3}{2}ZrO2(s) = Al_2O_3(s) + \frac{3}{2}Zr(s)$ $\Delta G^{\circ}_{(1273K)} = +17$ kJ [7]

$Si (l) + ZrO_2(s) = SiO_2(s) + Zr(s)$ $\Delta G^{\circ}_{(1273K)} = +174$ kJ [7]

$2Al (l) + Y_2O_3(s) = Al_2O_3(s) + 2Y(s)$ $\Delta G^{\circ}_{(1273K)} = +268$ kJ [7]

$3Si (l) + \frac{2}{3}Y_2O_3(s) = SiO_2(s) + \frac{4}{3}Y(s)$ $\Delta G^{\circ}_{(1273K)} = +342$kJ [7]

Therefore, at least in theory, it is expected that using the Y-PSZ substrate can be maximized be ensure correct results.

The Y-PSZ substrate (purity: 99.5 mass %) with 20 mm in square and 3 mm in

thickness was prepared by cold isostatic pressing using a pressure of 147 MPa, then was sintered at 1723 K for 3 hours. After polishing by diamond paste, the average roughness *R*a of the surface measured by 3D-SEM was 0.0025 μm ± 0.001 μm, indicating a highly polished surface.

6.2.3 Experimental apparatus and procedure

The surface tension of liquid alloys was measured by using the same experimental apparatus and method as the measurement of the wettability, and the experimental temperature were set to 1373 K for the Cu-Ti and Al-Ti alloys, and 1273 K for the Al-Si alloy. As for the setting of the image observation system in all the experiments, the focal distance must be fixed in order to give a constant magnification of the photographed image, and the focus was adjusted by changing the distance between the liquid drop and the camera fixed on a positioning stage, which could be moved three-dimensionally. This study adopted the algorithm put forward by Rotenberg et al. [8]. Therefore, after the experiments, the profile of the liquid drop was extracted from the photographs by an image analysis software and then was imported into a computer with a digitizer, to determine the curve giving best fit between the numerical solution to the classical Laplace's equation and the observed experimental drop profile. The magnification was determined by a picture of a standard steel ball (5 mm in diameter) taken with the same camera in the same focal distance. In the sessile drop method, the density was necessary for calculating the surface tension. Here, the density (g/cm^3) of the liquid Cu-Ti alloys reported by V. Krasovskyy et al. [9] and the density of the liquid Al-Ti alloys reported by M. Yokota et al. [10] were used in this study. For the Al-Si alloys, the density of it was investigated by D. Poirier et al. [11], as expressed by the following equation:

$$\rho = \left(0.3970 - 1.04 \times 10^{-3} C_{Si} + 4.0924 \times 10^{-5}(T - 273)\right)^{-1} \quad (6.2.1)$$

where C_{Si} was the weight percent of Si and T was the experimental temperature.

6.3 Results and Discussion

6.3.1 Surface tension of liquid Cu-Ti alloys

Table 6.3.1 shows the measured results of the surface tension of liquid Cu-Ti alloys in the present work. The data show that the surface tension increased from 1078 mN/m to 1237 mN/m with the increasing the Ti content from 4mass% to 10mass% at 1373 K. To estimate the effect of Ti content on the surface tension of the Cu-Ti alloy more accurately, the surface tension of other compositions of Cu-Ti alloys were required. S. Gruner et al. [12] have measured that the surface tension of pure Cu was approximately 980 mN/m in a high vacuum at 1373K. For pure Ti, the temperature dependence of the surface tension of liquid Ti was given by the following equation proposed by J. Zhu et al. [13]:

$$\gamma_{\mathrm{Ti}}(\mathrm{mN/m}) = 1962 - 0.26\mathrm{T(K)} \quad (6.3.1)$$

Where T was the experimental temperature. Therefore, the surface tension of liquid Ti at 1373 K was calculated to be 1605 mN/m. Moreover, Mao et al. [14] investigated that the surface tension of liquid Cu-20mass%Ti and Cu-30mass%Ti alloys were 1263 and 1417 mN/m, respectively at 1273 K. Although the experimental temperature were somewhat different from that of this work, its effect on the surface tension of liquid alloys was very

small and these data could be referenced roughly. Based on the above data, Figure 6.3.1 that shows the surface tension of liquid Cu-Ti alloys as a function of titanium content was drawn. Clearly, the surface tension of liquid Cu-Ti alloys increased monotonously with increasing the Ti content, and as it was common for binary alloys, the surface tension values of the Cu–Ti alloys ranged between the data of pure Cu and Ti. Moreover, it was noted that the composition dependence of the surface tension (see the dotted chain line in Figure 6.3.1) showed a large upward deviation from the linearity between the surface tension of pure Cu and Ti. A rule was given by Tanaka et al. [15] that could explain this phenomenon. They suggested that for binary alloys, in alloys with a positive deviation of the activity from the ideal solution in the bulk, the surface tension deviated negatively from the ideal solution, whereas in alloys with a negative deviation of the activity from the ideal solution in the bulk, the surface tension had the tendency to show a positive deviation from the ideal solution. Due to the existence of many intermetallic compounds according to the Cu-Ti binary phase diagram [16], the activity of Cu-Ti alloys presumably deviated negatively from the ideal solution. Therefore, the surface tension of liquid Cu-Ti alloys would show a positive deviation from the ideal solution, which was in agreement with the result obtained in this work.

Table 6.3.1 Surface tension for Cu-Ti alloys measured at 1373 K

Alloy compositions	Surface tension (mN/m)	Standard deviation (mN/m)
Cu-4mass%Ti	1078	41.1
Cu-6mass%Ti	1113	43.7
Cu-10mass%Ti	1237	31.3

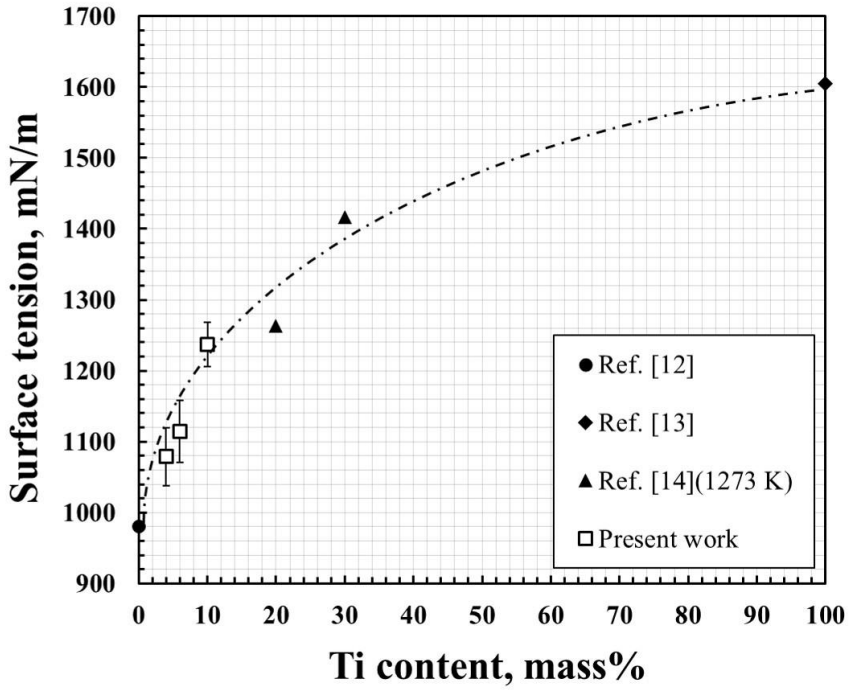

Figure 6.3.1 Surface tension of Cu-Ti alloys as a function of titanium content

6.3.2 Surface tension of liquid Al-Ti alloys

Table 6.3.2 shows the measured results of the surface tension of liquid Al-Ti alloys

in the present work. It was found that the surface tension decreased from 677 mN/m to 795 mN/m with the increase of Ti content from 1mass% to 5mass%. Rhee et al. [17] have reported that the temperature dependence of the surface tension of liquid Al could be best fitted by the following equation:

$$\gamma_{\mathrm{Al}}(\mathrm{mN/m}) = 948 - 0.202\mathrm{T(K)} \tag{6.3.2}$$

Where T was the experimental temperature. According to this equation, the surface tension of pure Al was calculated to be 670 mN/m at 1373 K. In addition, by referring the surface tension data for liquid Al-55mass%Ti alloy taken from the Ref. [18] and pure Ti calculated by using the equation (6.3.1), we could make Figure 6.3.2 that shows the surface tension of liquid Al-Ti alloys as a function of titanium content. The results basically were in good accordance with the principle that the surface tension values of the binary alloys ranged between the data of two pure elements, and we found that the surface tension of liquid Al-Ti alloys increased monotonously with increasing the Ti content. However, the values of the surface tension measured in this work were significantly lower than those measured by M. Yokota et al. [10], who reported that the surface tension values of liquid Al-Ti alloys with 1 ~ 5mass%Ti at 1373 K were in the range of 820 ~ 900 mN/m. In fact, at the high temperature of 1373 K, due to the evaporation of Al_2O gas according to the reaction (4.3.1), the reduction of the Al content in the Al-Ti alloy was inevitable. By comparing the total mass of the samples (including alloy and substrate) before and after the experiment, about 0.1~0.15g of mass reduction was indeed observed in all the experiments, and it would result in the increase of the actual density of liquid Al-Ti alloys. Therefore, since the density of the Al-Ti alloy used to calculate the values of the surface tension was set as a constant value, the calculated values of the surface tension were

smaller than the actual value of that according to the Bashforth and Adams equation [19]:

$$\gamma_{LV} = \frac{g\rho b^2}{\beta} \tag{6.3.3}$$

where γ_{LV} was the surface tension, g was the gravitational acceleration, ρ was the liquid density, and β was a shape factor of the liquid drop.

Table 6.3.2 Surface tension for Al-Ti alloys measured at 1373 K

Alloy compositions	Surface tension (mN/m)	Standard deviation (mN/m)
Al-1mass%Ti	677	38.2
Al-3mass%Ti	727	59.6
Al-5mass%Ti	795	35.0

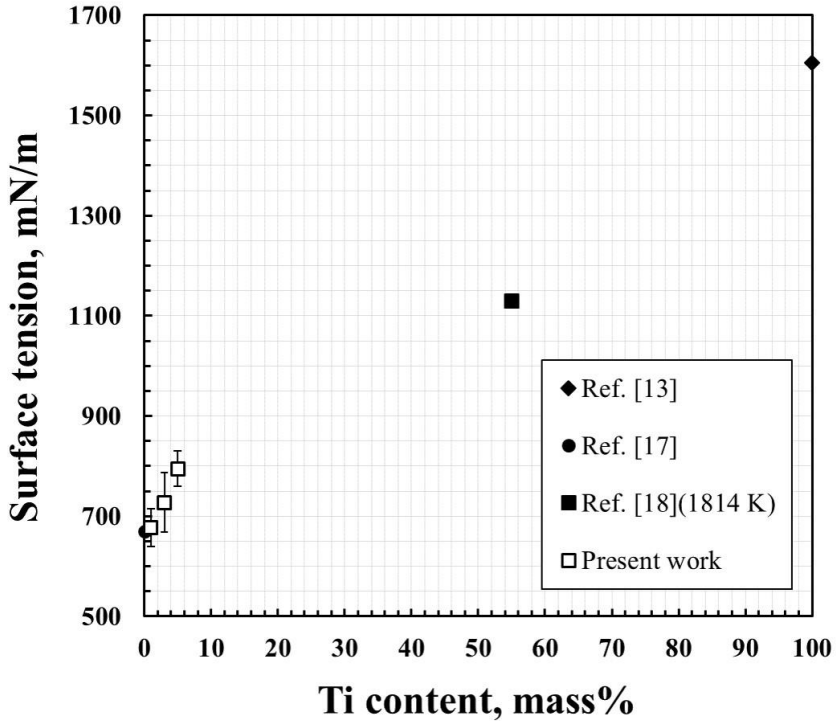

Figure 6.3.2 Surface tension of Al-Ti alloys as a function of titanium content

6.3.3 Surface tension of liquid Al-Si alloys

Table 6.3.3 shows the measured results of the surface tension of liquid Al-Si alloys in the present work. For the surface tension of pure Al, plenty of earlier studies [20-23] agreed that its value was in the range of 800 to 900 mN/m, which corresponded to a visible oxide film formed on the surface of liquid drop. Goumiri et al. [24] particularly investigated that the relationship between the surface tension of Al drop and the oxide thickness by means of the auger electron microscopy. They found that even a single monolayer could decrease the surface tension from approximately 1050 to 900 mN/m. Therefore, the value of 902 mN/m for pure Al measured in this work was basically within a reasonable range, which corresponded to an oxidized surface. The surface tension of liquid Al-Si alloys

exhibited lower values than that of Al in this work. Figure 6.3.3 shows the surface tension of liquid Al-Si alloys as a function of silicon content, which the data of liquid Si, about 728 mN/m at 1273 K, was estimated by the following equation proposed by Shergin et al. [25].

$$\gamma_{\mathrm{Si}}(\mathrm{mN/m}) = 791 - 0.05\mathrm{T(K)} \tag{6.3.4}$$

It was found that the surface tension of liquid Al-Si alloys decreased with increasing the Si content, and its values ranged between the data for pure Al and Si. Goicoechea et al. [26] have reported that the surface tension of liquid Al-Si alloys decreased from 866 to 838 mN/m as Si content increased from 1 to 19 mass % using maximum bubble pressure (MBP) method at 973 K. These values were higher than those measured in this work. This difference might be attributed to the different measured method of the surface tension. Generally, the measurement of the surface tension in the MBP method would not be affected by any impurities attached on the drop surface (i.e., the oxide film), and the surface was newly created for each bubble [27], thus it was believed that the MBP method would give more reliable and higher values for Al and Al alloys as compared with the sessile drop method. On the other hand, in our experiment, since both Al and Si were readily oxidized especially under the low vacuum (1.5 Pa) in this work, the measurement of the surface tension of liquid Al and Al-Si alloys should be associated with the oxidation film formed on the liquid drop. For pure Al, the oxidation reaction was as follows:

$$2\mathrm{Al(l)} + \frac{3}{2}\mathrm{O_2(g)} = \mathrm{Al_2O_3(s)} \qquad \Delta G^{\circ}_{(1273K)} = -635\ \mathrm{kJ}\ [7] \tag{6.3.5}$$

but for Al-Si alloys, due to the addition of Si, Al and Si would simultaneously react with

oxygen to form Mullite ($3Al_2O_3 \cdot 2SiO_2$) according to the following reaction equation:

$$6Al(l) + 2Si(l) + \frac{13}{2}O_2(g) = 3Al_2O_3 \cdot 2SiO_2(s) \qquad \Delta G^{\circ}_{(1273K)} = -5325\ \text{kJ}\ [7] \tag{6.3.6}$$

Because the activities of Al and Si in the Al–Si liquid have almost linear relations with respect to their contents, the molar mass of Al and Si could be employed as their activities [28]. Therefore, by taking the Al-20mass%Si alloys for instance, the equilibrium oxygen partial pressure of the reaction (6.3.5) and (6.3.6) was calculated to be approximately 1.3×10^{-30} Pa and 4.9×10^{-29} Pa, respectively, which indicated that both reactions would occur under this experimental condition (1.5 Pa). However, at 1273 K, it was expected that both the Al_2O_3 and Mullite films would be disrupted then, according to the following reaction equations:

$$\frac{4}{3}Al(l) + \frac{1}{3}Al_2O_3(s) = Al_2O(g) \qquad \Delta G^{\circ}_{(1273K)} = +189\ \text{kJ}\ [7] \tag{6.3.7}$$

$$3Al_2O_3 \cdot 2SiO_2(s) + 16Al(l) = 11Al_2O(g) + 2SiO(g)$$

$$\Delta G^{\circ}_{(1273K)} = +2318\ \text{kJ}\ [7] \tag{6.3.8}$$

It can be seen that the equilibrium partial pressure of Al_2O gas in the reaction (6.3.7) was calculated to be 1.7×10^{-3} Pa, while that of Al_2O and SiO gas in the reaction (6.3.8) were 3.3×10^{-5} Pa and 0.6×10^{-5} Pa, respectively. The equilibrium partial pressure in the reaction (6.3.8) was about two orders of magnitude lower than that in the reaction (6.3.7), which demonstrated that the Al_2O_3 film formed on the surface of liquid Al would disappear faster than the Mullite film formed on the surface of liquid Al-Si alloy at 1273 K.

Therefore, these results could explain the fact that the surface tension of liquid Al measured in this work did not deviate too much from the normal value, but its values of liquid Al-Si alloys were significantly lower than those measured by Goicoechea et al.

Table 6.3.3 Surface tension for Al-Si alloys measured at 1273 K

Alloy compositions	Surface tension (mN/m)	Standard deviation (mN/m)
Pure Al	902	33.0
Al-6mass%Si	801	2.9
Al-10mass%Si	770	3.8
Al-20mass%Si	744	1.6

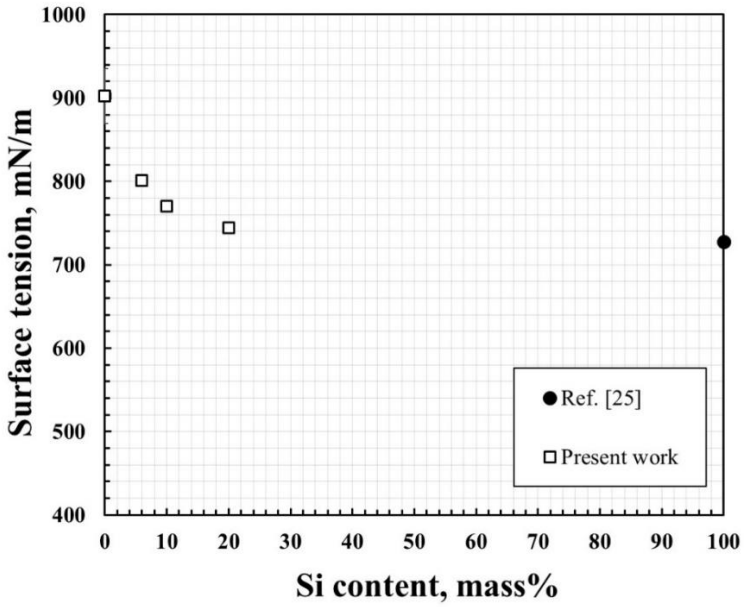

Figure 6.3.3 Surface tension of Al-Si alloys as a function of silicon content

6.4 Conclusions

In this chapter, the surface tension of liquid Cu-Ti, Al-Ti and Al-Si alloys as a function of composition was measured on the Y-PSZ substrate by using the sessile drop method. According to the results, the surface tension of both liquid Cu-Ti and Al-Ti alloys monotonously increased with increasing the content of Ti. On the contrary, with the increase of the content of Si, the surface tension of liquid Al-Si alloy showed a monotonous decrease. With the change in the composition, the surface tension values of three kinds of alloys varied within a reasonable range, since these values were between the corresponding values of two pure elements. The sessile drop method using the Y-PSZ substrate with chemical inertness could be successfully used to measure the surface tension of the alloys containing highly chemically active elements.

Figure 6.3.1 used in this chapter has also been published in the following paper: "Wettability, surface tension and work of adhesion of Cu-Ti alloys on Yttria Partially-Stabilized Zirconia at 1273K". Weiji Mao, Hiroki Sannamiya, Nobuya Shinozaki and Toshifumi Ogawa. Advanced Materials Research, 2014, 941: 102-107.

References

[1] Hepp E, Neves S, Egry I. High precision measurement of thermophysical properties for liquid metals–Requirements for simulation of foundry processes[J]. Modeling of Casting, Welding and Advanced Solidification Processes IX, Eds.: PR Sahm, PN Hansen and JG Conley, Aachen, 2000: 697-703.

[2] Dezellus O, Eustathopoulos N. Fundamental issues of reactive wetting by liquid metals[J]. Journal of Materials Science, 2010, 45(16): 4256-4264.

[3] Cheng P, Li D, Boruvka L, et al. Automation of axisymmetric drop shape analysis for measurements of interfacial tensions and contact angles[J]. Colloids and Surfaces, 1990, 43(2): 151-167.

[4] Iida T, Guthrie R I L. The physical properties of liquid metals[J]. Clarendon Press, Walton Street, Oxford OX 2 6 DP, UK, 1988., 1988.

[5] Anson J P, Drew R A L, Gruzleski J E. The surface tension of molten aluminum and Al-Si-Mg alloy under vacuum and hydrogen atmospheres[J]. Metallurgical and Materials Transactions B, 1999, 30(6): 1027-1032.

[6] Hannink R H J, Kelly P M, Muddle B C. Transformation toughening in zirconia‐containing ceramics[J]. Journal of the American Ceramic Society, 2000 (83): 461-487.

[7] Barin I. Thermochemical Data of Pure Substances, Thermochemical Data of Pure Substances[M]. Wiley-VCH, 1997.

[8] Rotenberg Y, Boruvka L, Neumann A W. Determination of surface tension and contact angle from the shapes of axisymmetric fluid interfaces[J]. Journal of colloid and interface science, 1983, 93(1): 169-183.

[9] Krasovskyy V, Naidich Y. Surface tension and specific volume of copper–titanium melts measured by the sessile drop method[J]. Journal of adhesion science and technology, 2004, 18(4): 465-471.

[10] Yokota M, Fujii T, Nagai H, et al. Wettability of Sintered Al2O3 Plates by Aluminum and Al--Ti Alloys[J]. J. Jpn. Soc. Powder Powder Metall., 1989, 36(4): 418-425.

[11] Yeum K, Poirier D. Predicting microporosity in aluminum alloys[J]. Light Met, 1988: 469-76.

[12] Gruner S, Köhler M, Hoyer W. Surface tension and mass density of liquid Cu–Ge alloys[J]. Journal of Alloys and Compounds, 2009, 482(1): 335-338.

[13] Zhu J, Kamiya A, Yamada T, et al. Surface tension, wettability and reactivity of molten titanium in Ti/yttria-stabilized zirconia system[J]. Materials Science and Engineering: A, 2002, 327(2): 117-127.

[14] Mao W J, Sannomiya H, Shinozaki N, et al. Wettability, surface tension and work of adhesion of Cu-Ti alloys on Yttria Partially-Stabilized Zirconia at 1273K[C]//Advanced Materials Research. 2014, 941: 102-107.

[15] Tanaka T, Hara S. Thermodynamic evaluation of binary phase diagrams of small particle systems[J]. Zeitschrift für Metallkunde, 2001, 92(5): 467-472.

[16] Murray J L. The Cu− Ti (Copper-Titanium) system. Bull. Alloy Phase Diagrams 1983; 4(1): 81-95.

[17] Rhee S K. Wetting of ceramics by liquid aluminum[J]. Journal of the American Ceramic Society, 1970, 53(7): 386-389.

[18] Zhou K, Wang H P, Chang J, et al. Surface tension measurement of metastable liquid Ti–Al–Nb alloys[J]. Applied Physics A, 2011, 105(1): 211-214.

[19] Bashforth F, Adams J C. An attempt to test the theories of capillary action: by

comparing the theoretical and measured forms of drops of fluid[M]. University Press, 1883.

[20] Eustathopoulos N, Joud J C, Desre P, et al. The wetting of carbon by aluminium and aluminium alloys[J]. Journal of Materials Science, 1974, 9(8): 1233-1242.

[21] Lang G. Casting Properties and Surface Tension of Aluminum and Binary Aluminum Alloys. Pt. 3. Surface Tension[J]. Aluminium, 1973, 49(3): 231-238.

[22] Nakae H. Wettability of liquid aluminum to non-metallic materials[J]. Journal of Japan Institute of Light Metals, 1989, 39(2): 136-146.

[23] Sinozaki N, Hatano K, Morita J, et al. Influence of oxide layer formed in surface of molten aluminum on wetting in aluminum/MgAl2O4 spinel system [J]. Journal of Japan Institute of Light Metals, 2003, 53(8): 337-341.

[24] Goumiri L, Joud J C. Auger electron spectroscopy study of aluminium-tin liquid system[J]. Acta metallurgica, 1982, 30(7): 1397-1405.

[25] Shergin L M, Popel S I, Tsarevskii B V. Temperature Dependence of the Density and Surface Tension of Cobalt–Silicon and Nickel–Silicon Melts[J]. Tr. Inst. Metall., Ural. Nauchn. Tsentr Akad. Nauk SSSR, Fiz. Khim. Metall. Melts, 1971, 25: 52-62.

[26] Goicoechea J, Garcia-Cordovilla C, Louis E, et al. Effects of wetting and surface oxidation on the measurement of the surface tension of Al by the maximum bubble pressure method[J]. Scripta metallurgica et materialia, 1991, 25(2): 479-484.

[27] Fainerman V B, Miller R, Joos P. The measurement of dynamic surface tension by the maximum bubble pressure method[J]. Colloid and Polymer Science, 1994, 272(6): 731-739.

[28] Murray J L, McAlister A J. The Al-Si (aluminum-silicon) system[J]. Bulletin of Alloy Phase Diagrams, 1984, 5(1): 74-84.

Chapter 7 Summary and Future Work

7.1 Summary

Carbon materials reinforcing metal matrix composites (MMCs) have been widely used in aerospace, civil engineering, military and automobile fields due to their high specific strength and stiffness, good thermal and electrical conductivities, low coefficient of thermal expansion and superior tribological property without the use of lubricant, etc. Among many metals, MMCs based on copper and aluminum matrices with a broad range of different reinforcements show great promise. However, during the fabrication of these two composites, there are some unavoidable issues that need to be improved. For the copper/carbon system, the liquid copper does not wet the carbon, and neither the mutual solubility nor the formation of carbides would occur at high temperature. For the aluminum/carbon system, it is well known that the wettability between carbon and liquid aluminium is poor at temperature close to the melting point of Al since Al is readily oxidized even if under a high vacuum. Although increasing temperature could improve it, Al_4C_3 phase would be formed at the interface in the meanwhile, which is brittle and water soluble, and thus significantly results in the weakening of interfaces and reduces the mechanical properties and corrosion resistance of composites. Therefore, it is necessary to improve the wettability for both the copper/carbon and aluminum/carbon systems and simultaneously avoid the formation of Al_4C_3 at high temperature for aluminum/carbon systems.

Generally, wetting between liquid copper/aluminium and carbon materials can be improved by alloying other reactive elements, such as Ti, Mg, Si and Cr, etc, due to a reduction of interface energy contributed by the negative free energy of the chemical reaction between the reactive element and the substrate, or by the formation of a reaction product at the liquid-substrate interface. Furthermore, for aluminium/carbon system, addition of suitable alloying elements in Al matrix is also expected to replace the formation of Al_4C_3 by that of other wettable compound at the interface. Among many reactive elements, titanium and silicon has been increasingly utilized as carbide-forming element for studying the wetting behavior between carbon materials and liquid copper/aluminium. Therefore, the understanding of interfacial phenomenon of copper/carbon and aluminium/carbon systems as adding elements of titanium and silicon is of crucial importance in producing these composites.

In present work, a major effort was made to investigate the wettability and interfacial reaction between Cu-Ti, Al-Ti and Al-Si alloys and graphite substrates with changing the composition of each alloy and the placement state of matrix and alloy elements by using the sessile drop method under vacuum. For this purpose, Cu-Ti alloys with titanium content of 4, 6 and 10 mass%, Al-Ti alloys with titanium content of 1, 3 and 5 mass%, and Al-Si alloys with silicon content of 0, 6, 10 and 20 mass% were employed in present work, and they were placed on the graphite substrate in three different placement states, which from top to bottom, was settled as (pre-alloyed sample)/graphite, (alloying metal)/(matrix metal)/graphite, and (matrix metal)/(alloying metal)/graphite, respectively. The latter two placement states aimed to prepare the drop of alloys in situ by directly melting alloying metal and matrix metal which were piled on the graphite substrate. The experimental temperatures were set to 1373 K for Cu-Ti/graphite and Al-Ti/graphite

systems, and 1273 K for Al-Si/graphite system, respectively. Besides, due to carbon fiber with some excellent properties that graphite does not possess, such as higher specific strength and lower CTE than graphite, high specific modulus, light weight, and good fatigue resistance, the composites reinforced by carbon fiber have been more widely used in many practical productions. Therefore, the penetration phenomena of Cu-Ti, Al-Ti and Al-Si alloys into carbon fiber felt were also investigated under same experimental condition.

On the other hand, the surface tension of liquid metals or alloys, which is both an intrinsic property and a key parameter of technological importance, contributes to deeper understanding the world of wettability. Especially, for a full analysis of capillary systems, the knowledge of adhesion characteristics (e.g. work of adhesion and adhesion tension) is required, and the surface tension value is necessary for these calculations according to the Young–Dupre equation. From this discussion, the surface tension of liquid Cu-Ti, Al-Ti and Al-Si alloys as a function of composition was also investigated using the sessile drop method, and Yttria Partially-Stabilized Zirconia was selected as the contacting substrate due to its chemical inertness.

The results of this work are summarized in the following statements.

1. **In Chapter 2 (Wettability and Interfacial Reaction between Cu-Ti Alloys and Graphite)**, it was observed that a TiC layer was formed at the interface between Cu-Ti alloy and graphite substrate in all cases. The wettability improved with increasing titanium content from 4 to 10 mass %. And with the same Ti content, the best wettability was obtained in the placement state of Cu/Ti/C, followed by Ti/Cu/C and pre-alloyed Cu-Ti/C. The different wetting behaviors of three kinds

of placement states can be attributed to the contact area between the generated Cu-Ti liquid phase and the graphite substrate during the heating process, as well as the actual content of molten Ti in the generated Cu-Ti liquid phase.

2. **In Chapter 3 (Wettability and Interfacial Reaction between Al-Ti Alloys and Graphite)**, it was found that addition of less than 5 mass% Ti in Al could accelerate the spreading of the droplet on the graphite, but had no measurable effect on the final contact angle. The values of the equilibrium contact angle did not be affect by changing the placement state of the Al-Ti alloys on the graphite substrate. Addition of Ti in Al led to the formation of a bilayer of Al_4C_3 and TiC at the interface of the Al-Ti/ graphite systems. Since only Al_4C_3 layer existed at the vicinity of the triple line in all cases, the formation of TiC improved the wetting of the Al-Ti/ graphite systems only in the initial wetting stage, and after all of Ti was consumed, the rest of the wetting was dominated by the formation of Al_4C_3.

3. **In Chapter 4 (Wettability and Interfacial Reaction between Al-Si Alloys and Graphite)**, the wetting result was not affected by the placement state of the Al-Si alloys on the graphite substrate. The wettability did not be improved significantly as increasing Si content from zero to 10 mass %, whereas a notable decrease of 22° in the contact angle was observed as adding Si content from 10 mass % to 20 mass %. This was attributed to the transformation of the interfacial reaction product from Al_4C_3 into SiC, provided an addition of sufficient Si to Al. It was verified that the liquid Al can wet the SiC substrate very well in nature, which might explain why the occurrence of SiC would improve the wettability of

the Al-20 mass %Si alloy on graphite substrate.

4. **In Chapter 5 (Composite of Carbon Fiber and Cu-Ti, Al-Ti and Al-Si Alloys)**, for the Cu-10mass%Ti/carbon fiber and Al-5mass%Ti/carbon fiber systems, the liquid alloy droplet totally penetrated into the carbon fiber felt spontaneously, due to the porous structure of the carbon fiber felt and the formation of wettable TiC at the interface between liquid alloys and the carbon fiber. For the Al-Si/carbon fiber systems, spontaneous penetration of the liquid alloys only occurred at 20mass%Si, and it resulted from the formation of the different reaction products as increasing the Si content from 10 mass% to 20 mass%, as well as the constraint of the critical contact angle of penetration.

5. **In Chapter 6 (Surface Tension of Liquid Cu-Ti, Al-Ti and Al-Si Alloys)**, the surface tension of both liquid Cu-Ti and Al-Ti alloys increased with increasing the content of Ti, whereas the surface tension of liquid Al-Si alloy showed a monotonous decrease with the increase of the content of Si. With the change in the composition, the surface tension values of three kinds of alloys varied within a reasonable range, because these values were between the corresponding values of two pure elements.

In conclusion, the core and achievements of this thesis can be generalized as the following flow chart:

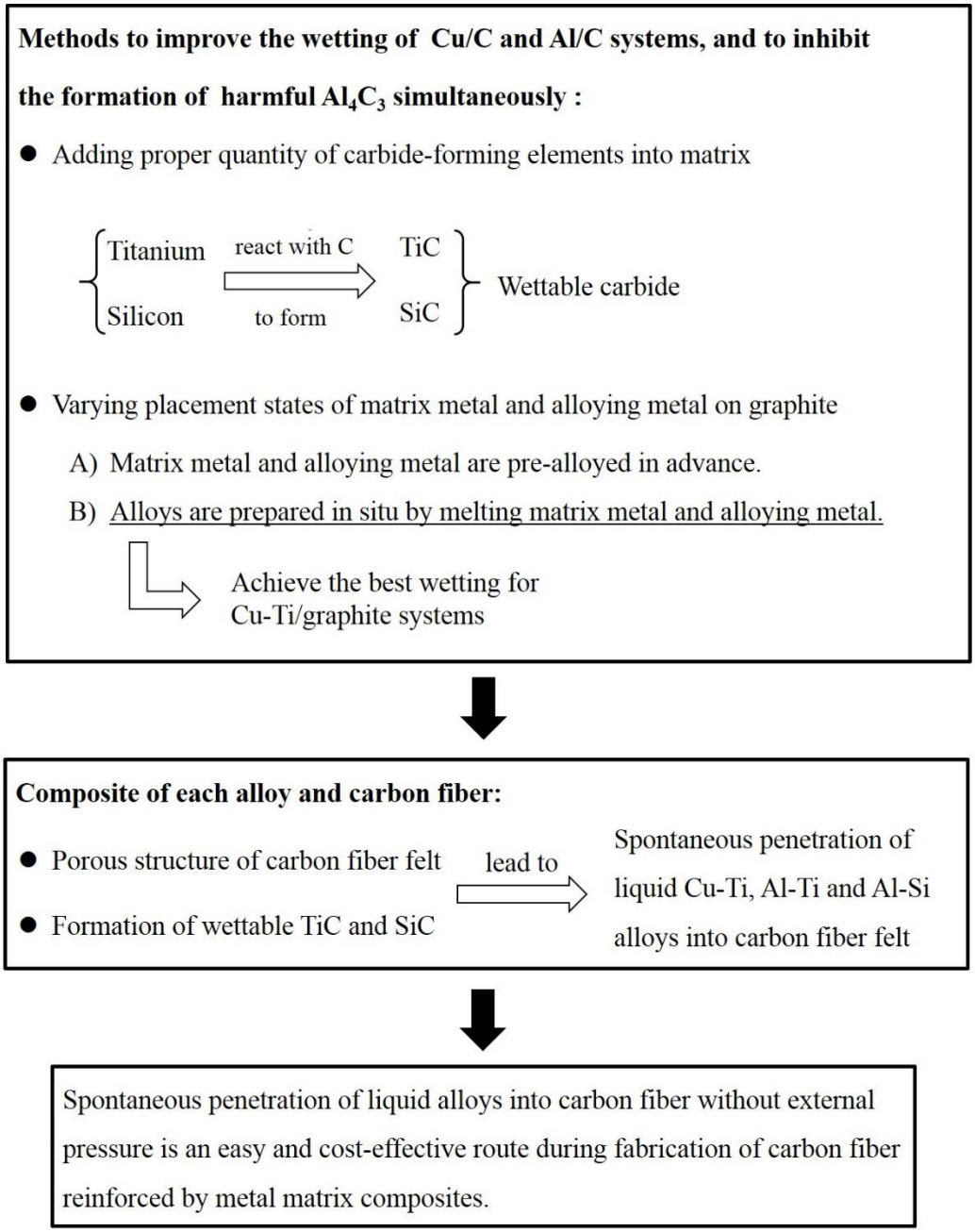

Figure 7.1.1 Core and achievements of this thesis

7.2 Future work

During fabrication of graphite reinforcing Cu-Ti composites, if the addition of Ti was less than approximately 20 mass%, sandwiching Ti plates or foils between Cu and graphite was a good configuration to cause a great wetting due to the higher content of Ti in the prior Cu-Ti liquid phase in this configuration. Future researchers should increase the configuration to further refine contact angle response behavior, such as a cylinder of Ti over a plate of Cu, to produce melting from the center of the drop out, as opposed to the observed behavior of the place statement B. For Al-Ti/graphite systems, using Al-Ti alloys oversaturated in Ti might enable the formation of TiC to extend to the triple line, but the rapid increase of the liquidus temperature of Al-Ti alloys would increase the difficulty of fabrication and raise the production cost at the same time. Therefore, suitable balance between the wetting and the cost should be considered comprehensively. Nevertheless, Al_4C_3 was formed even at high Ti content, and future work should test different fabrication methods (e.g. temperature, holding time and fabricating procedure) to try to avoid its formation. For Al-Si/graphite systems, although the formation of Al_4C_3 did not occur at 20mass%Si in present work, the critical Si content that can suppress the formation of Al_4C_3 should be clear by experiments, and adding less amount of Si is favorable to the material performance during fabrication process, since increasing Si content would lower the strength of Al-Si alloys. However, the present work only focused on the wetting and interfacial phenomenon, mechanical tests (e.g. tensile strength, hardness and ductility etc.), therefore, are suggested to be conducted in future work, to estimate the improvement of mechanical properties of materials, and to provide important information in the selection of suitable applications. Furthermore, since the data of work

of adhesion is of vital importance to evaluate the bonding strength of the interface between alloys and graphite substrate, push-off shear tests deserve to be conducted for producing actual work of adhesion values.

Acknowledgment

Firstly, I would like to express my sincere appreciation to my supervisors, Prof. Nobuya Shinozaki, for his constant encouragement and patient guidance throughout whole course of my research. He was not only available when I needed counsel regarding the direction of my research, but he was also there when I needed career and even personal advice. Without his consistent and illuminating instruction, this thesis could not have reached its present form.

I also would like to thank Prof. Kazumasa Nishio, Prof. Tomiko Yamaguchi and Ms. Liying Zhang for providing an opportunity to pursue my doctoral study in Kyushu Institute of Technology.

I want to express my gratitude to Ms. Noriko Miyoshi for her experimental assistance and helpful advice in the field of EPMA. I am also grateful to Mr. Katsumi Yamamoto for XRD analysis, to Ms. Rika Umegane for chemical analysis, and to Dr. Toshifumu Ogawa for production of alloy samples.

Last my thanks would go to my beloved family for their loving considerations and great confidence in me all through these years. I also owe my sincere gratitude to my friends and every students in my lab who gave me their assistance and time in listening to me and helping me work out my problems during the difficult course of my research.

Appendix Publication List

Publication in paper

1. “Wettability, surface tension and work of adhesion of Cu-Ti alloys on Yttria Partially-Stabilized Zirconia at 1273K”. Weiji Mao, Hiroki Sannamiya, Nobuya Shinozaki and Toshifumi Ogawa. Advanced Materials Research, 2014, 941: 102-107.

2. “Wettability of Cu-Ti Alloys on Graphite in Different Placement States of Copper and Titanium at 1373 K”. Weiji Mao, Tomoko Yamaki, Noriko Miyoshi, Nobuya Shinozaki and Toshifumi Ogawa. Metallurgical and Materials Transactions A, 2015, 46(5): 2262-2272.

3. “Wettability and surface tension of liquid aluminium-copper alloys on graphite at 1273 K”. Weiji Mao and Nobuya Shinozaki. CRC Press/Balkema. **(In press)**

4. “Wettability of molten aluminium-silicon alloys on graphite and surface tension of those alloys at 1273 K”. Weiji Mao, Takayasu Noji, Kenichiro Teshima and Nobuya Shinozaki. Metallurgical and Materials Transactions A. **(Under review)**

Presentations in conference

1. The 5th International Conference on Manufacturing Science and Engineering. April, 2014, Shanghai, China.

2. The 1th International Conference on Civil, Architectural, Structural and Constructional Engineering. August, 2015, Busan, Korea.